Electronically Generated Cover-Page

Measurement and analysis of alkaline battery performance for low power wireless applications

A THESIS SUBMITTED TO THE UNIVERSITY OF MANCHESTER FOR THE DEGREE OF MASTER OF PHILOSOPHY IN THE FACULTY OF ENGINEERING AND PHYSICAL SCIENCES

2011

ANDREW FLOYD

SCHOOL OF ELECTRICAL AND ELECTRONIC ENGINEERING

LIST OF CONTENTS

Word Count: 28,947

List of Figures

LIST OF TABLES

ABSTRACT

THE UNIVERSITY OF MANCHESTER

ANDREW FLOYD

MASTER OF PHILOSOPHY

MEASUREMENT AND ANALYSIS OF ALKALINE BATTERY PERFORMANCE FOR LOW POWER WIRELESS APPLICATIONS

2011

Alkaline batteries provide an inexpensive and readily available energy source for low power wireless devices. These devices can spend as much as 99 % of their operating life in an inactive state, consuming currents in the micro-Amp range. The operating current can be up to one hundred times higher. This causes a pulsed current discharge from the battery.

From existing academic research and manufacturers' data it is difficult to estimate how the service life of an alkaline battery is affected by this pulsed discharge, and discharge currents in the micro-Amp range.

This research project focuses on understanding the behaviour of the alkaline batteries, in particular the battery voltage, and analyses the effect on the service life under varying experimental conditions.

To achieve this, in excess of 100 batteries have been discharged, contributing to more than 350 days worth of experimental results. The results show that through a combination of pulsed current discharge and long periods of inactivity the service life continues to extend at a linear rate. With further experimental work, a model for estimating the achievable service life could be developed.

These results have also assisted the design of a low power wireless node that presents a method of power management to increase the efficiency of the power drawn from the alkaline batteries during the long inactive periods.

DECLARATION

No portion of the work referred to in this thesis has been submitted in support of an application for another degree or qualification of this or any other university or any other institute of learning.

COPYRIGHT STATEMENT

I. The author of this thesis (including any appendices and/or schedules to this thesis) owns certain copyright or related rights in it (the "Copyright") and he has given The University of Manchester certain rights to use such Copyright, including for administrative purposes.

II. Copies of this thesis, either in full or in extracts and whether in hard or electronic copy, may be made **only** in accordance with the Copyright, Designs and Patents Act 1988 (as amended) and regulations issued under it or, where appropriate, in accordance with licensing agreements which the University has from time to time. This page must form part of any such copies made.

III. The ownership of certain Copyright, patents, designs, trademarks and other intellectual property (the "Intellectual Property") and any reproductions of copyright works in the thesis, for example graphs and tables ("Reproductions"), which may be described in this thesis, may not be owned by the author and may be owned by third parties. Such Intellectual Property and Reproductions cannot and must not be made available for use without the prior written permission of the owner(s) of the relevant Intellectual Property and/or Reproductions.

IV. Further information on the conditions under which disclosure, publication and commercialization of this thesis, the Copyright and any Intellectual Property and/or Reproductions described in it may take place is available in the University IP Policy (see http://campus.manchester.ac.uk/medialibrary/policies/intellectual-property.pdf), in any relevant Thesis restriction declarations deposited in the University Library, The University Library's regulations (see http://www.manchester.ac.uk/library/aboutus/regulations) and in The University's policy on presentation of Theses.

ACKNOWLEDGEMENT

First and foremost I would like to express my gratitude towards my academic supervisor, Mr Peter R Green, for all of his advice, support, guidance and encouragement during my research. Peter has been a constant source of motivation and always extremely helpful throughout my studies. I would also like to acknowledge my Line Manager, Adrian Rice, at Pactrol Controls Ltd, who has supported me whenever he can throughout my part-time postgraduate studies. Finally I would like to thank my family and all of my close friends who have supported me throughout.

Chapter 1.

Introduction

Over the previous decade there has been an increased use and advancement in wireless communications. One use is for wireless sensor networks (WSN); whilst other examples include wireless local area networks, and the mobile phone cell network.

Wireless sensor networks are designed to autonomously monitor and collect real-time information whilst requiring little maintenance. The data and periodic readings provide environmental feedback in what can sometimes be from a hostile or hard to reach environment [1]. They are used across a wide variety of application fields, from Medical Care [2] and scientific observation, to environmental [3] and structural monitoring [4].

The major advantage of wireless sensor networks is the flexibility when integrating and installing into the intended environment. In comparison, wired sensor networks often suffer from installation delays and higher costs in order to install the power and communication connections [5].

One of the most challenging aspects of deploying a wireless sensor network is the selection and management of the primary energy source. Batteries are the general choice but hold only a finite amount of energy.

Whilst there have been advancements in wireless communications, the energy density of batteries for portable applications has seen very little increase [6] since the introduction of the first alkaline battery for consumer electronics in 1959.

The same alkaline batteries now last only 40 times longer [7] than the original commercial batteries, due to changes in cell structure and manufacturing techniques in the 1980's [6].

The batteries used in wireless sensor networks come in various forms and can be selected based on properties such as capacity, size or cost. It is important that the chosen battery can provide the required service life for each of the sensor devices.

An alternative to batteries is the use of a renewable energy source [8] such as solar energy. This method is often ruled out on cost and the difficulties associated in harvesting enough power, for example once scaled for use with a wireless sensor node, solar energy can only provide 10-25 % efficiency [8] providing there is good luminance in the location of installation.

Wireless sensor networks can consist of anywhere up to 100 or 200 sensor devices, all requiring their own energy source. This means that cost can be a deciding factor in the choice of energy source.

Standard AA Alkaline-Manganese batteries are inexpensive and readily available. The UK market in 2009 was worth £370 million, with Alkaline-Manganese batteries taking a 79 % share of the market sales [9] and on average costing 65 pence per cell. The market leaders are Duracell taking a 43 % share in the value of sales in 2009.

Based on the market research and partly on the availability and price of large quantities, the Duracell Procell range aimed at industrial end users, has been selected to be used in this research project.

A wireless sensor device, or 'node', is a single point within a wireless network that performs some form data processing or data gathering and then communicates this data to other nodes within the same network. To achieve this, every node contains an embedded microcontroller.

Due to the popularity of battery powered electronics, manufacturers of embedded microcontrollers have turned their attention to producing devices that require less power when active or sleeping. Microcontrollers, from manufacturers such as Microchip, are now available with sleep currents that are in the sub 1 μA range [10].

Since the amount energy available in a standard alkaline battery is unlikely to improve, it raises the question, when operating a wireless sensor node for long periods of time, with extremely low sleep currents, how long can the service life of the batteries be prolonged? Can the service life be prolonged to operate a wireless sensor node for two years or more?

1.1 MOTIVATION

The motivation for this research project comes from the difficulty in obtaining the necessary information to determine the expected service life of an alkaline battery being discharged for long periods of time at very low discharge currents.

Data from existing research, simulation or experimental, is hard to come by and almost non-existent. Even data from the battery manufacturers does not provide data for batteries being discharged at currents less than 5 mA.

The main aim of this project is to analyse the performance of alkaline batteries through experimental measurement. Performing controlled discharges to investigate the behavioural effects from variables such temperature and the magnitude of the discharge current.

The research then aims to suggest ways of improving the performance of alkaline batteries when used in low power wireless sensor applications.

1.1.1 Contribution of knowledge

In summary this thesis contributes to the following areas of research knowledge:

- Experimental analysis of standard Alkaline-Manganese batteries.
    - Cell behavior under pulsed discharge conditions
    - Changes in cell behavior due to temperature

- Suggestion of battery lifetime estimation model for Alkaline-Manganese batteries
    - Due to lack of models from existing research focusing on the alkaline battery chemistry.

- Low power node hardware design
    - Improvements in power management.
    - Reduction in node sleep currents compared to existing hardware.

1.2 Document Structure

The thesis will begin in Chapter 2 by discussing in more detail the areas of technology that are closely related to this project, including the alternative energy sources available and the expected behaviour of the batteries, and some background on wireless communications.

The area of wireless sensor networks covers a broad range of related research and in Chapter 3 this research is reviewed and brought into context with the aims of this research project. In the same chapter, existing research on battery modelling and lifetime estimation is also reviewed.

As previously stated this project aims to experimentally measure the behaviour of the batteries under discharge. The experimental framework used to achieve this has been discussed in Chapter 4, including the measurement system that has been designed specifically for the purpose of performing controlled battery discharges.

The results from the experimental work have been broken down into two separate areas, the behaviour exhibited from different forms of discharge in Chapter 5, and then the effects on the battery performance from temperature changes in Chapter 6. Both areas of results will then be analysed and put into context of the batteries being used in low power wireless applications in Chapter 7.

Chapter 8 outlines the low power node prototype design that has been implemented based on the analysis of the results and suggested methods of improving the service lifetime of a wireless sensor node using alkaline batteries.

The project is concluded in Chapter 9, summarising the knowledge that has been gained from the experimental work, and what further work could be carried out on this research topic.

Chapter 2.

Technology Review

Wireless sensor networks already have a large number of possible applications, but the technology required to operate autonomous networks with more than 100 devices, is relatively young.

This chapter reviews the key areas of technology required to operate a wireless sensor network. Including the finite energy sources required to power the individual wireless sensor nodes, and possible forms of wireless communications and configurations.

2.1 ENERGY SOURCE

The deployment flexibility of wireless sensor nodes is due to each node having its own primary energy source. The most common energy source is a battery, of which the greatest disadvantage is that they can only provide a limited amount of energy. Power efficiency becomes one of the major factors in the design of a wireless sensor node intended for a long service life.

The ideal battery [11] is one that is inexpensive, has infinite energy, can operate over the full temperature range and environmental conditions, and has unlimited shelf life.

In reality only a finite amount of energy is available as materials are consumed, varying with temperature and discharge rate during the discharge process. The shelf life is also limited as during storage chemical reactions and physical changes can reduce the available energy to 90 % or less [11].

When selecting a battery energy source there are a number of characteristics that should be considered:

- **Type of battery:** Primary or secondary, rechargeable or non-rechargeable
- **Voltage:** Operating voltage, maximum and minimum, and profile of discharge curve
- **Load Current and Profile:** Constant, variable or pulsed load
- **Temperature Requirements:** Temperature range over which operation can occur
- **Service Life:** Length of time operation is required
- **Physical requirements:** Size, shape, weight
- **Shelf Life:** State of charge during storage, a function of temperature, humidity and other conditions
- **Cost:** Initial cost, operating or life-cycle cost

The batteries for wireless sensor nodes are selected based predominantly on the service life and the ability to hold charge and not self discharge. Cost also plays an important role, especially in large sensor networks that can reach 100-200 nodes [3][12].

2.1.1 Primary Energy Source

In the application of wireless sensor networks, non-rechargeable batteries are commonly used as the primary energy source. The characteristics of non-rechargeable batteries mean that they have a much greater shelf life than their rechargeable counterparts and are more suited to low drain applications.

Rechargeable batteries are often more expensive, but in high drain applications they offer greater value as they can be re-used. In low drain applications it is the service life that is more important and the self discharge characteristics of a rechargeable battery means that they are less suitable for use as the primary energy source.

Given the flexibility in installation location of wireless nodes, it makes it nonsensical to have to perform the maintenance of retrieving the nodes to recharge the battery. It is preferred that the energy source chosen will reach the required service life for the sensor network without being revisited.

An alternative to using batteries as the primary energy source is the use of renewable energy. Until recently this has been deemed a costly alternative to using limited energy sources. The argument being that it would be cheaper to let the nodes 'die' than to employ technology such as photovoltaic cells to recharge a secondary energy source.

Recent developments by Texas Instruments and industrial partners [13], has introduced forms of energy harvesting for use with small autonomous devices. The energy can be harvested from ambient energy such as light, heat, motion, and RF.

Different technologies are used for the energy harvesting circuit depending on the environment it's in, and its efficiency and size. The design article contained within the *EE Times* [8] gives a summary of the challenges that are faced when using energy harvesting.

A good example of a challenge faced is the efficiency of the conversion, for example in 2009 the most efficient solar panels available were only roughly 41 % efficient, and that is without considering the reduction in size necessary for a solar panel to be practical for an autonomous embedded device. This value of efficiency reduces to 10-25 %, as shown in Table 2.1, despite advances in photovoltaic cells. A summary of the other possible power outputs can also be found in the same table.

Energy source	Characteristics	Efficiency	Harvested power
Light	Outdoor	10–25%	100 mW/cm²
	Indoor		100 µW/cm²
Thermal	Human	~0.1%	60 µW/cm²
	Industrial	~3%	10 mW/cm²
Vibration	~Hz-human	25~50%	4 µW/cm²
	~kHz-machines		800 µW/cm²
Radio frequency (RF)	GSM 900 MHz	~50%	0.1 µW/cm²
	WiFi 2.4GHz		0.001 µW/cm²

Table 2.1 - Sources for Energy Harvesting [8]

It would be very difficult to run the embedded device directly from the harvested energy, for example during transmission of a wireless sensor the power required can peak at 100 mW. It would be unrealistic to assume that the energy source would be available all the time, so the energy harvested needs to be stored in a secondary energy source.

The secondary energy source can be a rechargeable battery, a super capacitor, or the more recent development of solid state energy storage [14]. The harvested energy is used to trickle charge the secondary energy storage over long periods of time, making the energy available when required. The selection of the secondary energy source would depend on, for example how often the ambient energy is available for harvest.

The use of energy harvesting is still very much dependant on the application, for example a wireless sensor deployment that only needs to last 2 years could be achieved with a set of batteries. So not all applications will be suitable candidates and there is a high cost associated with development to ensure that there is sufficient reliability. However applications where installation and maintenance costs are high due to the application environment, the cost of developing with energy harvesting technology could be outweigh the maintenance costs.

2.1.2 Battery Chemistry

There are numerous battery chemistries that are available as primary energy sources, each having their own advantages and disadvantages. The two chemistries that are most commonly used for wireless sensor nodes are Alkaline Manganese Dioxide, and various combinations of Lithium chemical compounds.

Although inherently different chemistries, their behaviour is comparative. They share the common attributes; high energy density, low internal resistance, long shelf life, and low leakage currents.

The major difference in behaviour between the two chemistries is with the cell voltage over the lifetime of the cell. Lithium batteries exhibit an almost flat curve, as seen in Figure 2.1(b). This is for almost the entire lifetime of the cell, but at the end of the service life the cell voltage falls sharply.

In comparison Alkaline Manganese Dioxide cells have a more gradual decline of cell voltage over the lifetime of the cell before a sharp fall as shown in Figure 2.1(a).

An advantage of the flat curve exhibited by the lithium chemistry is that the supply voltage for the embedded hardware will not change a great deal over the service life of the battery. This means that any voltage regulation can be refined to operate at its highest efficiency for the given supply voltage, or the voltage regulation bypassed completely.

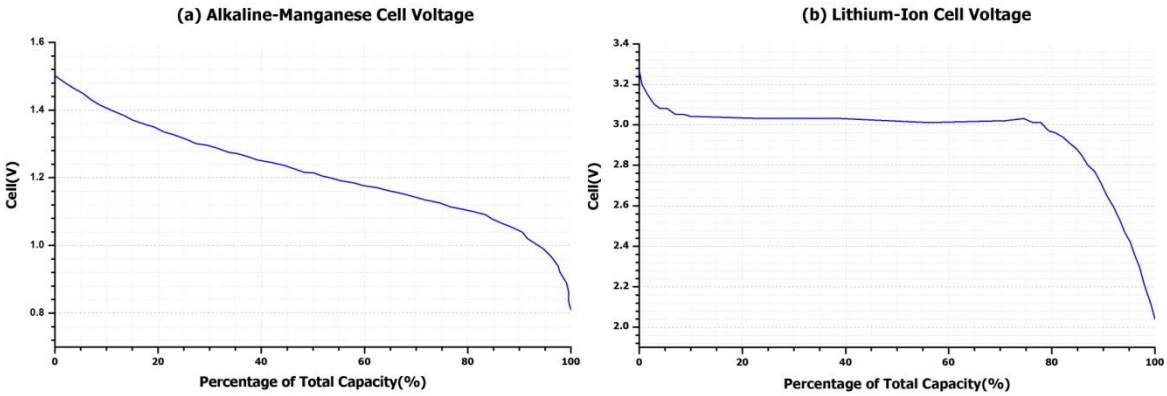

Figure 2.1 - Cell voltage of (a) Alkaline Manganese [15] and (b) Lithium-Ion batteries [16]

The cell voltage from the alkaline chemistry does change over the lifetime by as much as half the cells original value. There is an advantage of the gradual decline since it is possible to predict the nearing end of life of a cell based on the cell voltage. The lithium chemistry falls sharply and therefore puts onus on battery models for calculating impending end of life.

Despite both chemistries having their similarities and differences, the main point of comparison comes down to price and availability. Alkaline batteries are lower in cost and easier to acquire. Which points back to one of the motivations for this research project as mentioned in Section 1.1

Wireless sensor networks often result in the deployment of a large number of sensor nodes [3][12] and in large deployments the price can become a major factor in design, especially for an item that is effectively disposed of at the end of its life cycle.

2.1.3 Battery Behaviour

The cells in question are constructed of two electrodes, an anode and a cathode. The electrodes are separated by an electrolyte which varies depending on the cell chemistry. When the cell is connected to a load, electrons are transferred from the anode to the cathode.

The amount of energy deliverable by the cell is defined as the cell capacity. At full charge the theoretical capacity [17] is based on the amount of active material available in the cell after manufacture. The actual capacity delivered from the cell depends on the load applied to the cell and the temperature conditions.

It is possible that the actual delivered capacity is less than the theoretical maximum capacity. To describe this phenomenon, Ma et al. [18] present several simplified diagrams of the cell in its various states, as summarized in Figure 2.2 and Figure 2.3.

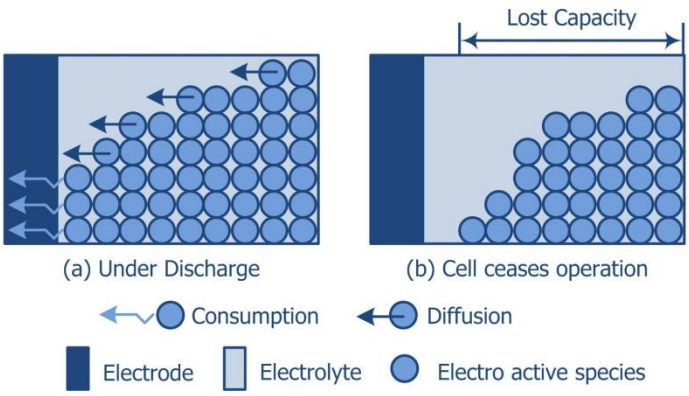

Figure 2.2 - Models [10] of (a) a discharging cell and (b) a discharged cell

When a load is applied to the cell, the electro active species move towards the electrode of the cell Figure 2.2(a). The higher the load applied the more species that are consumed. This in effect forms a concentration gradient across the electrolyte, dependant on the rate of discharge.

Should the gradient increase to the point where there are no longer any active species at the electrode, there becomes a situation where the electrochemical process can no longer be sustained. This results in the remaining capacity being inaccessible, Figure 2.2(b).

Should a sustained load either be significantly reduced or removed during discharge, the cell enters a charge recovery state, Figure 2.3(a). This 'rest period' allows for the concentration of electro active species at the electrode to increase, reducing the gradient, as shown in Figure 2.3(b).

The system designer can use the recovery process to their advantage. If the discharge rate is reduced sufficiently low enough during the rest period, then it is theoretically possible to extract much closer to the theoretical maximum capacity of the cell. This method is referred to as 'Pulsed Discharge' [19] and is a technique that will be used experimentally to explain the benefits.

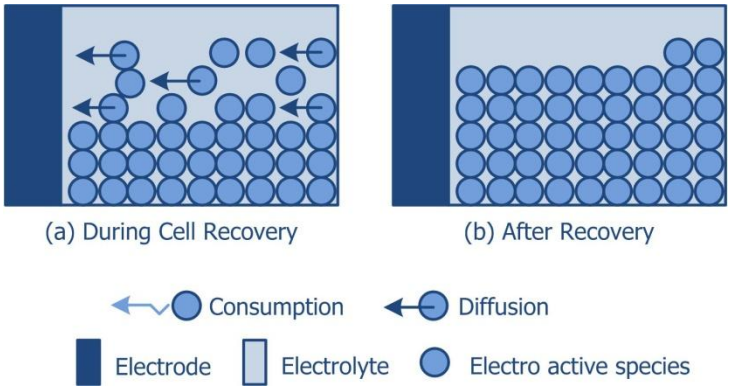

Figure 2.3 - Models [10] of (a) a cell in recovery and (b) a cell after recovery

During the operational lifetime of an alkaline cell the voltage decreases as previously shown in Figure 2.1(a). This is because as the bulk of the electro active species becomes further away from the electrode the cell's internal resistance increases. With the increase in resistance, there is a fall in cell voltage.

Temperature strongly affects the behaviour of the cell [17] and more specifically the behaviour of the electro active species. At temperatures below room temperature, roughly 25 °C, the chemical activity decreases, effectively reducing the available capacity of the cell when under discharge.

At temperatures above room temperature the chemical activity increases and the internal resistance decreases when under discharge. This in effect increases the available capacity from the cell.

When in storage the cells can exhibit the behaviour of self discharge, which is linked with the shelf life characteristic of each cell. It is recommended by the battery manufacturers [20] that when in storage the cells are kept below room temperature. The reason being that storing them below room temperature, takes advantage of the reduced chemical activity and the cell self discharging.

2.2 WIRELESS COMMUNICATIONS

Wireless sensor networks as mentioned revolve around large numbers of low cost, and low speed devices that have a battery life between months to years. The networks themselves are often based on proprietary communications that are designed to meet the application demands. This type of network is known a Wireless Personal Area Network (WPAN).

The popularity of WPANs has risen in the last decade, prompting international standards to be introduced. The standards are defined and managed by the IEEE Standards Association [21] and are implemented across the globe. The standards set out the requirements of the devices that operate in the various unlicensed frequency bands that are available in different countries.

2.2.1 Communications Protocol

The requirements set out by the standards are in relation to two areas, the PHY (Physical) layer and the MAC (Medium Access Control) layer, with the latter being part of the DLL (Data Link Layer). Both are part of the OSI (Open Systems Interconnect) model that has been defined by the International Standards Organization, and is depicted in Figure 2.4.

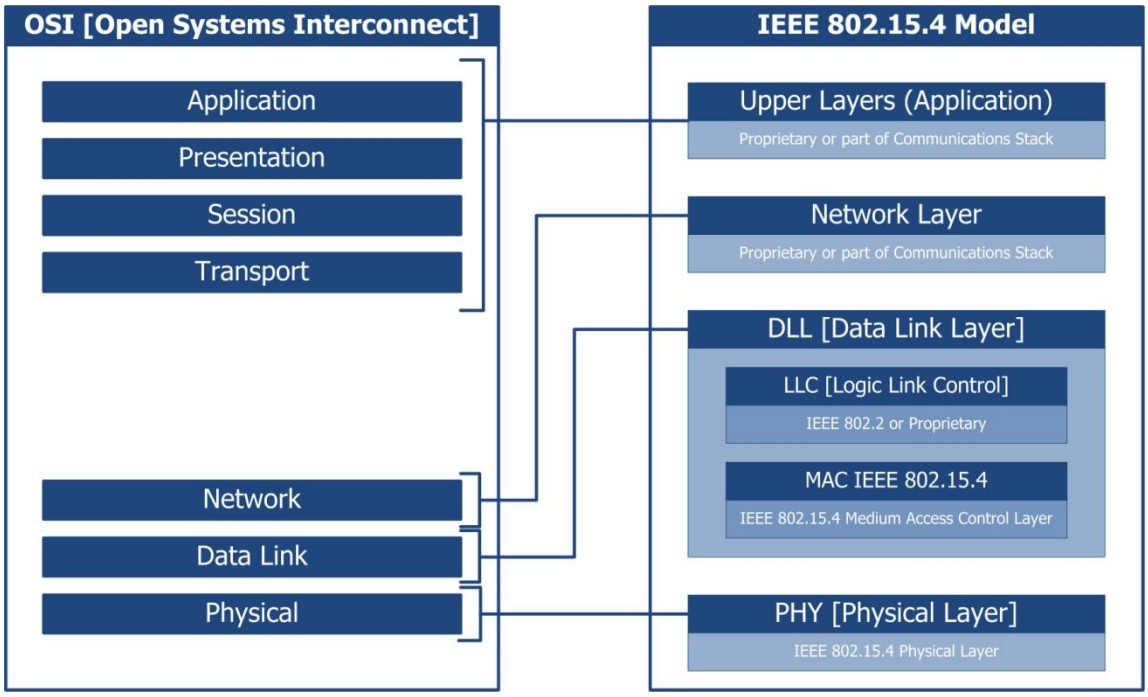

Figure 2.4 - Comparison between OSI and IEEE 802.15.4 Model

The following is a short description of the layers contained within the IEEE 802.15.4 Model:

- The **Network Layer** handles the network connection, routing, security, and delivery of the data.
- The **DLL Layer** is constructed of the LLC (Logical Link Control) and MAC layers.
- The **MAC Layer** handles the physical addressing of the device and the following [22]:
    - Network association and disassociation
    - Frame delivery acknowledgement
    - Wireless channel access
    - Frame validation
    - Time slot management
- The **PHY Layer** contains the RF transceiver and translates the data packets into an electrical signal.

It is the MAC layer that has overall control over the radio, and has a large effect on the overall energy consumption and therefore the lifetime of the node.

The standards that relate to low data rate and low power consumption wireless networks comply with the IEEE 802.15 standard. The most common applications of IEEE 802.15 are Bluetooth and ZigBee. Both of these technologies focus on the application and network layers of the OSI model in order to provide a full communications stack.

Bluetooth uses the 802.15.1 standard and was primarily aimed at peer to peer communications through a process known as pairing. The Bluetooth radios operate in the 2.4 GHz spectrum and have range between 1 and 10 meters. An example use of Bluetooth is communication between a mobile phone and a hands free ear piece.

ZigBee is based on the 802.15.4 standard and aims at providing a low complexity communications stack that is reliable and secure, with low power consumption. The high level stack aims at providing a solution for companies that are looking for a low cost, and a low risk implementation of a wireless network. This is because to produce a proprietary wireless network it can require substantial research hours to produce a commercially viable solution.

2.2.2 Network Topologies

The network topology is the layout or arrangement of devices that form interconnections. There are several forms of topology and an advantage of the ZigBee communication protocol is that it allows for multiple topologies to be formed, giving the end user maximum flexibility when the wireless devices are being located.

The most common topologies are star, mesh and cluster, all of which are shown in Figure 2.5 and are commonly applied using the ZigBee communications stack. In general a wireless sensor network will have a gateway or access point.

The gateway, or gateways, are the access points into the network and are where the data gathered is retrieved and stored on a larger and possibly more stationary device. Most wireless sensor networks are based on the mesh topology as this configuration brings about the most redundancy since all the nodes can have multiple nodes with multiple routes for the data to travel to the gateway or access point.

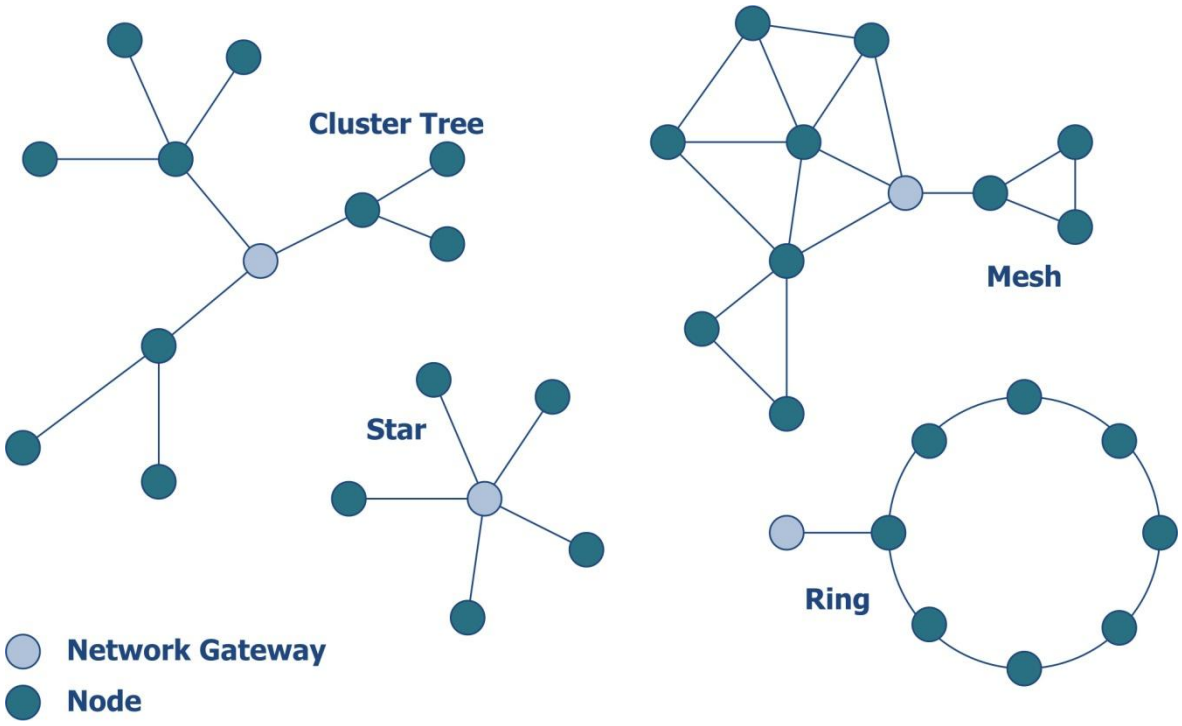

Figure 2.5 - Collection of example network configurations

The ring topology is not a common configuration, but in applications where a perimeter is being monitored it could offer greater efficiency using a reduced number of nodes to cover the same perimeter distance. The implementation of a ring network would require a proprietary protocol in order to improve on communication efficiency.

An important factor in the design of a low powered wireless network is the amount of traffic that each node must handle. Taking the cluster tree in Figure 2.5 for example, there are three nodes that have the responsibility of relaying data packets from two or more connected nodes. Assuming that all the nodes are battery powered, it would mean that theses three nodes would see an increased amount of activity and it is likely that they would have a lower service life than the nodes at the extreme end of the network.

It is therefore a clear advantage of having redundancy in the network design, as it allows for network traffic to be spread across multiple paths. This is an area of the related research that will be discussed in the following chapter.

2.3 Summary of Technology

In summary this chapter has covered the energy sources that can be used for wireless sensor nodes, and the basics of the communications protocol.

The focus on alkaline cells complies well with the need for low cost, long shelf, and a suitably large capacity required for a wireless sensor node.

It could well be that some applications could be suited to using renewable energy sources but until efficiency can be increased, the cost incentive will remain with non-rechargeable batteries.

Chapter 3.

Performance Analysis

The focus of this project is to analyze the performance of alkaline batteries for use in wireless sensor networks. The combination of wireless sensor networks and alkaline batteries is not an area of research that commonly exists.

The aim of this section is to identify the areas of research related to both alkaline batteries and wireless sensor networks, and understand the links or possible voids in the research.

As previously introduced, wireless sensor networks are a growing area of research and have been applied to applications such as habitat [23], building [4], and health [2] monitoring.

In order to apply the technology to a real life application there are numerous design considerations to take into account. The structure of the network, or network topology as explained in Section 2.2.2, can have a great bearing on connectivity and network coverage. A miscalculated design can have an effect on the service life of the network or individual nodes.

The network topology is managed through the communications protocol, and part of that protocol is the MAC layer as discussed in Section 2.2.1. A great deal of related research is aimed at producing an energy efficient MAC layer [24][25] for wireless sensor nodes, whereas traditional MAC protocols concentrate on attributes such as throughput, latency, fairness, and bandwidth utilization.

The expected service life of the wireless network depends a great deal on the choice in energy source, i.e. the batteries. Research focused around the batteries is generally related to estimating the remaining capacity of the cells [26] or how the lifetime of the cells can increase through pulsed discharge [19].

Battery models play a key role in being able to simulate the behaviour, but no models are directly aimed at the simulation of alkaline cells.

Before considering network design or energy management it is worth considering what practical deployments have been implemented by various research groups, and the service life that has been achieved by them.

3.1 DEPLOYMENT

In the area of wireless sensor networks a great deal of research is concluded on simulation results. When the theories or algorithms are applied to a real world application it is common for problems to appear. The research in the area of wireless sensor networks is continually growing, and with it the number of network deployments to compare.

The earliest successful large scale deployment was reported by the Berkeley research group [23][3]. The application was to monitor the habitats of nesting birds on the Great duck Island, in Maine State USA.

The use of a wireless sensor network lends itself well to environmental monitoring where the simple task is to observe. The wireless network nodes can be designed to be unobtrusive to the surrounding environment and can be located in the environment without affecting the habitat. In this example the wireless sensor network was able to observe a large area uninhabited by people, whilst being unattended.

The deployment was not without problems. In the analysis [3] of the second generation deployment a clear problem was the unexpected end of life for a large portion of the nodes. The second generation deployment used lithium cells for the energy source due to the flat voltage curve; this meant that the device could operate without the need for a DC to DC convertor.

The problem experienced with lithium batteries was that when nearing the end of service life the drop in cell voltage was severe enough to mean that the nodes were unable to report a fall in cell voltage. The nodes simply disappeared from the network without warning, putting a burden on local nodes to realize that an alternate routing path was required.

The solution identified was to implement an energy counter to monitor the number of times given operations occurred e.g. sensing, receiving, transmitting, and active CPU time.

Problems with the energy source were apparent in the LOFAR-agro project [12], undertaken by researchers at the Delft University of Technology in the Netherlands. The project faced multiple problems during the deployment process and the published work goes at length to try and share all their experiences.

The aim of the LOFAR-agro project was to deploy a large scale sensor network in a potato field to warn against possible signs of a fungal disease in the potatoes.

The deployment involved multiple trials and faced problems with the operation of the MAC layer but also with reduced battery lifetimes. The batteries originally used were AA alkaline cells but on the first trial the batteries lasted only 4 days. The alkaline batteries were later replaced by larger Lithium-thionyl chloride 7.2 Ah capacity batteries, which equated to over twice the capacity of the alkaline batteries.

The problem with the batteries existed due to the communications protocol behaving in an unexpected manner that did not occur during testing or simulation.

The experiences from this project provide a good advocate for the importance of detailed design and careful preparation when deploying a wireless sensor network.

Despite the bad experiences in the LOFAR-agro project [12], there are several successful deployments that have lasted between two months [4] and eighteen months. The latter involved researchers from the University of Southampton and Leicester [1] who deployed a sensor network to monitor the behaviour of glaciers in Norway.

The wireless nodes were deployed and located in the glaciers to measure the water pressure and movement over the winter period. This is a clear example of an environmental monitoring situation that would be almost impossible to achieve through human observation.

Although overall a successful deployment, there were a few technical problems, and in order to rectify them it had resulted in an expensive maintenance visit. The project concluded on the lesson that to never assume that the predicted or simulated behaviour of the sensor network will match the actual behaviour once the network is actually deployed.

Researchers from Switzerland [27], part of the SensorScope project have put together a comprehensive guide to the common problems faced with deployment of a wireless sensor network. This is split into hardware and software development, testing and deployment preparation, and then the actual deployment.

The success of a deployed network is down to careful design decisions and matching communication protocols and algorithms with the intended target application.

3.2 NETWORK TOPOLOGY & ROUTING ALGORITHMS

Network topology algorithms and strategies, like those suggested by *P. M. Wightman and M. A. Labrador* [28], suggest ways to improve the lifetime of the network, or perform maintenance on the topology when it no longer becomes optimal during operation.

A topic closely related to the network topology is how the data is routed through the network to the gateway or data sink. There are a number of challenges associated with data routing in a wireless sensor network.

The energy spent performing computation and transmitting data means that there is a balance to be found between energy consumption and the potential cost of losing nodes from the network. Losing nodes from the network could potentially result in losing data accuracy.

Should a node be lost from the network due to a failure or lack of power, as illustrated in Figure 3.1, the network needs to be able to re-route the data so that the overall operation is not affected. This can result in problems such as data bottle necking near the access point. This is just one of the problems that could be faced if energy consumption is not managed correctly.

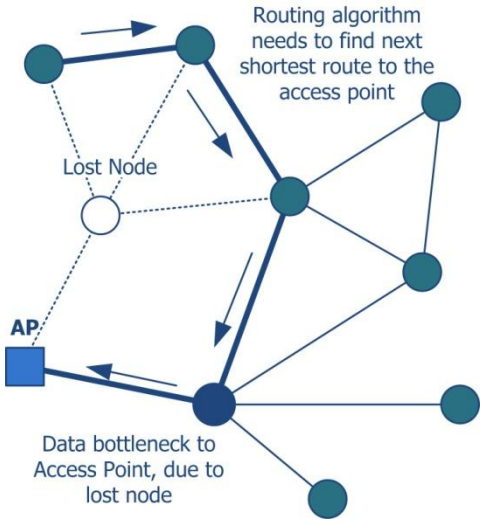

Figure 3.1 - Example of network routing and the loss of a network node

A detailed survey of routing techniques has been carried out by *Al-Karaki et al.* [29], summarizing and grouping or categorizing them based on the network structure.

The different network structures include flat or hierarchical and can be applied to any of the topologies discussed in Section 2.2.2. In a flat network structure all the nodes are treated the same; they all have the same responsibilities for routing traffic, where as in a hierarchical structure the network is split into clusters of nodes that then report to a cluster head.

Using a flat network structure means that it is possible to find the optimal route to the access point but can add complexity to the routing algorithm. Data traffic patterns have a huge effect on the energy consumption, and using the a flat structure does mean that the nodes close to the access point may need to route increased amounts of traffic.

In a hierarchical structure the network is split into clusters of nodes that then report to a cluster head. This approach [30] means that responsibilities can be removed from the sensor nodes to reduce energy consumption, and allows the cluster heads to perform data aggregation and remove possible redundant data. This avoids the problem of data traffic bottle necking near the gateway or access point of the network.

Although routing algorithms and network topologies can improve energy efficiency, there are areas much closer to the control of the wireless transmission such as the MAC layer of the communications stack, as previously introduced in Section 2.2.1.

3.3 MAC Protocol

Since the MAC layer has direct control over the RF transceiver it is a suitable point in the communications stack to implement energy saving techniques. The primary role of the MAC layer is to manage and decide when competing nodes can access the shared medium, in an attempt to prevent interference between nodes.

The majority of energy consumption in a sensor node is through transmission and receiving. In the 2.4 GHz frequency band there is very little difference in energy consumption between transmit and receive states.

If a traditional MAC protocol was applied to a wireless sensor network then there would be key areas of wasted energy, as discussed by *Wei Ye et al.* [24]:

Collision – This is when transmitted packets have to be discarded due to corruption from collisions. This causes for additional energy to be consumed re-transmitting the corrupted packets of data.

Overhearing – When a node picks up and receives packets that were meant for other nodes, this can depend on the application and protocol used.

Idle listening – This is similar to over hearing but instead the node is in receive mode but no packets are being transmitted and instead the device idly listens, consuming energy in the process.

A good example of excessive energy consumption from overhearing was exhibited in the network deployment from the LOFAR-agro group [12]. In this application the lifetime of the wireless network was well below estimations, and it was concluded that overhearing was one of the reasons for the reduced performance.

There are a number of variations in the MAC layer and the research by *Langendoen et al.* [31] presents a good comparison between the more popular protocols. The following is a brief summary of some MAC protocols that have been applied in a practical deployment:

3.3.1 Low Power Listening

To increase energy efficiency the low power listening scheme suggested by *J. L. Hill et al.* [32], reduces the time spent by the wireless node in idle listening. This is achieved by extending the pre-amble period of the data frame, increasing the transmission time.

Pre-amble is used at the beginning of a data packet in order for receiving devices to recognize data is being transmitted and so that the radios can become synchronized with the sending device.

In order to recognize the pre-amble the receiving nodes must periodically wake up and sample the channel as shown below in Figure 3.2.

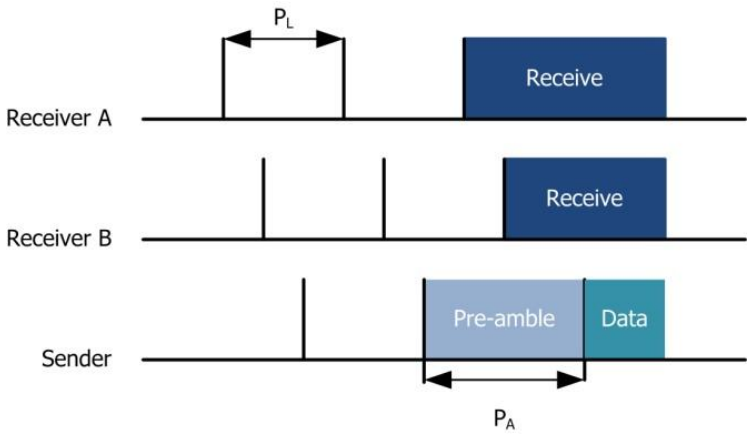

Figure 3.2 - Low power listening sequence

Providing the pre-amble period P_A is greater than the periodic listening P_L then all listening nodes in range will be able to detect the preamble transmission and leave their radios on until the end of the meaningful data has been transmitted.

Despite the simple nature of this scheme it cannot be applied to IEEE 802.15.4 compatible RF transceivers due to the maximum programmable length of the pre-amble not being long enough. Research by *Moon et al.* [33] however presents an alternative scheme VPCC (Virtual Preamble Cross Checking) that can be used by IEEE 802.15.4 compatible RF transceivers.

The protocol is however implemented in the Duck Island deployment [3]. Although a successful deployment the conclusions indicated that lost data packets could be reduced significantly through some form of synchronization between the nodes. In this scheme the nodes could spend a lot of time overhearing data not meant for them.

3.3.2 S-MAC (Sensor MAC)

The S-MAC [24] protocol is based on the principle of synchronization between local nodes. Activity is split into time slots, and at the beginning of each slot there is a period of synchronization packets, as shown in Figure 3.3. The synchronization packets allow for clock synchronization and each node acquires an allotted period for transmission during the active period.

Figure 3.3 - Time slots implemented in the S-MAC protocol

The active period is a fixed period of between 500 ms to 1 second and allows for full RTS (Request to send) and CTS (Clear to send) handshaking to avoid collisions. The disadvantage, as discussed by *K. Langendoen and G. Halkes* [31], is that the duty cycle must be decided upon before network start up.

There may be a case where the duty cycle would want to be changed to adapt to network traffic. Another problem is the amount of energy wasted through overhearing due to the nodes keeping their receivers powered for the duration of the active period. This is something that the T-MAC protocol [34] aims to prevent.

3.3.3 T-MAC (Timeout MAC)

The T-MAC [34] protocol aims to improve upon the S-MAC by introducing an adaptive duty cycle to each node. This is achieved by introducing a timeout on the active period. Should no activity be seen by any node for the pre-programmed timeout then the node will go to sleep. This method reduces the amount of time that the node remains active.

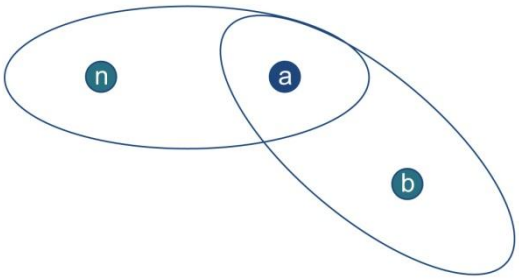

Figure 3.4 – Example situation that exhibits the flaw of early sleeping

This protocol does have a design flaw as it is possible for nodes to timeout and go to sleep too early. The problem is illustrated in Figure 3.4, where there are two nodes 'b' and 'n' that are in range of the node 'a', but nodes 'b' and 'n' are out of range of one another.

If node 'a' wanted to send to node 'b' but loses out to node 'n' for contention of the shared medium, it means that node 'b' will see no activity and will timeout and go to sleep. When node 'a' gains contention of the medium, it can no longer send to 'b' because the node is asleep.

No solution to this problem has been published but providing that energy saving has a bigger priority over network performance then the protocol remains appropriate for some applications.

The protocol itself was implemented by researchers at Delft University in the Netherlands in the LOFAR-agro project [12]. In this deployment they configured the T-MAC to run with a period of 6.1 seconds between 'sync' periods, resulting in an 11 % duty cycle.

In three weeks of operation only 2% of all packets were received which clearly highlights that network performance has been compromised for energy efficiency. Although in this deployment the nodes were found to still be consuming more energy than expected.

3.4 BATTERY ANALYSIS

The benefit of wireless sensor operation is the independence from wired installation, but the nodes must instead operate on a finite energy source. A critical design requirement in any application is ensuring the network will meet with the required lifetime, i.e. the service life of the batteries will match the required network operation time. The lifetime could range from a few weeks to being left unattended for numerous years.

Existing research approaches the area of batteries in two different ways, calculating the batteries state of charge during operation, or simulating the service life of the battery based on the energy requirements of the hardware.

This research project is looking specifically at the use of alkaline batteries in long duty cycle wireless sensor nodes. In many related pieces of research the focus has been on using simulations to clarify the work.

The work by *da Cunha et al.* [26] is the only example found of existing published research that combines the topics of wireless sensor networks and alkaline batteries. The focus is somewhat different, with the paper proposing techniques and calculations to give wireless sensor nodes the ability of measuring the remaining capacity of alkaline batteries.

The experimental work carried out [26] resulted in alkaline batteries being pulse discharged between 18 to 25 mA, and lasting no more than 6 days. This experimental work aims at verifying the suggested methods of measuring the remaining capacity and does not reflect the behaviour of a wireless sensor node, nor does it take into consideration any effect from temperature.

There are numerous methods of calculating remaining capacity or modelling the expected lifetime of a battery, however they are generally applied to Lithium battery technology. The question is what simulations or models exist and how do they apply to alkaline batteries?

3.4.1 Simulating Battery Behaviour & Lifetime Estimation

In the design of a battery operated system it is important for the designer to understand the behaviour of the battery. Through modelling and simulation the designer can gain an understanding of how to take advantage of behaviour such as the charge recovery effect.

Modelling of batteries varies from simple linear models, to complex models that try replicating the electrochemical process that takes place. The two main outcomes from using the battery models is either to simulate the expected lifetime of a battery, or to produce a method or algorithm for calculating the battery state of charge during operation.

Researchers have developed numerous different models to simulate battery behaviour, and *Ravishankar Rao et al.* [17] present a clear summary of these models by splitting them into different categories:

- Physical – detailed description of physical processes taking place in the battery.
- Empirical – parameters are fitted based on experimental data.
- Abstract – present the batteries as equivalent circuits, or discrete-time equivalents.
- Mixed – a mixture of physical and empirical methods to provide a simplified model.

The more complex models can require a large number of input parameters, sometimes in excess of 30-50 parameters [17]. The advantage is that they take into account the phenomenon of the 'relaxation effect', also known as charge recovery. The models can be evaluated based on their accuracy, computational complexity, and the ability to simulate behaviour such as time varying loads.

One model that takes into account varying loads and the relaxation effect is that suggested by Rakhmatov et al. [35]. The model is configured using the parameters α and β, where α is the original capacity of the battery, and β is the rate of non-linear recovery during discharge.

$$\alpha = \sum_{k=1}^{n} 2I_{k-1}A(L, t_k, t_{k-1}, \beta) \qquad (1)$$

The model shown in (1) represents the impact of the discharge profile on the battery service life. Where I_{k-1} is the discharge current for the period $k-1$, and function A computes the impact on the batteries non linear behaviour. Function A uses four parameters, where L is the battery service life, t_k is the duration of period k, t_{k-1} is the duration for $k-1$ and β as previously described. More details on function A can be obtained from the original research paper [35].

The advantage of this model is that it takes into account the relaxation effect and also allows for a variable load. The drawbacks are that it is required that the discharge profile is known completely in advance, and the model focuses only on the simulation of lithium batteries.

The model itself is verified by comparing against the Dualfoil [36] simulator which is a FORTRAN program for the simulation of electrochemical systems. This simulation program uses in excess of 75 parameters and models the chemical behaviour of lithium ion cells using partial differential equations. No model is available for the alkaline-manganese chemistry.

The Rakhmatov model has also been adapted by *Handy and Timmermann* [37] for calculating a runtime estimation of battery service life. The algorithm presented removes the requirement of knowing in advance the discharge profile. It instead uses continuous sampling of the discharge current to calculate the runtime estimation. This adaption to the model is also verified against the Dualfoil simulator.

The question is whether the model can be used for alkaline batteries. The parameters α and β provided for lithium batteries are estimated based on simulations using Dualfoil, making it difficult to estimate the β value for alkaline batteries. The Rakhmatov model is however applied by *Spohn et al.* [38] using parameters estimated for alkaline batteries. However this is the only evidence of parameters for alkaline batteries and it is difficult to assess the credibility of the values of α and β. In section 7.1.2 the parameters given by *Spohn et al.* [38] will be used to compare the Rakhmatov model to the experimental results.

The problem with the available battery models is that there is a lack of real world scenarios. None of the suggested models [17] have been compared to experimental results.

There could be several reasons for the lack of comparison. Batteries are very difficult to simulate due to the nature of the electrochemical process that takes place, and it is also very expensive in terms of time to record battery behaviour instead of modelling.

One of the aims of this research project is to look at battery behaviour experimentally and attempt to compare to the expected results found in various research papers [38] [39].

3.4.2 Estimating Remaining Capacity

An alternative use of battery modelling is to estimate the remaining capacity of the batteries at run time. In some applications of wireless sensor networks it may be a requirement to have the current state of charge for each node reported back for analysis.

Research by *da Cunha et al.* [26] explores the possible methods of calculating state of charge for alkaline batteries used in a wireless sensor node. It is suggested that one of three measurements are required to determine the state of charge; impedance measurement, cell voltage, or discharge current

The state of charge estimation through impedance measurement implies calculating the complex impedance of the cells; this would be impractical in terms of hardware complexity and cost, for a wireless sensor node. The alternative two are more feasible.

Estimation of state of charge through measuring the cell voltage has the advantage of requiring few additional parts; however it does present some inaccuracies. It is true that as the cell voltage decreases so does the cell remaining capacity [20], but if the cell voltage was used to estimate the state of charge then the value would vary depending on the temperature [40].

Estimation through measuring the discharge current is deemed to offer better accuracy [26], but this is a trade-off between the additional components required and ensuring that the technique used to measure the current does not uses excessive amounts of energy to perform the measurement.

The work by *da Cunha et al.* [26] uses the MICA2 node hardware with additional hardware to measure the current drawn during operation. In the practical measurements the MICA2 nodes were configured to continuously switch between 18-25 mA, to result in a shortened experimental duration.

The voltage and current were measured using both the MICA2 ADCs and an external powered data acquisition unit. The results compare the final measured capacities, from which the models both under and over estimated the point at which the node ceased to operate.

Although this research presents a good case for current based estimation techniques, the experiments do not take into account the effects of the node sleeping for extended periods, i.e. long duty cycle.

It is questionable as to how the capacity estimation models would perform over an extended lifetime for example node running for more than a year, given the inaccuracies when discharging for only 6 days.

3.5 Performance Analysis Conclusions

The aim of this research is to focus on the performance of alkaline batteries in wireless sensor networks that operate with long duty cycles. In the few deployment examples [12][4] where alkaline batteries have been deployed, the service life has lasted no more than 2 months.

This is far from the expected lifetime of years that is thought possible. It is however important to note that the lifetime is always dependant on the application of the sensor network. It is difficult to compare a network that exists in a difficult and changing environment [12] to one that is located in a more stable environment such as a building [4].

One thing that is noticeable about all the deployments is that there is very little attention paid to the power management of the nodes, instead the focus is very much on the communications protocol. In order to prolong node lifetimes there has to be a good balance between them both.

Based on the research areas covered there is certainly a gap when it comes to alkaline batteries. No battery models are available for alkaline batteries and without experimental results or a physical model it would be difficult to confirm if the existing models applied to lithium batteries can be applied to alkaline batteries as well.

Chapter 4.

Experimental Framework

The motivation behind the experimental framework is to closely monitor and record the behaviour of the battery voltage during the discharge cycle. This must be achieved through performing controlled battery discharges with measurement or control of environmental conditions.

The experiments are built around being able to simulate and compare to the expected behaviour of a wireless sensor node, whilst ensuring that the time to completion of the experiment remains manageable and within the timeframe of the research project.

The behaviour of most interest from a wireless sensor node is from the repeated change between inactive and active states. This behaviour is referred to as a pulsed discharge.

The environmental conditions during the experiments have been controlled with one of two approaches. Either performing experiments at a changing or stable ambient temperature, or performing experiments with the batteries held at a controlled and stable temperature.

This chapter summarizes the measurement system and aluminium temperature controlled enclosure that have been designed and built specifically for this research project.

The experimental framework focuses on the key variables; discharge current, temperature, discharge profile, and cell to cell variation. It is expected that all of these variables will have a noticeable effect on the battery service life and inevitably the performance of a wireless sensor node.

The batteries were bought new in boxes of 10 cells and in batches of 5 or more boxes. When in a new and unused state the initial state of charge is an unknown variable and influences the cell to cell variation and the theoretical maximum capacity.

4.1 EXPERIMENTAL TERMINOLOGY AND ASSUMPTIONS

Before considering the experimental framework, a set of notations will be defined and explained in relation to performing the controlled discharges.

Battery – The term battery refers to the combination of one or more cells in a series or parallel configuration. This experimental framework will refer to a battery as two Alkaline Manganese cells in series, characterized by three voltage values:

V_{OC} - Open circuit voltage, i.e. the initial cell voltage

V_L - The operating voltage when under load

V_{Cut} - The cut-off voltage which the point at which the battery is considered discharged or the point at which the connected hardware can no longer function reliably. The value of 1.6 V has been selected for this based on the datasheet [20].

Only one brand of cell will be used for the experiments, the Duracell Procell, which is also known as the Duracell Coppertop and differentiated only by packaging and purchasable quantities. The cell datasheet can be found in Appendix A. If more brands were to be used it would be difficult to know if the behaviour differences were down to the differing chemistries or constructions.

Battery Relaxation – This is a behaviour exhibited in the cell voltage when the load is significantly reduced [39]. The cell chemistry is able to recover from a high rate of discharge, as discussed in Section 2.1.3. This results in the cell voltage recovering to a higher voltage.

Discharge profile – This term is used to describe how the battery is discharged and all of the test variables that are defined to perform a particular battery discharge.

Constant Current Discharge – This is a discharge that consists of a single magnitude of current.

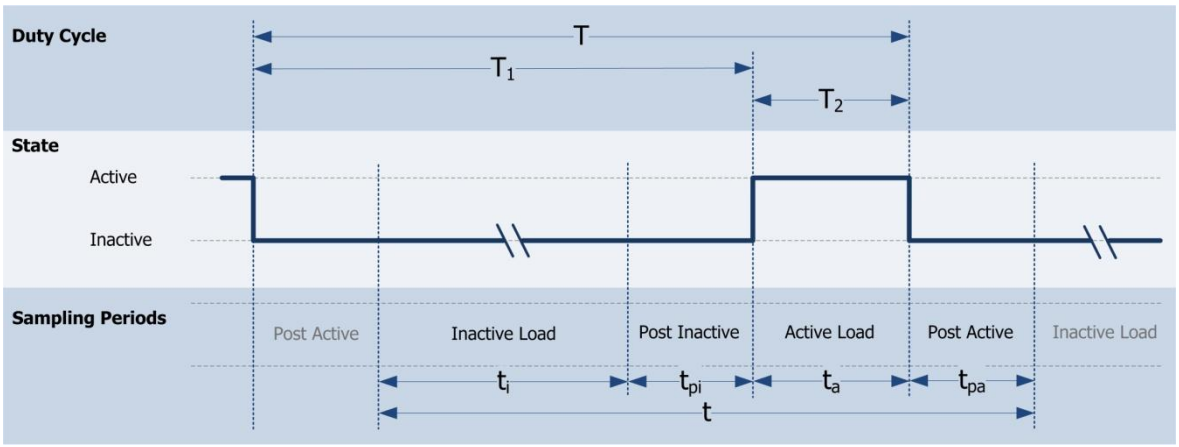

Figure 4.1 - Discharge duty cycle

Pulsed Discharge – This is the discharge of a battery using a pulse train of different magnitudes of discharge current. By varying the periods of the pulse train it is possible to achieve more efficient discharge of the batteries [19].

- **Duty cycle** – This is the period T that encompasses a period of inactivity T_1, and an active period T_2, as displayed in Figure **4**.1.
- **Active and Inactive State** – The pulse train is constructed using two alternating states, an active period when the discharge current is largest, and an inactive period when the discharge current is lowest, see Figure **4**.1.
- **Sampling Periods** – These are periods during the duty cycle that the measurement system can be setup for different sampling frequencies.
- **Duty Ratio** – This is the ratio between the two periods T_1 and T_2 where $R_C = \frac{T_2}{T_1}$
- **Control Frequency** – This is the rate at which the duty cycle is repeated where $f_C = \frac{1}{T}$

Assumptions are made by the measurement system based on the behaviour of a battery under an 'inactive' and 'active' load, in order to simplify the setup.

- It is assumed that the 'Inactive' Load will be of a lower value than that of the 'Active' load.
- It is assumed that the period of time in the 'Inactive' state will be greater than the 'Active' state.
- Based on the expected battery behaviour [39] the point of interest is in the region of switching between the two different loads.

The measurement system allows for a variable sampling frequency between the different periods. Given the expected behaviour of the cell voltage, it is possible to decrease the sampling frequency during the 'Inactive Load' period t_i of the discharge cycle.

Likewise during the 'Active Load' period t_a, the 'Post Inactive' period t_{pi} and the 'Post Active' period t_{pa}, the sampling frequency can be increased in order to capture the changing cell voltage due to a changing load.

4.2 PRELIMINARY EXPERIMENT

The challenge faced when discharging batteries at very low discharge currents is the length of time to completion for the experiment. Potentially, a battery being discharged at an average of 100 µA could last for up to 3 years based on an estimated capacity of 2800 mAh [41]. However there is no data from the manufacturer's battery datasheet (see Appendix A) or existing research, that gives details below a discharge rate of 5 mA.

With a period of just under 2 years for the completion of this research it would be impossible to achieve the discharge of a battery at for example 100 µA, whilst all variables being measured and recorded using the proposed measurement system.

The aim of the preliminary experiment was to begin the discharge of several batteries under a constant current load that can be related to the average load that a wireless sensor node might be discharged at. The cell voltages can then be manually recorded and used for later analysis.

Discharging the cells at 100 µA was based on the early research and the following estimated values and ratios for a single duty cycle:

Sleep Current – 1 µA for 6 hours

Active Current – 20 mA for 2 minutes

$$I_{Mean} = \frac{(I_{Sleep} \times t_{Sleep}) + (I_{Active} \times t_{Active})}{t_{Sleep} + t_{Active}} \quad (2)$$

$$I_{Mean} = 112\ \mu A\ \approx 100\ \mu A$$

Rounding down to the nearest decade will make it easier for future analysis and comparison. To achieve the constant discharge current of 100 µA, the JFET Constant Current Module circuit as later described in Section 4.4.3 has been duplicated and connected to four pairs of alkaline cells.

With no measurements being stored for this experiment, the intention instead is to use the cell voltage at any chosen time as an indication as to how far the batteries have discharged.

With the length of time some experiments may take, it is expected that the measurements taken in this research project will not be able to be repeated enough to achieve statistically significant results.

4.3 MEASUREMENT SYSTEM

The measurement system has been designed specifically for the task of performing controlled battery discharges, sampling battery voltage and recording the time to perform the discharge.

A system level diagram can be found in Figure 4.2, which shows how the system is distinctly broken down into the measurement core, and attached modules for each battery module. A battery module refers to the pair of cells under test and the attached loads and measurement module.

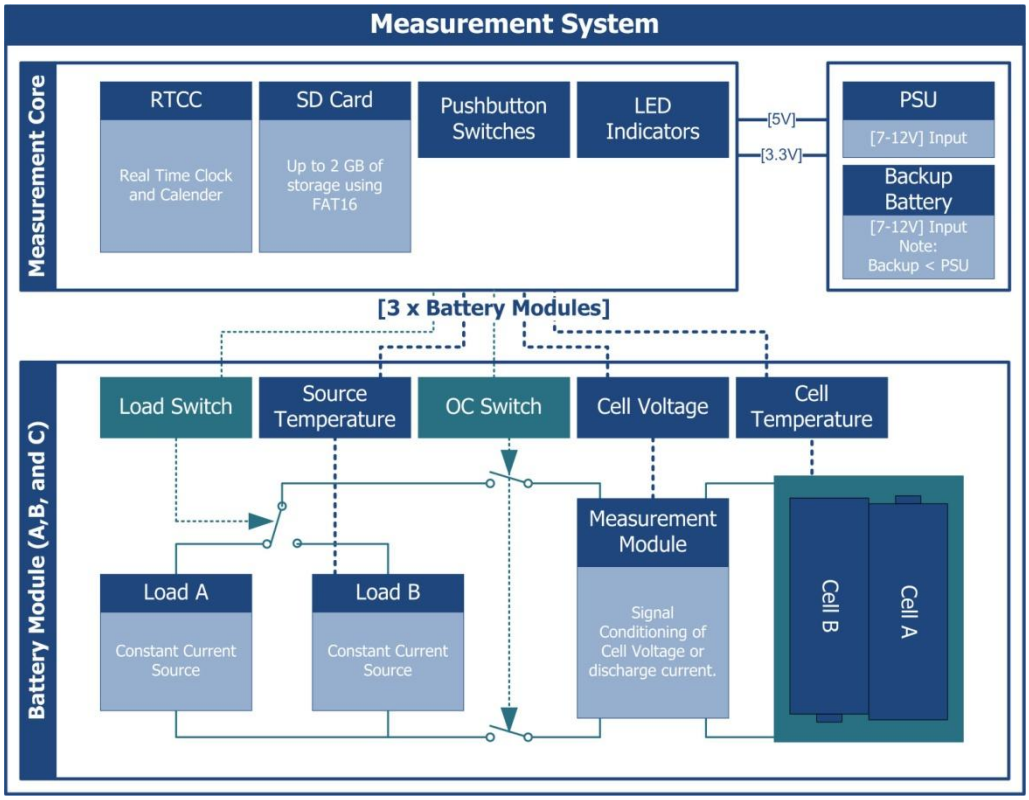

Figure 4.2 - Measurements system, system level diagram

The system can accommodate for 3 pairs of cells to be discharge at any one time, as visible in Figure 4.3, all with identical discharge profiles. Each pair of cells is connected to a measurement module that allows either the cell voltage or discharge current to be sampled by the measurement core.

Each pair of cells can be switched between two different loads and also put into an open circuit condition. The loads themselves are contained on changeable modules. This allows for different types of load such as a resistive load or constant current sink/source.

Further features of the system are summarised below:

- Measurements are logged and stored on a standard removable SD Card.
- Each battery module has a set number of measurement channels, cell voltage, source temperature and cell temperature.
- A Real Time Clock and 32 kHz watch crystal is used for time keeping
- Temperature measurements can be taken in a combination of four separate locations
    - On the connected load.
    - At the voltage reference IC
    - The cells under load
    - Ambient

The system diagram and overview provides a glimpse at the system design, for the full design including schematics and further photographs; please see Appendix B. All design files can be found on the attached DVD with the contents listed in Appendix H.

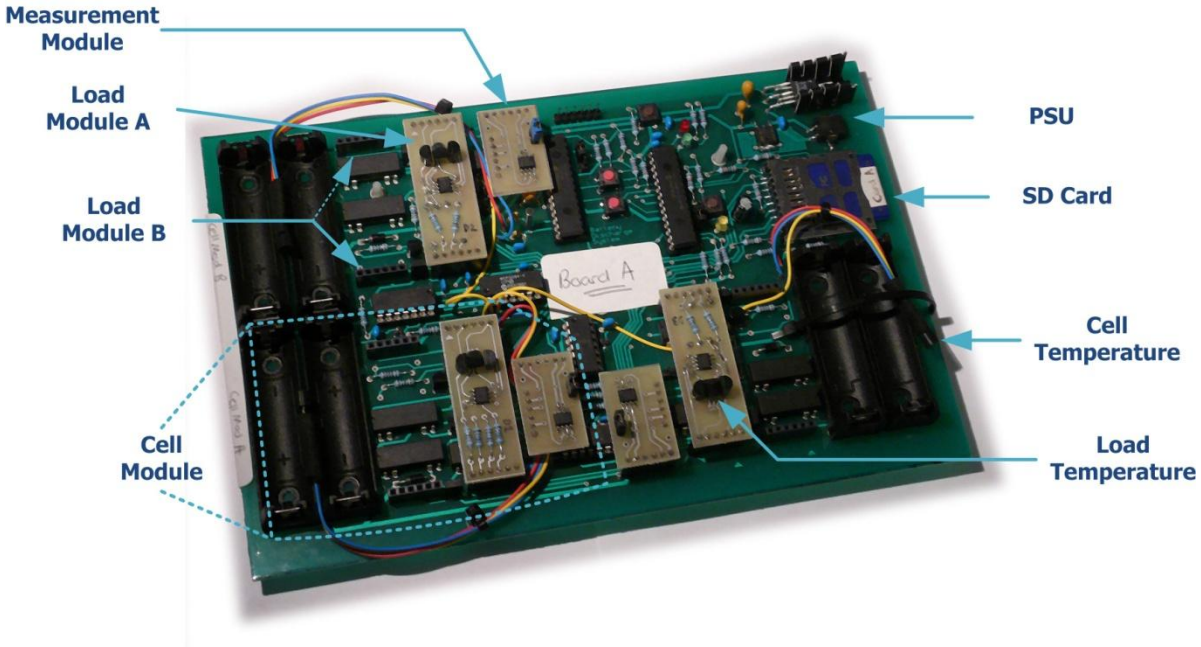

Figure 4.3 - System level overview showing the key features of the measurement system

4.4 MEASUREMENT HARDWARE

In the system level diagram the measurement system is split into distinct sections. The following aims to summarise in more detail the specification of those sections and the configurability of the system.

The system configuration comes from choice of modules, so for example the connected load could be a constant current, a resistive load, or there is even the possibility of connecting a wireless sensor node.

4.4.1 Measurement Core

The measurement core comprises of a microcontroller and supporting devices that are all connected to the same SPI (Serial Peripheral Interface) communication bus. The measurement system can be summarised by its inputs and outputs.

Inputs

A total of 9 ADC channels:

- 3 x [10bit][1.25V - 3.3V] Measurement Module Channels (Cell voltage)
- 3 x [10bit][1.25V - 3.3V] Load Temperatures
- 1 x [10bit][1.25V to 3.3V] Voltage Reference Temperature
- 4 x [12bit][0V - 1.25V or 3.3V] Auxiliary Channels

The measurement module channels are directly from the measurement modules and could be either the measurement of cell voltage, or the discharge current. There is also the availability of four auxiliary channels that in the majority of experiments have been used for temperature measurements of the cells or ambient.

Outputs

Each battery is controlled by a combination of two relays as illustrated in Figure 4.2. One relay for disconnecting the cells and putting them into open circuit, the second for switching between the two possible loads connected to the battery on test.

There are also two 12 bit DAC outputs per pair of cells to be used by the load modules if required, for example they can be used to control two voltage controlled current sources as detailed in Section 4.4.3.

Visually there are 3 LEDs on board for various indications to the end user. These LEDs highlight events such as end of test, sampling event, and activity on the SD card.

4.4.2 Measurement Module

The two measurements of interest from the cells under discharge are the cell voltage (open-circuit or closed circuit) and the discharge current. A physically separate measurement module means that any form of signal conditioning can be present before the ADC channel of the system core. For example to measure the discharge current a measurement module could simply use a shunt resistor for the current to voltage conversion.

The measurement module being used for this research uses a high impedance unity gain amplifier as illustrated in Figure 4.4. This ensures that any leakage currents can be accounted as negligible since they will be magnitudes smaller than the resolution of the ADC input.

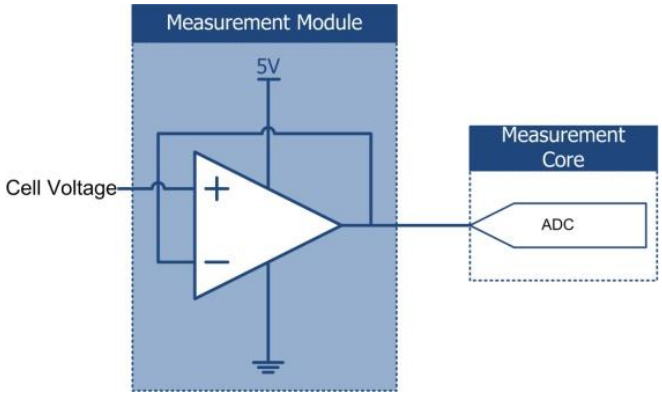

Figure 4.4 - Unity gain amplifier configuration

4.4.3 Constant Current Load Modules

The experiments carried out required discharge currents in decades ranging from 100 µA up to 100 mA. In order to achieve this, several different methods were used, each contained on different modules.

All modules had the common purpose of providing a constant current source/sink so that the discharge current can be accounted for as a controlled variable in all the tests and did not need to be measured only calibrated on setup.

JFET Constant Current Module

To achieve constant current sources in the region of 100 nA to 100 µA, the suggested configuration found in the Application Note published by Vishay [42] was used.

The circuit consists of a JFET and a variable resistor selected to bias the FET in the correct region. Through selection of the correct JFET device and resistors, the following constant current sources are achievable; 1 µA, 10 µA, 100 µA, and 1 mA.

Voltage controlled Constant Current Module

To achieve a constant current in the region of 1 mA and 100 mA a different constant current source was required. The circuit shown in Figure 4.5 uses a voltage follower to control the base voltage of the BJT transistor. The control voltage is configured so that the transistor is operated at an equivalent resistance in order to achieve the desired constant current through the load resistor.

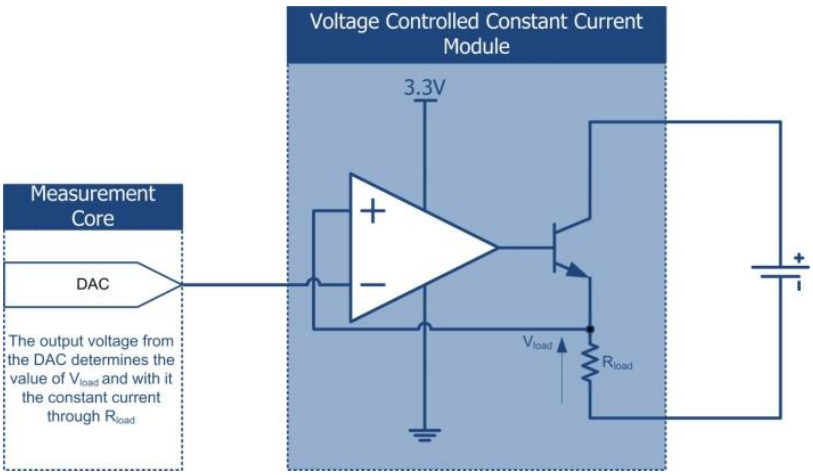

Figure 4.5 - Voltage controlled constant current module

The control voltage is provided from a DAC output from the measurement core. By having this control over the load it means that the measurement system could be configured to accurately mimic the discharge current profile of wireless sensor node, for example a change in load current between transmit and receive states.

4.4.4 Measurement Accuracy and Precision

The following briefly describes the measurement systems accuracy and precision, including the current sources, and analogue to digital conversion.

Since the discharge current is not measured by the system, the constant current source needs to be precise. All of the constant current sources were configured using a 6.5 digit digital multimeter and tested to provide ± 2% accuracy.

Given that the current sources will always operate at room temperature, change in the constant current due to the temperature coefficient of the load resistors was deemed negligible.

Temperature was measured using linear thermistor ICs, with a range of 0 °C and 70 °C and an accuracy of ± 2 °C. The advantage of the linear IC is that the device provided a voltage level output 10 mV/°C and required no lookup table or interpolation algorithms.

The ADC channels used for measuring the cell voltage and temperature channels use precision voltage reference ICs for the positive and negative reference, with a maximum error in accuracy of 0.2 %. With an input reference range of 1.25 V to 3.3 V the 10 bit ADC channels have a resolution of 2 mV.

For more details on the system accuracy and precision, see Appendix B.3.

4.5 MEASUREMENT SYSTEM SOFTWARE

The software required for the measurement system is split into two different parts, there is the embedded C code that operates the measurements system hardware, and then there is the windows application that deals with the post processing of the data taken from the SD card.

4.5.1 System configuration

The measurement system runs on embedded code written in C. Each experiment is configured through a set of definitions within the firmware of the measurement system. The full set of definitions can be found in Appendix C.

The definitions configure the different sampling periods described in Section 4.1, along with the type of loads connected, and the end of test point. Along with the definitions in Appendix C there is a full description of the data frame that is appended to the binary files contained on the SD card.

4.5.2 Data Processing

At the end of the test the SD card can be removed and connected to a PC running Microsoft Windows OS. The data is stored on the SD card within Binary files, with each file containing measurements for a 24 hour period during the length of the test.

All measurements are stored in their raw format, for example the ADC measurements are stored as their 10/12 bit value within 2 Bytes of the data frame. Each data frame is constructed of 32 Bytes which includes the 10 ADC channels, seconds, minutes, and hours at the time of measurement, the test state, and details on the sampling count for the current sampling period.

The data contained within the Binary files needs to be converted and conditioned into meaningful data. This is achieved through the Windows application written specifically for the measurement system in C#. The application output is in the standard '.CSV' format which allows import into other software packages for analysis.

The challenge with using the '.CSV' is that each data frame recorded by the measurement system equates to one line of the '.CSV' file. Given that the shortest full discharge test of roughly 12 days equates to a '.CSV' file of around 210,000 lines, the number of data points needed to be reduced before the data can be analysed or imported into different software packages.

The raw data is sampled and the data points reduced, averaging over different periods of time or over a single duty cycle and preserving the points of interest such as the period when the connected load changes.

4.6 TEMPERATURE CONTROL

In order to provide a temperature controlled environment for the batteries under discharge, a basic framework was constructed to heat or cool using thermoelectric effect exhibited by a Peltier module.

The Peltier module transferred heat to or from a machined aluminium encasement for two MN1500 Alkaline cells. Economies of scale were an important factor in design, as ideally temperature control would be provided by an industrial environmental chamber but this equipment was not readily available.

4.6.1 The Thermoelectric Effect

A Peltier module, also referred to as a thermoelectric device, is a semiconductor based component that functions as a heat pump. By applying a DC voltage to the module, heat is pumped from one face of the device to the other.

The thermoelectric device can be used to either heat or cool, depending on the direction of the current. For a full explanation see the document [43] provided by the manufacturer Tellurex.

The aim is to achieve a stable temperature close to the extremes of the alkaline battery specification. The operating temperature for the batteries is between -20 °C and 54 °C. It would be challenging to achieve a temperature as low as -20 °C, so in order to show the effect temperature change has on the battery performance the aim has been to achieve the extreme temperatures of -5 °C and 45 °C.

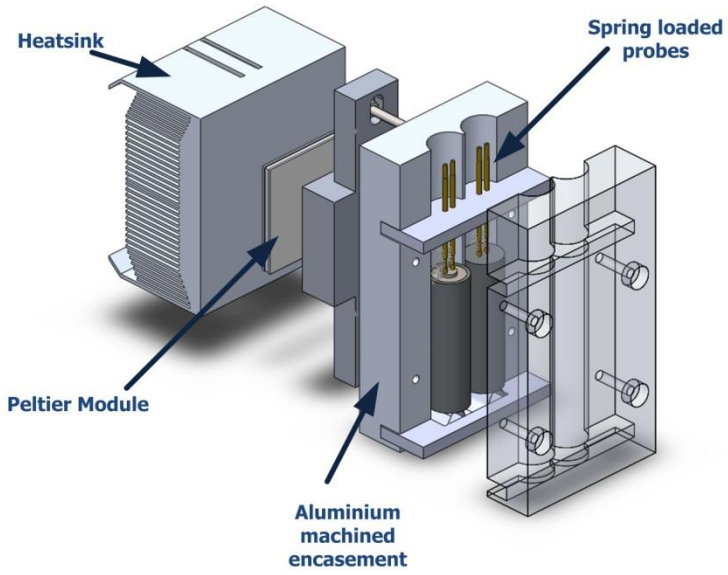

Figure 4.6 - 3D CAD model of temperature controlled encasement.

4.6.2 Mechanical Design

The mechanical design of the battery encasement, see Figure 4.6, was completed using the 3D CAD package Solidworks. It was important that the encasement clamped the cells so that it can be assumed that the cells operate at the same temperature as the aluminium casing.

There have been two iterations of the mechanical design. The original design performed well when heating the aluminium block but due to the arrangement between the Peltier module and the fan/heat sink assembly the design failed to achieve the low temperatures desired.

Using an assembly guide by Laird Technologies [44] a second iteration was manufactured. This provided the means to achieve a temperature as low as -15 °C, but without improved insulation, condensation became a real issue.

For full detail on the mechanical design and details on setup, see Appendix D.

4.7 CONCLUSIONS

The measurement system has been designed for multiple setup combinations to combat any changing ideas and hypothesis from the research. This includes different combinations of Loads connected to the batteries, different forms of signal conditioning before the ADC, and most importantly full control over how and when the batteries are under specific loads.

The constant current modules described in this chapter are the chosen method for applying loads to the batteries as they best resemble connection to a wireless communication device. It was decided that measuring the discharge current would not be required as the constant current sources/sinks were calibrated to within ±2 % accuracy.

The data collected by the measurement system can be easily transferred to a PC using the SD card and then can be converted by the windows application for further data analysis.

In conclusion the measurement system and temperature controlled encasement; provide an experimental framework capable of performing controlled discharges of the standard AA Alkaline-Manganese batteries.

Chapter 5.

Controlled Battery Discharge

The aim of this research has been to discover the behaviour of alkaline batteries under varying conditions and understand possible solutions for improving the performance when used in a wireless sensor node. The performance is quantified in the case of a wireless sensor node as the service life of the battery, i.e. the time before the node becomes inoperable.

The data and specification [45] of the batteries leave many questions unanswered, for example how is the service life affected from a changing load? Will the performance vary between cells? At what rate does the service life increase as the discharge current is reduced?

This chapter looks at the experimental results based on the framework discussed in Section 4.3. The analysis of the results is based on the achievable service life and the cell voltage behaviour under load, comparing and contrasting to related hypotheses. The results related to the environmental conditions will be considered in Chapter 6.

The results in this chapter and the subsequent chapter are not claiming statistical significance; instead highlight the behaviour of the batteries under discharge. Statistical significance would only be possible through significantly more discharge tests, but the time per discharge is one reason that has prevented this.

5.1 SERVICE LIFE

The definition of battery service life is the time taken for the battery to become discharged. In a practical sense the point at which the battery becomes discharged is the point in time that the battery powered system can no longer operate. It is assumed for the following experiments that the point at which the battery has become discharged is when the battery reaches the cut-off voltage of 1.6 Volts, or 0.8 V per cell. This in turn defines the end of battery service life.

The load applied to the cells under test is a constant current. Based on the typical constant current discharge characteristics curve in the battery datasheet (see Appendix A), no data from the manufacturer is available for discharge currents below 5 mA or at different temperatures. It is expected that based on the curve, the continuing trend will be that as the discharge current decreases, the service life will increase.

A total of ten full battery discharge experiments have been carried out and span a total of 358 days under varying conditions. All experiments have involved the discharge of three pairs of cells under the same conditions, referred to as batteries A, B, and C. Each experiment is identified by a test ID, and these ID's will be referred to throughout this and subsequent chapters.

The service life in hours of each individual pair of cells, from each experiment, is contained in Table 5.1. The 'Average' method of discharge refers to a pulsed discharge where the average discharge current is measured over a single duty cycle. Calculated from the service life and the average discharge current is the battery capacity measured in milliamp hours.

Test			DT001	DT002	DT003	DT004	DT005	DT006	DT007	DT016	DT017	DT020
Current			10mA	10mA	10mA	10mA	1mA	10mA	1mA	10mA	10mA	10mA
Environment			Lab	Lab	Lab	Stable(2)	Lab	Stable(2)	Stable(2)	Lab	Lab	Lab
Method			Constant	Average	Average	Average	Constant	Constant	Average	Average	Constant	Average
Load	High	Current	10mA	100mA	100mA	100mA	1mA	10mA	100mA	100mA	10mA	100mA
		Period	-	10 Min	1 Min	1 Min	-	-	1 Min	1 Min	-	10 Min
	Low	Current	-	1mA	1mA	1mA	-	-	100uA	1mA	-	1mA
		Period	-	100 Min	10 Min	10 Min	-	-	110 Min	10 Min	-	100 Min
Service Life	mAh	A	3170	2529	2728	2783	3428	3220	2856	2642	3159	2621
		B	3178	2676	2715	2783	3396	3234	2786	2666	NA(1)	2659
		C	3093	2694	2710	2770	3317	3288	2760	2659	NA(1)	2659
	Hours	A	317	252.9	272.8	278.3	3428.3	322	2856.3	264.2	315.9	262.1
		B	317.8	267.6	271.5	278.3	3396.5	323.4	2785.9	266.6	NA(1)	265.9
		C	309.3	269.4	271	277	3317	328.8	2760	265.9	NA(1)	265.9

Note: (1) Incorrect setup resulted in failed discharges
(2) Stable environment resulted in a smaller variation in temperature

Table 5.1 - Discharge Test Summary

The experiments can be split into three main groups for comparison based on the mean discharge current, the type of discharge, and the environment the experiment took place.

The hypothesis that the service life will increase as the discharge current is decreased, is proven correct when comparing the following similar experiments; DT001 with DT005 and DT004 with DT007. The service life in hour's increases but the experimental capacity remains almost identical between the tests compared.

In DT001 and DT005 the discharge method was a constant current discharge and the environment for both was in the lab. Comparing the service life in hours shows that through decreasing the discharge current by a factor of 10, the service life has increased by a factor of at least 10.

The same rings true when comparing DT004 with DT007 both have been discharged by applying a pulsed current discharge, and both were located in the stable environment. A reduction in discharge current by a factor of ten has resulted in an increase in service life by a factor of 10.

As previously mentioned the discharge characteristic curve in the battery datasheet [45], does not extend below 5 mA. Ideally to confirm that the curve remains linear below 1 mA it would require further discharges at 100 µA or 10 µA. Given the length of time to discharge at 100 µA could take over 3 years; it is not feasible to prove this hypothesis any further by completing a full discharge using the developed measurement system.

Despite this, early on in the research project an experiment was initiated with the setup described in Section 4.2, which involved four pairs of cells being discharged with a 100 µA constant current. The framework that was used meant that no measurements were being taken at regular intervals. The measurements that have been taken over an 18 month period are summarised in Table 5.2.

Date of measurement	Cell Voltage (Volts)			
	Battery A	Battery B	Battery C	Battery D
03/12/2009	3.222	3.217	3.224	3.22
12/02/2010	3.003	3.003	3.005	3.003
24/11/2010	2.801	2.803	2.8	2.801
27/05/2011	2.697	2.697	2.697	2.696

Table 5.2 - Preliminary Experiment

When comparing the value of the cell voltage measured on 27/05/2011 with the same corresponding cell voltage of the similar DT005 experiment, it can be estimated that the batteries have completed roughly 34 % of their discharge cycle.

On 27/05/2011 the batteries had been discharging for approximately 12960 hours, which means that theoretically the completion could equate to roughly 38880 hours or 4 years and 159 days.

Based on this estimation, there is reason to believe that the linear extrapolation of the datasheet discharge characteristic curve could still hold true, and a further reduction in discharge current by a factor of 10 is theoretically leading to a service life increased by a factor of 10.

5.2 PULSED DISCHARGE

There are two methods of discharge used in the experiments, constant current discharge and pulsed current discharge. Research suggests that battery service life can be prolonged by using a pulsed current discharge [19] [46]. This is due to the charge recovery process, as discussed in Section 2.1.3, that takes place at the electrode. The question is what are the visible signs of recovery during a pulsed discharge?

The measurement framework has the ability to switch between two constant current loads, creating a pulse train switching between an active and inactive load, as discussed in Section 4.1. Over a single duty cycle both loads are applied and the typical resulting cell voltage curve is shown in Figure 5.1. This graph also shows the 10 minute inactive load period T_1 and the active period T_2 which is 1 minute in length. In this example the inactive load is 1 mA and the active load 100 mA, which gives a mean discharge current of 10 mA over the duty cycle.

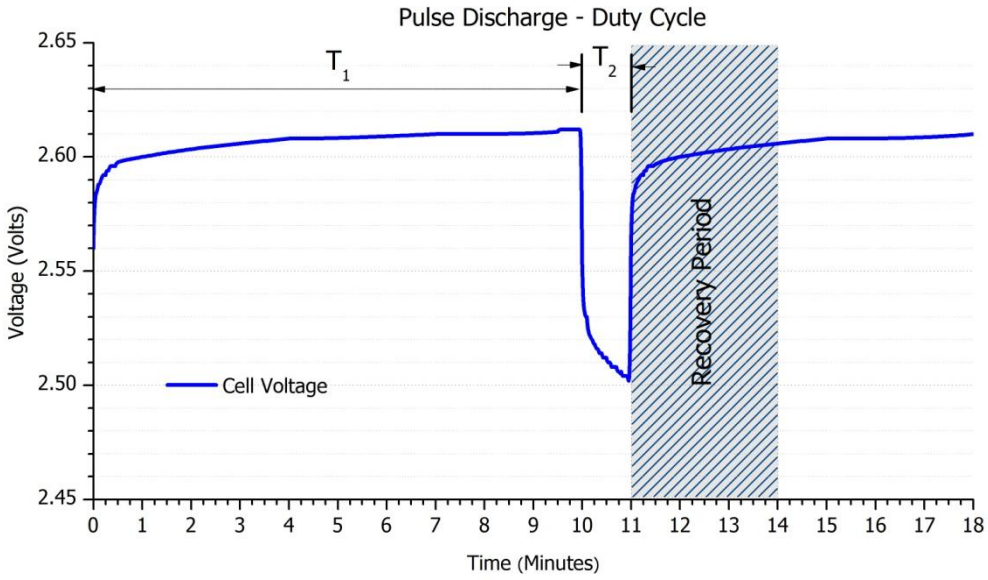

Figure 5.1 – Cell voltage during a single duty cycle, highlighting the recovery period.

When the active load is applied after T_1 the cell voltage drops dramatically, but when the active load is removed, the relaxation effect becomes evident and there is a period of recovery. There is no definition of when the recovery from the relaxation effect stops. By the end of the highlighted recovery period the cell voltage has recovered to 99.8 % of its value before the active load was applied and continues to increase after the highlighted period.

In the previous example there is a factor of 100 between the inactive and active discharge currents, what if this factor was increased to 1000 and the period T_1 increased to produce a 1 mA mean discharge current? It could be expected that for a lower average discharge current, the drop in cell voltage would be less.

To make this comparison the cell voltage data was taken from two experiments at an identical resting cell voltage of 2.612 V. The plots contained in Figure 5.2 show the cell voltage of (a) 10 mA and (b) 1 mA discharge current. The point of interest is the magnitude of the instant drop in cell voltage at the point the active load is applied.

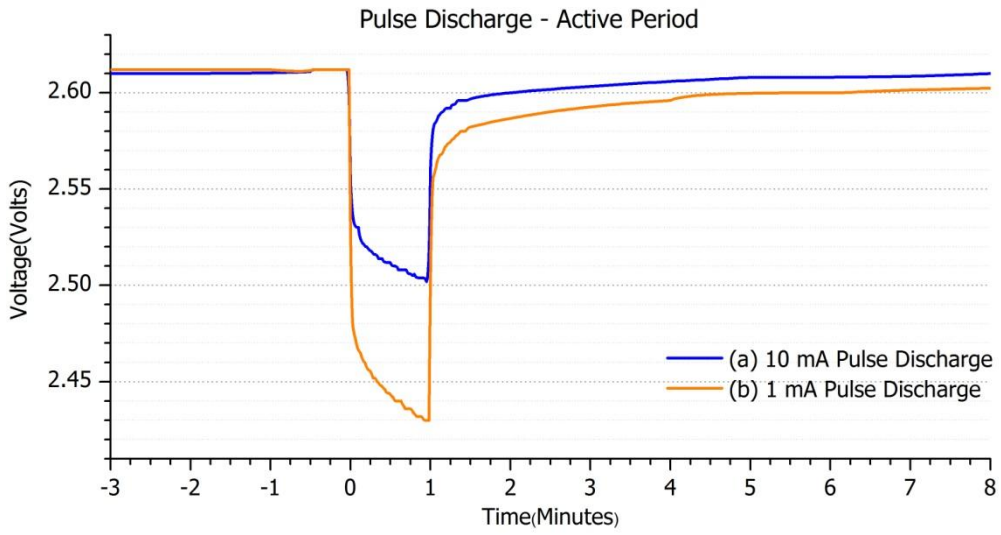

Figure 5.2 - Cell voltage behaviour during the active period at (a) 10 mA and (b) 1 mA

The pulsed discharge of 1mA shows an instant drop of 120 mV in comparison the 10 mA pulsed discharge where the instant drop is 70 mV. This goes against the expected result that a higher average current of the pulsed discharge would result in a larger instant drop.

The instant drop in cell voltage relates to the internal resistance of the cells defined by Equation (3). As the remaining cell capacity decreases the internal resistance increases.

$$InstantdropinCellVoltage = dV = I \times R_i \quad \textbf{(3)}$$

So on closer inspection the larger drop in cell voltage would suggest that the cells discharged at 1 mA average have been discharging for a longer period of time. This is true as the 1 mA pulsed discharge had been discharging for 75 days and 23 hours in comparison to the 10 mA pulsed discharge that had been discharging for 6 days and 12 hours.

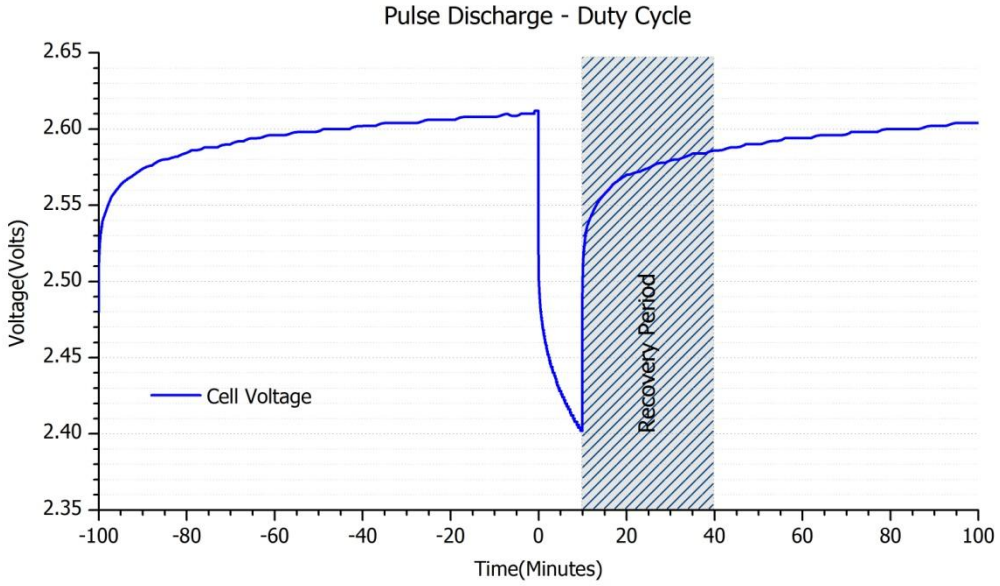

Figure 5.3 - Increased magnitude pulsed discharge to show the increased time for recovery

What if the active load period is increased whilst keeping the average at 10 mA? To achieve this T_1 is increased to 100 minutes and T_2 is increased to 10 minutes. The resulting duty cycle can be seen in Figure 5.3. The cell voltage curve shows that an increased active period has an effect on the time it takes for the cell voltage to recover.

The recovery period highlighted in Figure 5.3 is ten times greater than that shown in Figure 5.1, yet the cell voltage only recovered to 99 % of original capacity before the applied active load. The increased time with the active load applied has meant it is taking longer for the chemical recovery to take place.

It is possible to see visible signs of cell recovery but the real question is if the service life can be prolonged through applying a pulsed discharge.

5.3 Comparison of Pulsed and Constant Current Discharge

For experimental control purposes, every pulsed discharge is matched with a constant discharge based on the average discharge current over a single duty cycle, for example a 10 mA pulsed discharge is matched with a 10 mA constant current discharge.

The graph Figure 5.4 compares the cell voltage for both a pulsed discharge and a constant discharge of 10 mA, from tests DT004 and DT006 respectively. For the same comparison for batteries B and C, see Appendix E.

From the behaviour shown in Figure 5.1 we know that during a pulsed discharge the cell voltage moves between two levels depending on the load applied. To represent the pulsed discharge test DT004 graphically over the full length of the discharge, the cell voltage is split into the average for each duty cycle, the minimum, and maximum values recorded. This leads to three curves representing a single pulsed discharge.

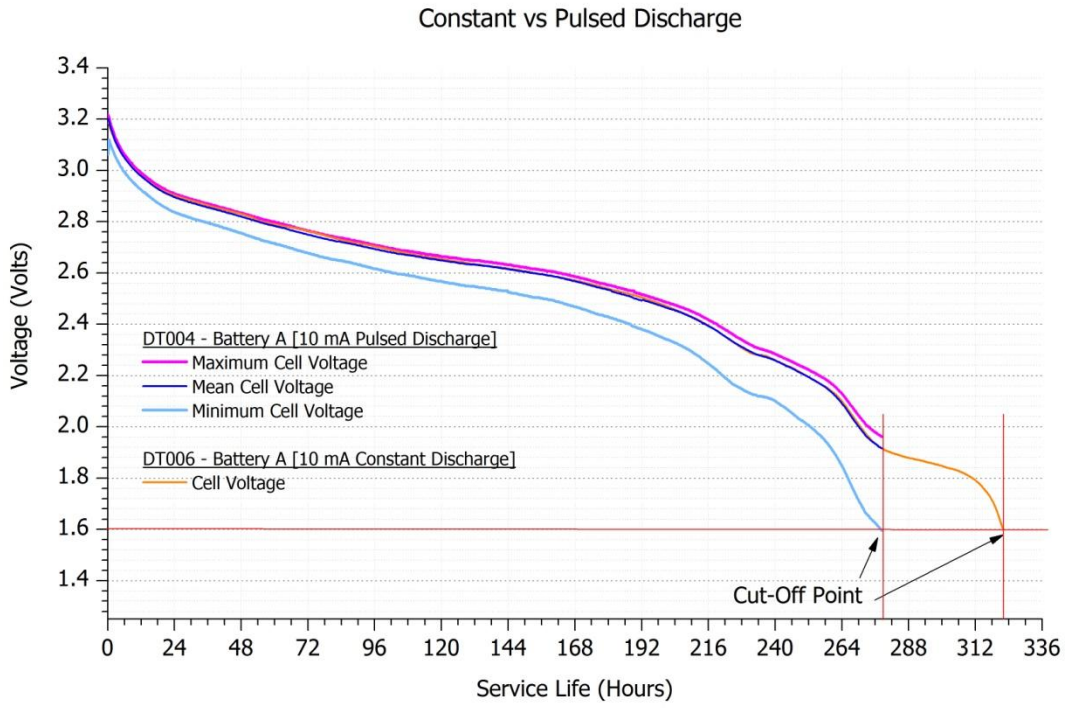

Figure 5.4 - Constant Discharge compared to Pulsed Discharge

The first thing that is noticeable from Figure 5.4 is that the constant discharge has a longer service life of 322 Hours in comparison to the service life of 278 Hours of the pulsed discharge. The end of the discharge test is defined by the moment the cell voltage drops below the cut-off voltage, as marked on the graph. As a result of the cell voltage dropping during the active load of the pulsed discharge, the cut-off point is reached by the minimum voltage curve some 44 hours before that of the constant current discharge curve.

Despite the reduced service lifetime of the pulsed discharge, it must be noted that the mean cell voltage follows the curve of the constant discharge cell voltage within ± 10 mV for the entire duration of the discharge.

Although in this example the pulsed discharge did not prolong the service life, in related research [19] the pulsed discharge would be compared to the constant current discharge of the active load.

The active load in this case is 100 mA. A constant discharge at 100 mA would last roughly 20 hours based on the typical constant current discharge characteristics graph in the battery datasheet (See Appendix A). Comparing against the 100 mA discharge shows that using a pulsed discharge prolongs the service life of the cell.

5.4 Cell to Cell Variation

When comparing the results in Table 5.1 it is clear that for every experiment there can be anywhere between a 1 to 6 % variation in the final service life between the three pairs of cells. Is there a reason for this variation between the batteries that were discharged at the same time, and under the same conditions?

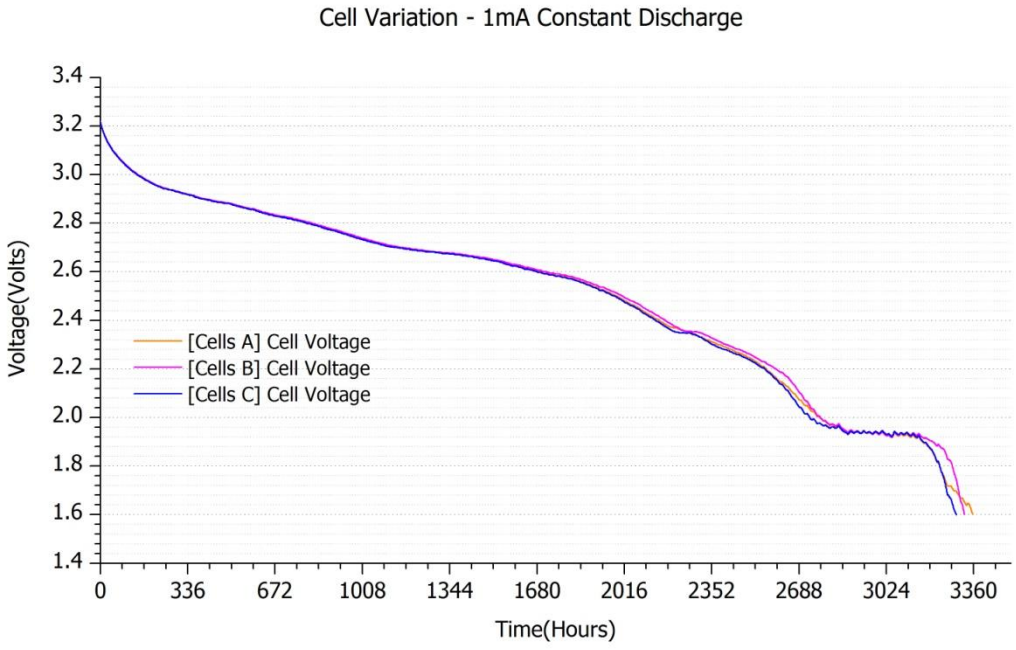

Figure 5.5 - Variation between cells discharged at 1 mA constant current

In Figure 5.5 there is a comparison between the three pairs of cells discharged at a constant current of 1mA as part of the test DT005. It is clear that there is little variation between the cell voltage curves until the last third of the discharge where it is visible that the cell voltage begins to vary. This final third has been expanded onto a second graph found in Figure 5.6. This variation leads to different final service life values.

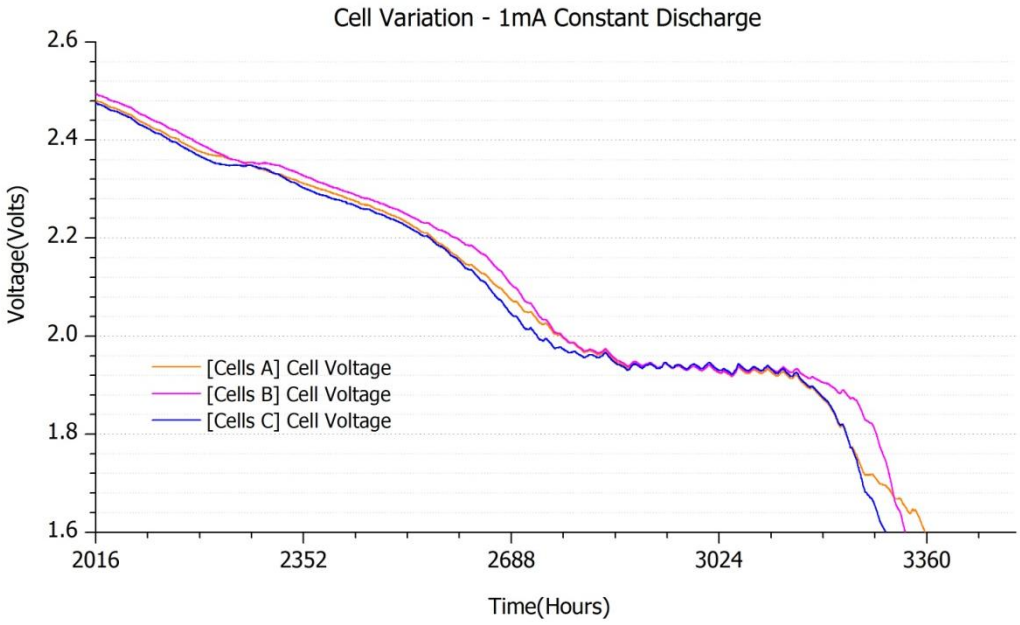

Figure 5.6 - 1 mA constant current discharge in the final third of the discharge cycle

Results from discharges tests DT001 and DT002 in Table 5.1 are an example of where cell to cell variation has resulted in a significant reduction in service life for just one pair of cells in each of the discharge tests.

The result of Battery C in DT001 is a service life of 309.3 hours, which is 2.5 % decrease on the other two pairs of cells in the same discharge test. Likewise the result of Battery A in DT002 which is a service life of 252.9 hours, has an even larger 6 % decrease in service life compared to the other two pairs of cells.

The variation can also result in an increase in performance, for example in DT007 the result of Battery A is a service life of 2856.3 Hours which is an increase of 3 % on the other two pairs of cells.

The cell voltage plots of all the aforementioned discharge tests can be found in Section E.2 of Appendix E.

Due to the nature of the electrochemical manufacturing process of alkaline batteries there is always likely to be a slight variation but advancements in manufacturing since the first alkaline battery has meant that the variation is kept to a minimum.

5.5 Experimental Conclusions

This chapter has summarised the behaviour of the cell voltage when under different loads and discharge patterns. There is clear evidence of the charge recovery process when considering the behaviour of a pulsed discharge. Including how the recovery period increases as function of the active load magnitude and the time the load is applied for.

The results summarised in Table 5.1 show that there is always a slight variation between the cells. This variation in battery service life could be cause for over estimation of the achievable system service life, so should not be ignored.

The interesting result from all of the discharge tests is the relationship between reduction in discharge current and increase service life, i.e. as the discharge current is reduced in magnitude, the service life is increased.

It could be possible that the data gathered can be used to predict the service life of the cells below the 5 mA constant current discharge that is available from the datasheet discharge characteristics graph.

From the number of discharge tests achieved it is possible to see that between constant current and pulsed current discharges, there is a slight correlation between the obtained service life from the batteries.

This leaves the question; can this possible relationship be used to estimate the service life of a pulsed discharge from the equivalent constant current discharge service life?

Chapter 6.

Environmental Effects

The key environmental variable is temperature. Each discharge test took place in one of two possible locations, both with different characteristics.

One location was an unregulated lab environment, which exhibited temperature swings between day and night and also temperature variation from changing weather such as high winds or large amounts of sunlight. This sort of behaviour could be faced by a WSN that is located outside.

The other location was within a small room that contained a domestic water heater and was well insulated, which resulted in a relatively stable temperature environment close to an ambient of 25 °C. The importance of this location is the removal of the large temperature swings between night and day, not necessarily the value of the ambient temperature. This sort of behaviour could be found within a well insulated and temperature controlled building that remains close to the same ambient temperature, 24 hours a day.

In addition to the two locations, discharge tests were completed using the temperature controlled framework described in Section 4.6. This provided a means for discharging cells at extremes of ±25 °C from the ambient temperature of 20 °C.

It is expected [15] that the higher the operational temperature, the longer the service life can be prolonged. As operating temperature decreases, performance decreases accordingly.

6.1 TEMPERATURE PROFILES

The two environments and also the effects from changing temperature can be compared through the discharge tests contained within Table 6.1. Each test has exactly the same discharge profile but they take place at different points in time and in one of the two described locations.

The question is why does the service life vary between each test? This will be investigated by firstly comparing the temperature profiles and then changes in the cell voltage due to temperature change.

These temperature histograms do not show the frequency of change in temperature, but instead the cumulative pattern at which the temperature is measured with the same value. The temperature values have been taken from one of the three batteries available from each discharge test as there is little variation.

Test			DT003	DT004	DT016
Current			**10mA**	**10mA**	**10mA**
Environment			**Lab**	**Stable**	**Lab**
Method			*Average*	*Average*	*Average*
Service Life	**mAh**	A	2728	2783	2642
		B	2715	2783	2666
		C	2710	2770	2659
	Hours	A	272.8	278.3	264.2
		B	271.5	278.3	266.6
		C	271	277	265.9
Temperature		Mean	24	27	19

Table 6.1 - Comparison of discharge tests in different environmental conditions

The two tests, DT016 and DT003, both take place in the lab environment yet the temperature distributions do differ, as shown in Figure 6.1. The temperature during DT003 has a well defined peak close to the mean of 24 °C and a data range of 10 °C. This is in comparison to the DT016 test that has no defined peak around the mean of 19 °C and has a more stagnated spread across a range of 9 °C.

In comparison the DT004 test that took place in the more stable environment, has a clear peak around the mean of 27 °C with a smaller range of 6 °C. Importantly the cumulative hours at the outer edges of the range, account for only 9 % of the total hours.

With the knowledge of the temperature profiles, how does this relate to the service life?

The one variable that is different between all three tests in Figure 6.1 is the mean temperature over the full discharge. There is a distinct correlation between the mean temperature and the resulting service life of the battery discharge. It can be observed from Figure 6.1 and the corresponding results in Table 6.1, the higher the mean temperature, the longer the service life of the battery.

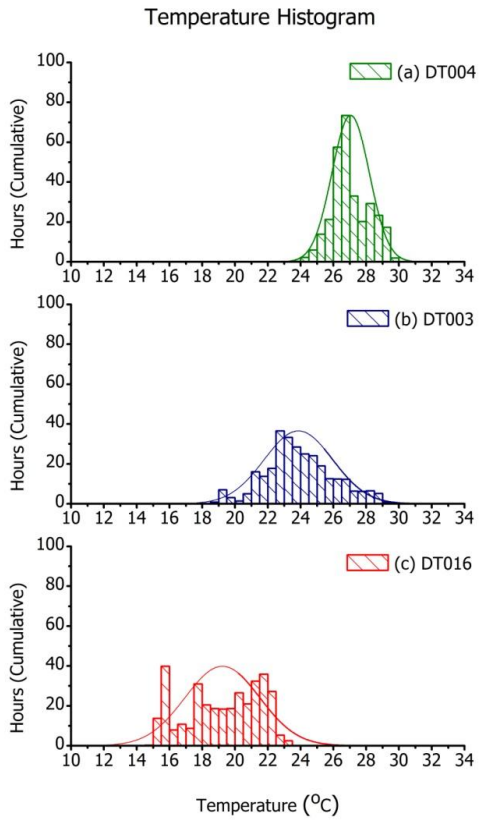

Figure 6.1 - Comparison of temperature histograms for discharge tests detailed in Table 6.1

6.2 TEMPERATURE CHANGE

The temperature profiles in Figure 6.1 show the frequency at which different temperatures have occurred over the lifetime of the test, but how does the changing temperature during the discharge affect the cell voltage?

To see the effects of temperature the focus will switch to the longer test DT007 that involved a 1 mA pulsed discharge. The test took place in the stable environment, and the temperature profile for this environment can be seen in Figure 6.2. The mean temperature for the duration of the discharge test was 26 °C, and temperature range was concentrated to 8 °C over a 3-4 month period.

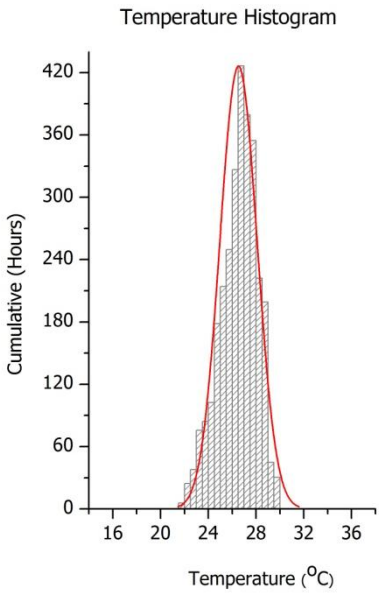

Figure 6.2 - Temperature histogram of discharge test DT007

When the mean cell voltage curves are compared in Figure 6.3 there appears to be very little effect from temperature change until about 90 % of the final service life. At this point there is a slight deviation by one battery. This could be due to cell to cell variation as discussed in Section 5.4.

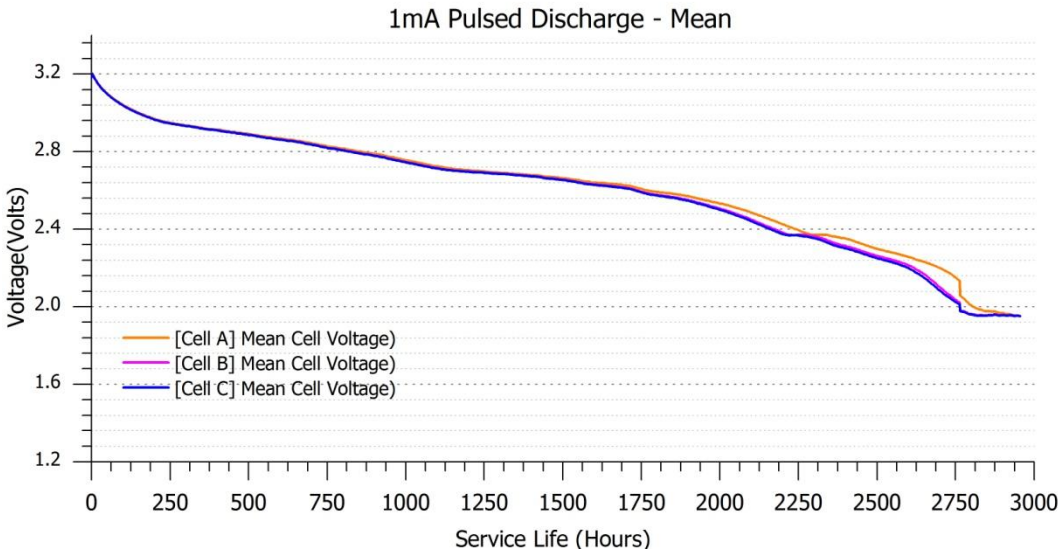

Figure 6.3 - The mean cell voltage from the 1 mA pulsed discharge

However by comparing the minimum and maximum cell voltage curves, in Figure 6.4, it is possible to see that there is a more significant variation between the cells after around 1800 hours. The cell voltage of Battery A appears to be holding a higher minimum cell voltage than the other two pairs of cells until at 2760 hours the cell voltage takes a very sudden drop of 200 mV.

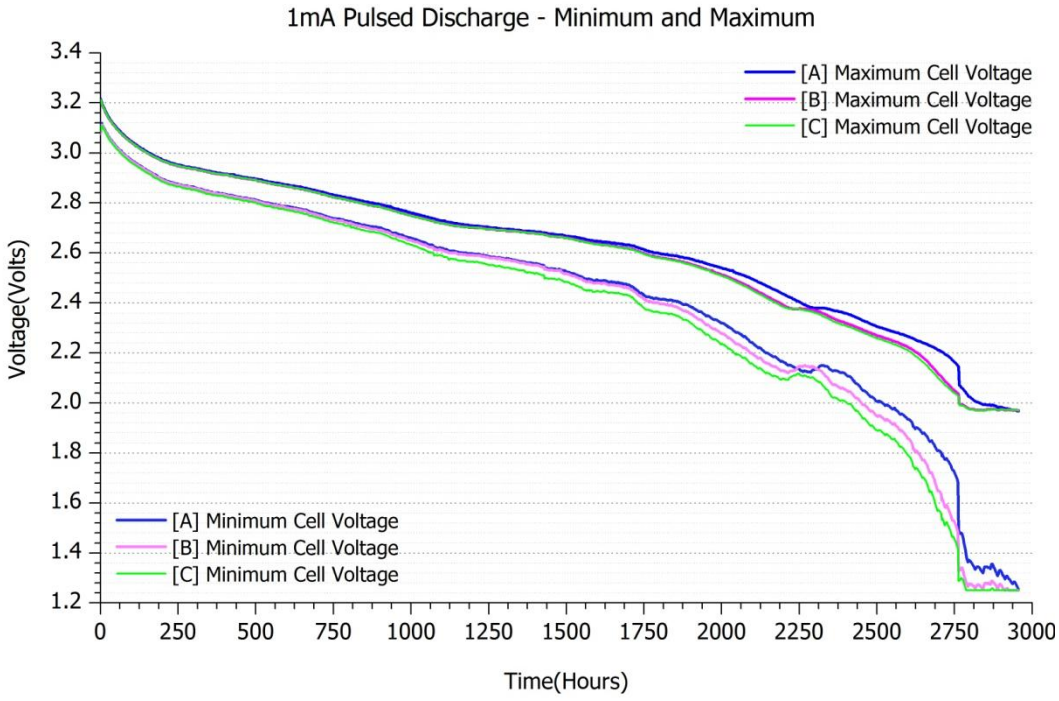

Figure 6.4 - Minimum and maximum cell voltage from the 1 mA pulsed discharge

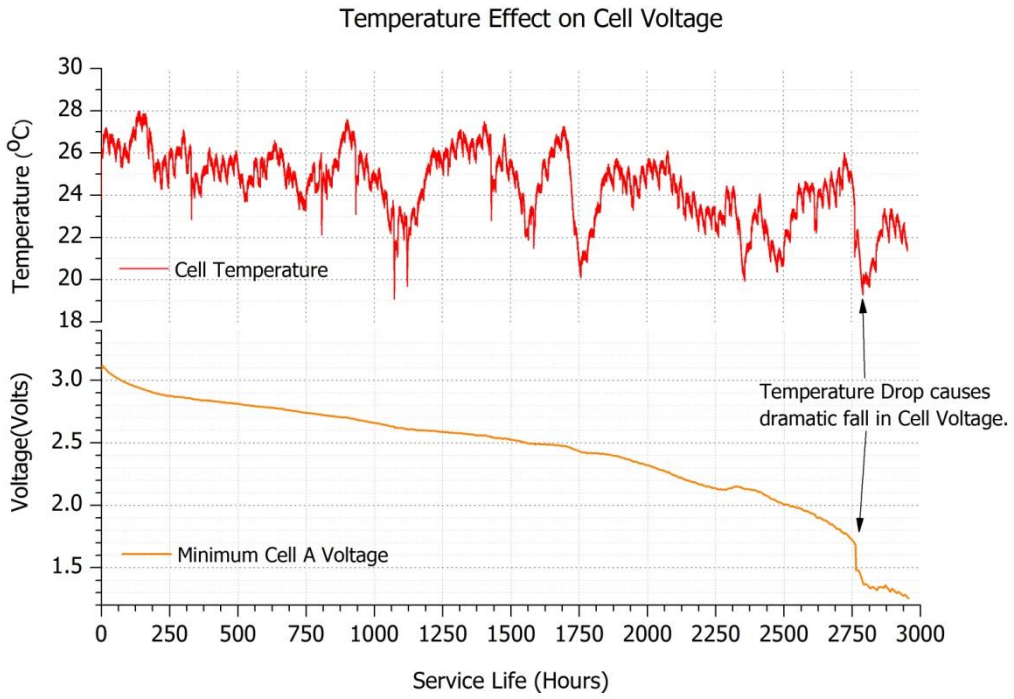

Figure 6.5 – Plot to highlight the effect that temperature can have on the minimum cell voltage

The sudden drop in cell voltage as mentioned could be due to cell to cell variation, but with closer investigation it appears that a change in temperature may have had an effect. In Figure 6.5 the cell voltage of the battery is compared with the temperature curve of the battery in question. Despite being in a stable environment, there is still some fluctuation in temperature, more noticeable due to the length of the discharge test. At the point the cell voltage takes a sudden drop there had been a sudden drop in temperature by roughly 5 °C.

From comparisons between temperature and cell voltage in other discharge tests, the period towards the end of the cells service life appears to result in the cell voltage to be more susceptible to environmental changes. Despite this the correlation between the fall in temperature and cell voltage is a clear indication of how temperature change can affect the cell voltage and ultimately the final recorded service life.

6.3 TEMPERATURE EXTREMES

The manufacturer's datasheet [45], in Appendix A, states the operating temperature of the MN1500 cells to be -20 °C to 54 °C. The question is just how much of an effect does operating the cells close to their operating temperature extremes have on their service life?

By using the experimental framework as described in Section 4.6, cells were setup to be discharged at the temperatures of -5 °C and 45 °C which is ±25 °C of a 20 °C ambient temperature. The equipment used only allowed for a single pair of cells to be discharged at the desired temperature, for this reason the test time was reduced by part-discharging all of the cells.

The discharge profile was the same used for tests DT003 and DT016, which was a 10 mA pulsed discharge at lab ambient temperatures. The cells were discharged at ambient to a cell voltage of 2.4 V, which equated to roughly two thirds of the way through the discharge, before continuing the discharge at a given temperature.

In order to compare the results at different temperatures it was important to have an equal number of control experiments discharging the cells from the part-discharge point at lab ambient temperatures.

6.3.1 High temperature Discharge

A comparison between the discharge at 45 °C and ambient can be seen in Figure 6.6, with the data for the graph being selected on the best case for comparison.

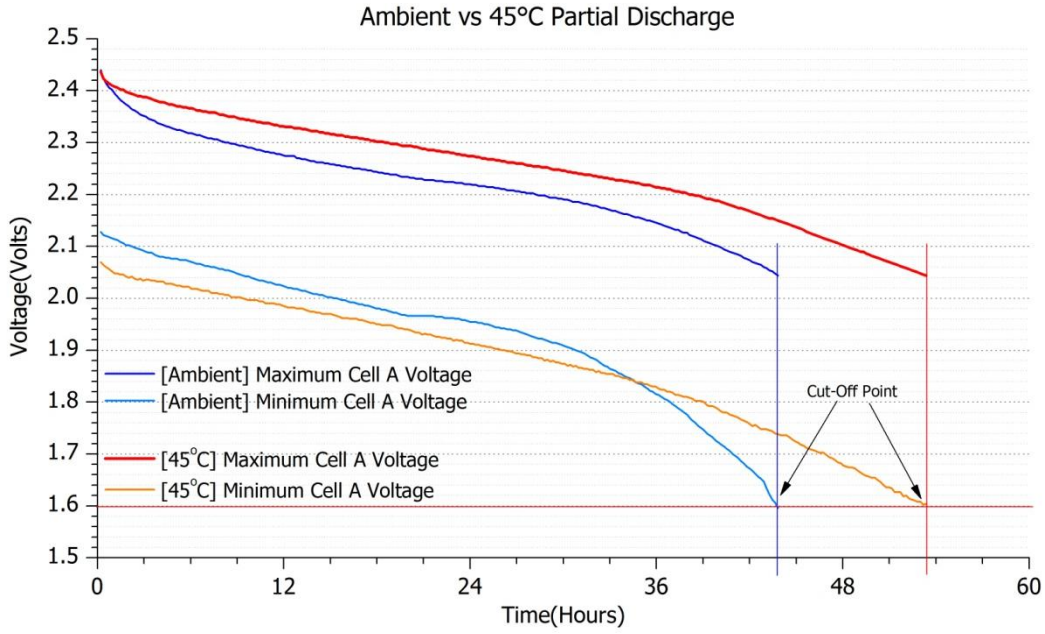

Figure 6.6 - Comparison between partial discharges at ambient and 45°C

Data on the battery chemistry [20] suggests that the performance of the battery chemistry will improve with higher temperatures, and the performance will degrade at lower temperatures. It can be seen that the length of time to reach the cut-off voltage has been increased for the cells being discharged at 45 °C by just under 12 hours, which is as expected.

Not all of the batteries discharged at 45 °C produced the same result. There was a great degree of variance despite the temperature profiles being almost identical. The full comparison and temperature profiles can be found in Section F.2.1 of Appendix F.

There is a 48 hour difference between the longest and shortest discharge test at 45 °C. The significant difference seems to be the minimum cell voltage curve as they are all different. There is also unusual behaviour at the start of DT009 as the minimum cell voltage falls below the cut-off voltage immediately on beginning the discharge, only to recover roughly 25 minutes into the discharge test. This sort of behaviour is unexplainable.

6.3.2 Low Temperature Discharge

The cells discharged at -5 °C produced mixed results, mainly due to inconsistent temperature control below freezing.

Due to the experiments operating below 0 °C the accuracy of the temperature IC's reduced to ±4 °C. To counter this all experiments were setup using a calibrated multimeter thermocouple to ±1 %, and regularly monitored throughout the experiment.

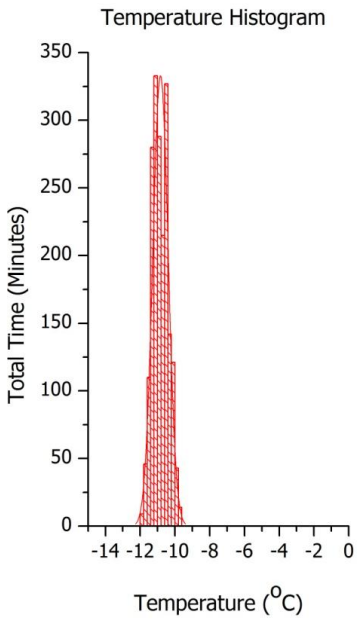

Figure 6.7 - Temperature histogram of partial discharge test DT015

From the temperature profiles recorded, four pairs of cells were discharged whilst operating between a range of -2 °C and -12 °C. The fixed temperature of -5 °C proved difficult to achieve.

The reliability of the temperature control below 0 °C became a real issue mainly due to condensation. Despite this the cell voltage behaviour of four pairs of cells was recorded and showed very unpredictable behaviour.

The plot of test DT0015 contained in Figure 6.8 has been selected to show the best case cell voltage behaviour. The corresponding temperature profile in Figure 6.7 shows that even with the reduced accuracy of the thermistor the temperature range remained very narrow and centred around -10 °C for the duration of the test.

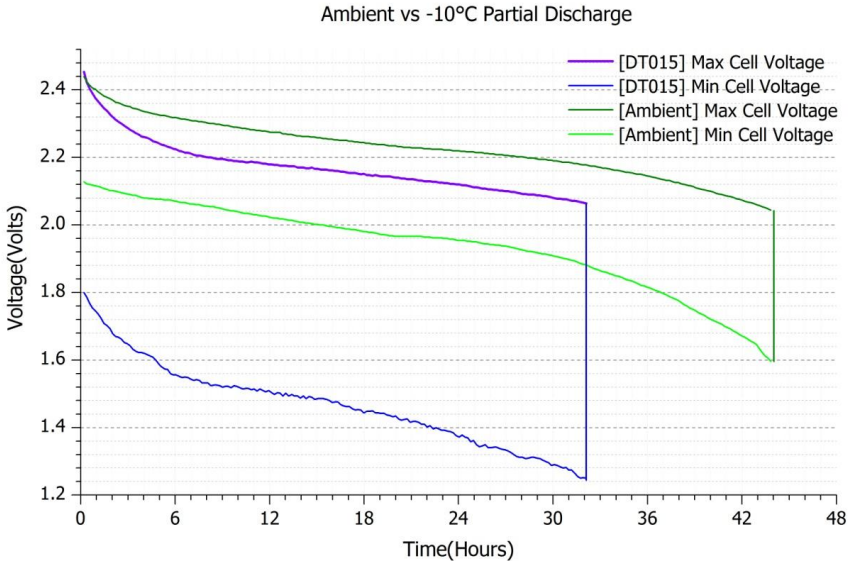

Figure 6.8 - Comparison between partial discharges at -10°C and ambient.

In comparison to the partial discharge at ambient, the service life for this best case discharge of DT015 shows that service life is reduced by 39 hours, to a very short partial service life of 5 hours. It is clearly the minimum cell voltage that shows the greatest degree of change and this is when the cells are under their greatest load.

As mentioned the behaviour of the cell voltage at these low temperatures is unpredictable and an example of the worst case, and all other examples, can be found in Appendix F. It is not known if the unpredictable nature of the cell voltage is due to the low temperature or the fact that the cells are already partially discharged. To try and investigate this, a full discharge was completed at freezing point.

6.3.3 Freezing Point

It is possible in some deployments of wireless sensor networks that the sensor nodes will see operational temperatures close to freezing point. In order to see how the batteries would operate at this temperature, a full discharge cycle identical to the DT003, DT004, and DT016 tests, has been used (See Table 5.1 in Section 5.1).

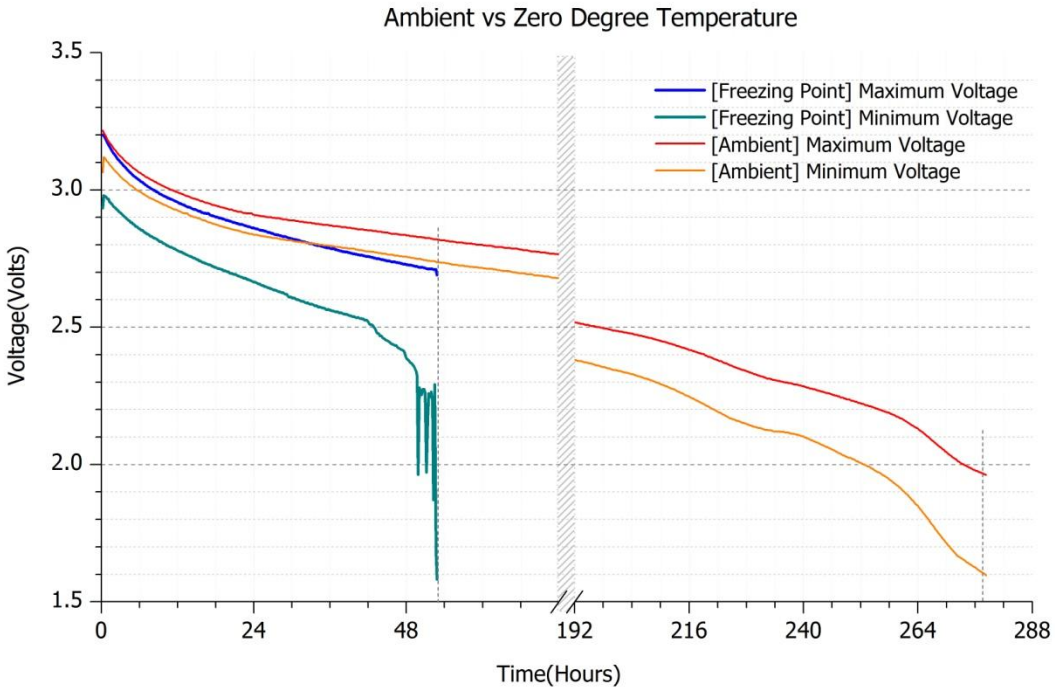

Figure 6.9 - Cell voltage of full discharge compared at freezing point and ambient

The temperature was successfully kept at 0 ±2 °C using the same experimental framework as previous temperature tests, but at this temperature there were no problems with condensation. It must be stressed that this experiment was only completed the once and therefore cannot represent any statistical significance.

It is evident from the minimum and maximum cell voltage curves shown in Figure 6.9 that there is a drastic reduction in service life when compared to the minimum and maximum curves of the same discharge completed at ambient temperatures.

Comparing the minimum voltage curves, after only 24 hours the difference between the minimum cell voltages is nearly 200 mV. Within 48 hours the discharge at zero degrees has begun to fall away sharply. In summary the discharge completed after 52.8 hours, only 20 % of the service life at ambient temperature.

6.4 Environmental Conclusions

The opening hypothesis was that the performance of the batteries increases with temperature, and likewise decreases accordingly with lower temperature.

It has been proven with the experimental results that if you perform the exact same discharge experiment in environments with varying conditions, the higher the mean operational temperature the greater the performance of the cells under discharge.

This hypothesis was further proven when operating the cells at high temperature close to the operational limits of the cells.

Operating at lower temperatures became a difficult task. The major problem was from condensation building up inside the insulation surrounding the aluminium encasement. The condensation caused problems with the temperature switch used and therefore prevented full control of the temperature. This explains the why experiments at -5 °C were instead measured at -11 °C.

To conclude the low temperature experiments, one pair of batteries were fully discharged at freezing point. The service life of the battery at this temperature was significantly reduced, again a result that was expected.

This chapter has explored the effects temperature can have on an Alkaline Manganese cell, and it is clear that operating temperature or change in temperature for a wireless sensor node should not be ignored.

Chapter 7.

Experimental Analysis

The results given in Chapter 5 and Chapter 6 have covered two main aspects of battery behaviour, pulsed discharge, and the environmental effects. This chapter will use the results and put them into context for the case of alkaline batteries in a wireless sensor node.

The alkaline batteries offer the great advantage over batteries of different chemistries that they are low cost and readily available. The question is, how long can the service life of wireless sensor node, using alkaline batteries, be prolonged?

Environmental variables are difficult to predict and even more so the effects these variables have on the behaviour of the cells. What the experiments have highlighted is the importance of considering the environment, in particular the temperature that a wireless network/node will have to endure.

This chapter will firstly consider the battery models discussed in Section 3.4, and if it is possible to base a model on the experimental results of this project. The following topics will then be considered in the context of prolonging the service life of the batteries:

- Controlling the discharge profile
- System operating voltage
- Deployment environment

7.1 BATTERY MODELS

In Section 3.4 a selection of battery models are discussed. With the experimental results gained, how can the models be compared to the results? The two models used for comparison with the experimental results are the Discharge Rate Dependant model [26], and the Rakhmatov model [35][37][38].

7.1.1 Discharge Rate Dependant Model

This model is a current based estimation for calculating the remaining battery capacity and relies heavily on the rated capacity given by the manufacturer.

The model calculates the capacity consumed based on an instantaneous discharge current for a given period of time. It is therefore possible to simulate the discharge profiles executed in the experimental work using equation (4):

$$C_{res} = C_{max} - \sum_{t=t_0}^{t=t_n} I(t)\Delta(t) \qquad (4)$$

Where C_{res} is the remaining capacity, C_{max} is the rated capacity, $I(t)$ is the instantaneous current consumed over the duration of time $\Delta(t)$. This model is very closely related to the linear model as it does not take into account cell recovery.

The initial or maximum battery capacity can be based on the rated capacity of 2850 mAh from the manufacturer's datasheet [20], but this is an estimate and does not take into account the discharge rate or the environmental factors.

The maximum battery capacity could instead be replaced by an average experimental value for a given discharge profile, such as that found in experiments DT003/004/016. So using the discharge profile of 100 mA for 1 minute, and 1 mA for 10 minutes, the resulting mean achievable capacity is 2717 mAh.

If both rated capacities are used the resulting time to reach zero capacity are as follows:

$285\ hours$ for $C_{max} = 2850\ mAh$ $271.8\ hours$ for $C_{max} = 2717\ mAh$

As you can see the time taken to reach zero capacity relies solely on the rated capacity and the average discharge rate. If the rated capacity from the manufacturer had been used the lifetime of the battery would have been overestimated, prompting the wireless node to stop operating before expected. This simple linear model would not give enough accuracy in estimating the lifetime of the battery, without prior experimental work

7.1.2 Rakhmatov Model

The main advantage of this model is that it takes into consideration the recovery in capacity during the relaxation period of a pulsed discharge. It is possible to produce a lifetime estimation based on two parameters α and β. A full description of the model can be found in Section 0.

To perform the simulation, the algorithm created by *Timmermann* [37] has been used, and parameters α and β presented by *Spohn et al.* [38]. On attempting to apply the model it became apparent that the parameters suggested [38] did not fit with the expected units of milliamp hours for capacity, instead mA per ms have been used. Even on conversion to milliamp hours the values presented did not produce lifetime estimation results that looked valid or even comparable to the experimental work.

Since the parameters from *Spohn et al.* [38] were the only values found for alkaline cells, a simulation and comparison with experimental results was not possible.

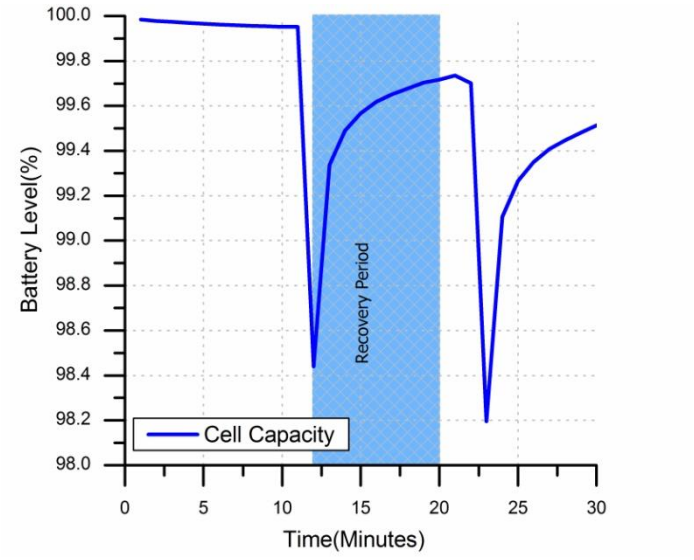

Figure 7.1 - Rakhmatov-Vrudhula Battery Model and example of cell recovery

However from using the parameters available the resulting simulation gave an example of how the Rakhmatov model takes into account cell recovery, as illustrated in Figure 7.1. Despite the cell recovery being present within the model, the discharge rate is different to that of the experimental results, and therefore does not present a good fit.

For this model to be used for alkaline cells, further research would be required to calculate the β parameter value for alkaline cells.

7.1.3 Proposed Battery lifetime estimation

The manufacturer's data sheet for the alkaline batteries, as previously mentioned, provides a graph of the typical constant current discharge characteristics [45], found in Appendix A. This graph could in theory be the first point of reference for system designers. The problem is that in the area of wireless sensor networks, it would be expected that the average operational discharge current would extend below the 5 mA that the manufacturer's graph covers.

The experimental work from this research has included the constant current discharge of batteries at 10 mA and 1 mA, the question is can this data can be used to extend the aforementioned manufacturer's graph?

The proposed method of lifetime estimation is to use experimental data and statistical analysis to extend the manufacturer's graph whilst providing estimation for cells that are pulse discharged.

To do this there are some general assumptions:

- The characteristics curve remains linear below the discharge current of 5 mA.
- The non-linear regions for discharge currents above 100 mA are ignored as loads that large are considered not applicable for WSN.
- The cells will be discharged to 0.8 V individually, with a combined a cut-off voltage of 1.6 V.

As well as the above assumptions, the results from discharge tests DT004, DT005, DT006 and DT007 are shown in Table 7.1. The results in Table 7.1(a) have been used to gather a mean value for constant current discharges at 1 mA and 10 mA respectively. The results in Table **7**.1(b) provide the corresponding mean service life for pulsed discharge tests, where the average current over a single duty cycle is matched with the constant current values used in Table **7**.1(a).

Test			DT005	DT006
Current			1mA	10mA
Environment			Lab	Stable(2)
Method			*Constant*	*Constant*
Load	High	Current	1mA	10mA
		Period	-	-
	Low	Current	-	-
		Period	-	-
Service Life	Hours	A	3428.3	322
		B	3396.5	323.4
		C	3317	328.8
		Mean	3380	324.7

(a) Constant Current Discharge

Test			DT007	DT004
Current			1mA	10mA
Environment			Stable	Stable
Method			*Average*	*Average*
Load	High	Current	100mA	100mA
		Period	1 Min	1 Min
	Low	Current	100uA	1mA
		Period	110 Min	10 Min
Service Life	Hours	A	2856.3	278.3
		B	2785.9	278.3
		C	2760	277
		Mean	2800.73	277.867

(b) Pulsed Current Discharge

Table 7.1 - Experimental data for lifetime estimation model

Based on these mean values a straight line equation on a logarithmic scale has been generated similar to that provided by the manufacturer on a logarithmic scale. Using the line equation (5) with the y intercept value of $3380\ mAh$, and the value of m calculated in (8), the final line equation can be found in (9).

$$y = x_1 \times x^m \text{ where } m = \frac{\Delta \log Y}{\Delta \log X} \quad \textbf{(5)}$$

$$\Delta \log Y = \log 324.7 - \log 3380 \quad \textbf{(6)}$$

$$\Delta \log X = \log 10 - \log 1 \quad \textbf{(7)}$$

$$m = \frac{\Delta \log Y}{\Delta \log X} = -1.0174 \quad \textbf{(8)}$$

$$y = 3380 \times x^{-1.0174} \quad \textbf{(9)}$$

The extrapolated graph in Figure 7.2, using equation (9), has allowed for the estimated service life of the batteries to be extended to below 5 mA, all the way down to 10 µA. Realistically no embedded device is likely to operate at a constant current of 10 µA and to experimentally back up this estimation up could take in excess of 26 years! In reality the maximum service life is limited by the cell's shelf life of 5-7 years, or time to self discharge.

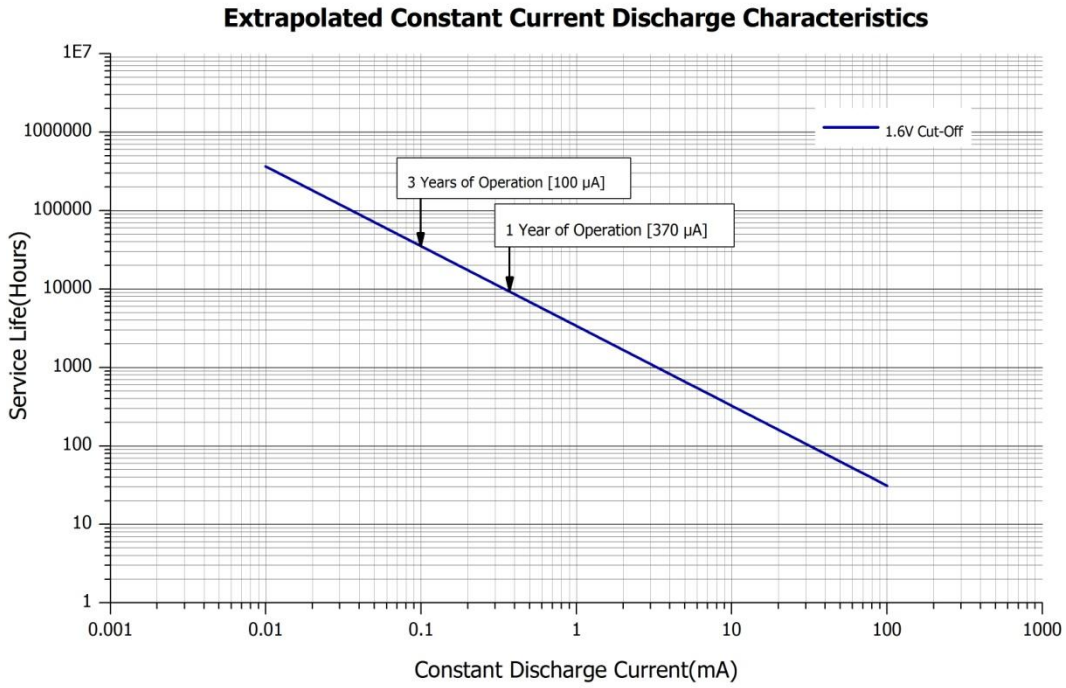

Figure 7.2 - Extrapolated Constant Current Discharge Characteristics

In a wireless sensor node, current communications radio technology dictates that the radio operational current draw is in the region of 20 mA. Based on this estimation and an assumed sleep current in the region of 1 μA, the mean discharge current for a wireless sensor node would be between 100 and 500 μA.

This range is based on the assumption that the sleep duty ratio is 99:1, so 1 % of each duty cycle is spent operational; the average discharge current over a single duty cycle is calculated in (10).

$$I_{Avg} = \frac{(99 \times 1\mu A) + (1 \times 20mA)}{100} = 201\mu A \qquad \textbf{(10)}$$

Marked in Figure 7.2 are two points of interest. To achieve one year of operation, an estimated constant discharge current of 370 μA would be required. With a constant current discharge of 100 μA, it could be possible to achieve three years of operation. It is worth noting that a service life of this length could be approaching the manufacturer's marked shelf life of the cell. Beyond this time it would be very difficult to predict the cells behaviour.

The generated straight line omits an important aspect in relation to wireless sensor nodes. How can the service life of a battery that has a pulsed current discharge applied be predicted?

The simple answer is that it would require an incredibly large number of experimental discharges covering all major steps in duty cycles and inactive and active discharge currents, in order to provide a reliable estimation curve.

In theory it could be possible to generate a graph, like that in Figure 7.2, containing plots of duty ratios in steps of decades, and a similar graph containing plots of inactive and active discharge current in steps of decades. This would at least give a straight line plot that could be used for estimation of the battery capacity.

There does appear to be a correlation between the constant current discharge capacity and the pulsed current discharge. Taking data from Table **7**.1(b), the mean service life works out to be roughly 85 % of the equivalent constant current discharge. With more experimental data, a fraction could be calculated to work out the pulsed discharge lifetime based on the constant current lifetime.

Even with all this experimental work, a significant sample would need to be carried out to claim statistical significance. This is something that has been difficult to achieve in the length of this research project, and would require substantial investment in time for any future research project.

7.2 DISCHARGE PROFILE

The experiments looked at two types of discharge profile, constant current and pulsed discharge. In the context of wireless sensor node, or any embedded electronics, it would be very difficult to design hardware to operate as a constant current load low enough to provide a suitably long service life. The behaviour of a wireless node instead results in active and inactive periods of operation.

The experimental pulse discharge profiles use only two levels of constant current load. In reality a sensor node could have multiple levels of current demand depending on the operations taking place. It is often during the transmission and receive mode that there is the highest current demand.

An example current profile [47] can be found based on the MICA2 hardware that operates in the 916 MHz frequency band and will be discussed in Section 8.1. The summary of the different contributions highlights that the largest current draw of 22 mA, is during transmission and the sleep current reduces to roughly 100 µA.

These are two areas that can be improved upon, minimizing the active load, and reducing the inactive load.

7.2.1 Period of Activity

It is the active load that has the greatest influence on how quickly the cell capacity is drained. The higher the load, the more chance there is of the cells not recovering and capacity being lost, as discussed in Section 2.1.3.

Reducing the active load in magnitude or the period of activity would aid in the cells charge recovery. As mentioned the largest load in existing hardware is the transceiver, improvements in the magnitude of the current draw might not be possible whilst achieving the same transmission power. Instead attention should be paid to reducing the amount of time active.

The importance of reducing the period of activity can be indentified through the comparison of DT020, and DT003. In both the discharge rate was an average of 10 mA, but notably the length of the active period was increased by a factor of 10 in DT020. This resulted in a 2.5 % reduction in service life in DT020 compared to DT003.

In reality the period of activity is determined by the configuration of the wireless network the node is part of. Network requirements such as the number of retries, the time spent listening for network activity, all contribute to the time the node spends active.

7.2.2 Inactive Period

An advantage of alkaline cells is their long shelf life, but even after 4 years of storage and no use, only 89 % of capacity is still attainable [20]. This is due to the leakage currents and the degradation of the chemical compound, even when in open circuit conditions. What if the inactive load could be reduced to the same magnitude of the cell leakage currents?

Well in theory the lower the inactive current, the closer the cell becomes to having almost open circuit conditions. The advantage of this would be that the cells could chemically recover a larger proportion of the cells capacity after each active period, and reduce the chances of cell capacity being inaccessible at the end of the cells service life. In turn this would allow for the service life to be prolonged.

Reducing the inactive load only becomes beneficial providing that the inactive period is long enough for the cells to recover. The inactive period is predominantly determined by the wireless network MAC protocol, as discussed in Section 3.3.

A combination of reducing the inactive load and increasing the inactive period will bring the average discharge current down. An example of this can be seen from comparing the DT007 and DT004 test. From reducing the inactive load to 100 µA from 1 mA, and increasing the inactive period from 10 minutes to 110 minutes, the average discharge current has been reduced by a factor of 10 and the service life increased.

Reducing the magnitude of the inactive current very much depends on the connected hardware. Careful consideration must be given to the possible leakage currents from each component and the manufacturing/soldering techniques used.

A good example of this is from the MICA2 node that as mentioned is commonly used in related research. The value given in the product datasheet [32] for processor sleep current is less than 15 µA. Based on other research projects using the MICA2 hardware [3], when the sleep current of the node is measured, a value in the region of 100 to 300 µA is quoted.

One of the causes for the value being quoted at 300 µA was due to the leakage current consumed by the DC to DC Boost converter. It could be possible that through alternative part selection this figure could be improved or through alternative methods of power management. This improvement could come at a monetary cost however; therefore there will always be a trade-off between a low cost design and a design that will prolong the battery service life.

7.3 OPERATING VOLTAGE

A key design decision for any wireless node is how to manage the operating voltage rail of the connected ICs. It is clear from the graph, Figure 5.4 in Section 5.4, that the cell voltage does not remain the same through the lifetime of the cell and is ever decreasing. This is a major disadvantage of the alkaline cell as the majority of semiconductor ICs must operate within a certain stable input voltage range.

The preferred method of provided the operating voltage is using a DC to DC boost convertor as the efficiency can be as high 95-96 %. An example of the efficiency curve for a DC to DC boost convertor that best illustrates this can be seen below in Figure 7.3.

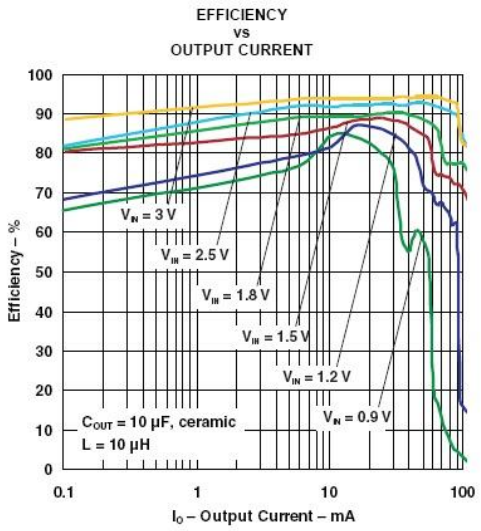

Figure 7.3 - Efficiency curves for DC to DC Boost Convertor [48]

As the output current, i.e. the active load increases to 10-20 mA the efficiency of the device peaks, but as the input voltage from the battery decreases the efficiency also decreases. The graph shows that to operate the DC to DC convertor close to maximum efficiency regardless of the cell voltage input, it would be ideal only to operate the boost convertor during the active load.

The catch is that the minimum cell voltage input to the boost convertor would be during the active period, due to the cell voltage dropping during the active load. This means that the efficiency would gradually fall away from the maximum value. However the efficiency would still remain higher, if not the same, than if the boost convertor was to be operated during the inactive period.

If the boost convertor was operating during the inactive load, i.e. all devices were in sleep mode, the efficiency of the boost convertor would never reach above 90 %. This poses the question of whether the boost convertor can be bypassed during the inactive state. However the implication of the boost convertor being bypassed would be not having a regulated operating voltage during the inactive state. A possible solution to this problem is discussed in Chapter 8.

7.4 DEPLOYMENT ENVIRONMENT

From the experimental results in Chapter 7, it is clear that the temperature of the node's environment clearly affects the performance of the cells. Discharging the cells at the extreme temperatures in essence exaggerated the point that temperature has a key part to play in the cells service life.

The main observation from the temperature tests results was that the higher the mean temperature, the longer the battery service life is extended.

In the context of a wireless sensor node, it is the node behaviour that must be adjusted to suit the environment of its deployment, whether it is a forest, or a building. Controlling the environment to extend the service life of a wireless network would be unjustifiable.

Take for example a network that is going to be placed in a forest, like the GreenOrbs project [49]. It could be of great advantage during the design stages of the network if some of the following are known:

- The full range of the temperature swing
- Temperature above, below and at ground level
- Temperature under the tree canopy or foliage
- Temperature in open space or direct sunlight

With this information it would be possible to try and optimize the locations and behaviour of individual nodes or the network as a whole.

Using the example given, if two nodes are located one under the tree canopy and the other in direct sunlight during the day, it could be safe to assume from the test results this research has produced, that the nodes located under the tree canopy will have a shorter service life than the node located in direct sunlight.

The placement of wireless sensor nodes could have a significant effect on the network, for example the difference in service life between nodes located in the shade and those located in direct sunlight could be significant enough to cause a portion of the network to outperform another. Solutions could be:

- More nodes in the lower temperature locations to burden the load and reduce the time spent active
- Try and locate all node in similar micro environments, i.e. always in direct sunlight
- Route data around the network based on the temperature of the nodes.

7.5 Experimental Conclusions

The experimental work has provided measured cell lifetimes and capacities. For a wireless network system designer it is an important process for estimating the potential lifetime of the network, and battery models can be used to achieve this.

This chapter has summarised two possible models, but it should be stressed that no models, to the author's knowledge, are available specifically for alkaline cells. This led to the proposal of battery lifetime estimation through the extrapolation of the constant current discharge characteristics provided by the manufacturer.

This graph could be extended to include estimation plots for pulsed discharged cells, but would require a large amount of further experimental work. This model is not claiming to be accurate but instead is suggesting a possible method of generating a lifetime estimation based on experimental work.

Along with battery models, other aspects have been considered in relation to improving performance of a wireless sensor node. This includes the discharge profile of the node, minimizing the active period, and increasing the time and decreasing the magnitude of the inactive period.

The system voltage of a wireless sensor node or any battery powered embedded device needs to be carefully considered. Efficiencies in any voltage regulation in the system can affect the sleep currents and in essence reduce the lifetime performance.

The work on the effects of temperature has shown that the design of any wireless sensor network should carefully consider the environment of deployment. Failure to do so could result in a significantly reduced lifetime compared to what may have been estimated.

With the knowledge gained from the experimental work, the question now is if it can be used to design and implement a wireless sensor node and network powered from alkaline cells.

Chapter 8.

Low Power Node Design

In order to further the research on battery performance, a wireless sensor node has been designed for use with two alkaline cells based on what has been learnt. The aim has been to build a node that could be implemented as part of ring topology network and be able to gather network performance data for future research. This has been achieved by meeting the following requirements:

- 2.4 GHz wireless communications using the IEEE 802.15.4 standard,
- Provide sufficient Flash memory for storage of performance data,
- The antenna should be located external to the PCB,
- Low cost solution.

The ring topology has been used in previous research projects to provide a method of monitoring a perimeter through nodes being buried at ground level encircling the desired area. The design of the low power node will be based on meeting the requirement of developing a ring topology network.

The nodes themselves will be designed to monitor temperature conditions and network performance. The network performance will hopefully provide data and statistics for future development work. Data such as dropped network packets will be stored locally on each node.

8.1 EXISTING HARDWARE

The design of the low power node is based on the knowledge gained from this research project and also through hardware gains when compared to existing hardware that is available. Comparing through datasheets is not enough; instead through comparing results from research projects of different institutions it is possible to see the disadvantages of the existing hardware and ways that the hardware could be improved.

The benchmark hardware is the MICAZ or the MICA2 node. They are both the 3rd generation of wireless nodes that are product of research work carried out by Berkeley University in collaboration with Crossbow Technology Inc. of California. Both nodes offer comparative specifications to the design requirements set out for this research project.

Importantly they are both powered by two standard AA batteries. Both nodes also offer Flash for data storage. The difference between the two is the radio frequency band, the MICA2 node operates in the 868/916 MHz range, whilst the MICAZ node operates in the 2.4/2.48 GHz range. Despite this difference, the specifications for the required power are almost identical, which leaves both open to comparison with this project.

Research in Section 3.1 identified several research projects that gave insight into the deployment of a wireless sensor network using the MICA hardware. The Duck Island Deployment [3] highlighted the problems associated with a high current draw when the MICA2 node is in sleep mode.

The paper highlights the high current draw being down to the DC to DC boost converter which is used to continually provide a stable voltage even when in sleep mode. This causes the converter to draw between 200 and 300 µA during sleep compared to the 15 µA that is quoted in the datasheet.

Out of the research projects that have used these nodes, deployments have lasted no longer than 6 months on standard AA batteries, and even the researchers for the Duck Island deployment were only able to predict a service life of six months after modification to the boost converter configuration.

There are clearly some design changes that if addressed could improve on the possible service life of a wireless node using two standard AA cells.

8.2 Design Decisions

The main design requirements of this node are related to the power management and behaviour between different states. The aim is to achieve an inactive current draw of less than 1 µA, whilst considering the following:

- Cell cut-off voltage
- Component selection to provide low sleep current and dynamic load control
- Component leakage currents when inactive
- Component supply voltage, i.e. the range and stability

As noted from the design of existing hardware, the configuration of the DC to DC boost converter is important. Parts exist that allow the system to shutdown and bypass the boost converter, providing a supply rail based on the battery voltage that could be anywhere between 1.8 V and 3.2 V. This poses some problems as devices such as the radio transceiver require a stable supply voltage, and based on the cell voltage curves in Section 5.3 it could prove difficult to achieve with alkaline batteries.

A solution is to have all auxiliary loads to the microcontroller enabled through a load switch. This load switch can be controlled by the microcontroller and enabled only when the boost converter has been enabled. This way it ensures that all auxiliary loads see a stable voltage and the boost converter is only required when the node is active. A full system overview can be found below in Figure 8.1, showing the main components of the system.

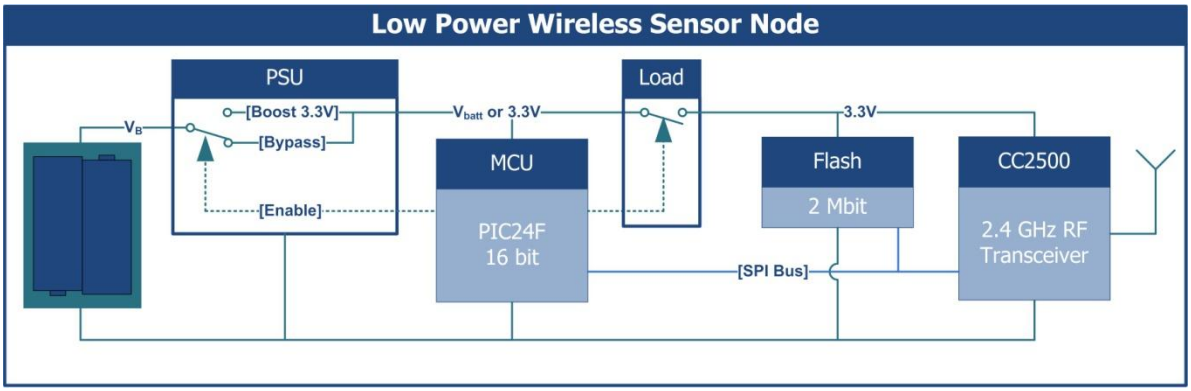

Figure 8.1 - Low power wireless sensor node system diagram

When the node is in deep sleep and inactive the boost converter is bypassed and the microcontroller is powered from the battery voltage. Since when in a deep sleep the current draw from the microcontroller will be less than 1 µA, the change in the cell voltage will be minimal and can be assumed to be stable for the duration of the deep sleep.

When in the sleep mode there is only the deep sleep current from the microcontroller, and the leakage current from the boost converter and load switch being drawn from the battery. One disadvantage of this system is that because the power is removed from the transceiver, all of its registers must be re-programmed before it can be used.

8.2.1 Component Selection

In recent years there has been increased attention by microcontroller manufactures to reduce power consumption of embedded devices. Two manufacturers in particular are Microchip with their XLP range of devices and Texas Instruments with their MSP430 devices.

Both manufacturers claim it possible to achieve deep sleep currents of less than 1 µA. Achieving sleep currents this low however is dictated by the system design. This is includes how the device is used, the peripherals that are required, and how the device is woken from deep sleep.

For this design the comparison of the microcontrollers extends beyond the electrical properties, to considerations such as hardware required for programming or debugging, practical experience with the manufacturers' development environment, and the cost of the development kit.

The two parts under consideration were the 'PIC24F16KA101' and the 'MSP430 F2132'. The operating specifications of the device are very similar, however based on previous experience with Microchip development tools and parts; the Microchip PIC24 was selected.

The DC to DC boost converter was selected on being able to meet the required design criteria and the availability and cost of the device, as was the load switch.

Another important part was the radio transceiver. The existing hardware, the MICAZ node uses the part from Texas Instruments, the CC2500, and given the design support material [50] available from the manufacturer, this component was selected.

A full bill of materials can be found in Appendix G, along with the system schematics.

8.2.2 Cell Voltage Operating Range

From the specifications of the DC to DC boost converter it should in theory be possible to achieve the stable operating voltage from an input voltage as low as 0.9 V. Assuming the cell voltage remained linear throughout the cells lifetime then this could be of a great advantage.

However from the cell voltage curves in Figure 5.4 in Section 5.3, it is clear that when the cell capacity is nearly reached, the drop in the cell voltage during the active load begins to exponentially fall away.

In doing so the current required by the boost converter to provide the operating voltage of 3.3 V will equally begin to increase. The increase in current then reducing the remaining capacity further, entering a vicious cycle.

The advantage however of the minimum input voltage being as low as 0.9 V is that it provides an additional length of time, however slight, to detect the nearing end of service life when the node is active. The detection could then be relayed over the network and the batteries replaced in due course.

The operating range of the selected microcontroller is between 1.8 V and 3.6 V. This means that at some point during the nodes operational life the boost converter will be required even during the inactive period in order for the microcontroller to remain operational and have the ability to wake from sleep.

The particular point can be determined by the node measuring the cell voltage and can be set with a safety threshold, such as at 2.0 V the boost converter remains on constantly. This gives time for warning to be sent out over the network that the node is approaching its end of life.

All of these details would eventually be determined by the network configuration but the option is available for full control over the voltage regulation.

8.3 PROTOTYPE

In order to test the theories behind the design decisions, a prototype PCB was designed and manufactured. The initial aim of the prototype was to use up to ten devices in a small network and gather data on the batteries whilst in operation. The PCB needed to be able to fit into enclosures that had been designed for a related research project.

Due to time restrictions towards the end of the research project, the aim was reduced to achieving the intended power management scheme suggested in Section 8.2. This was achieved and the prototype node can been seen below.

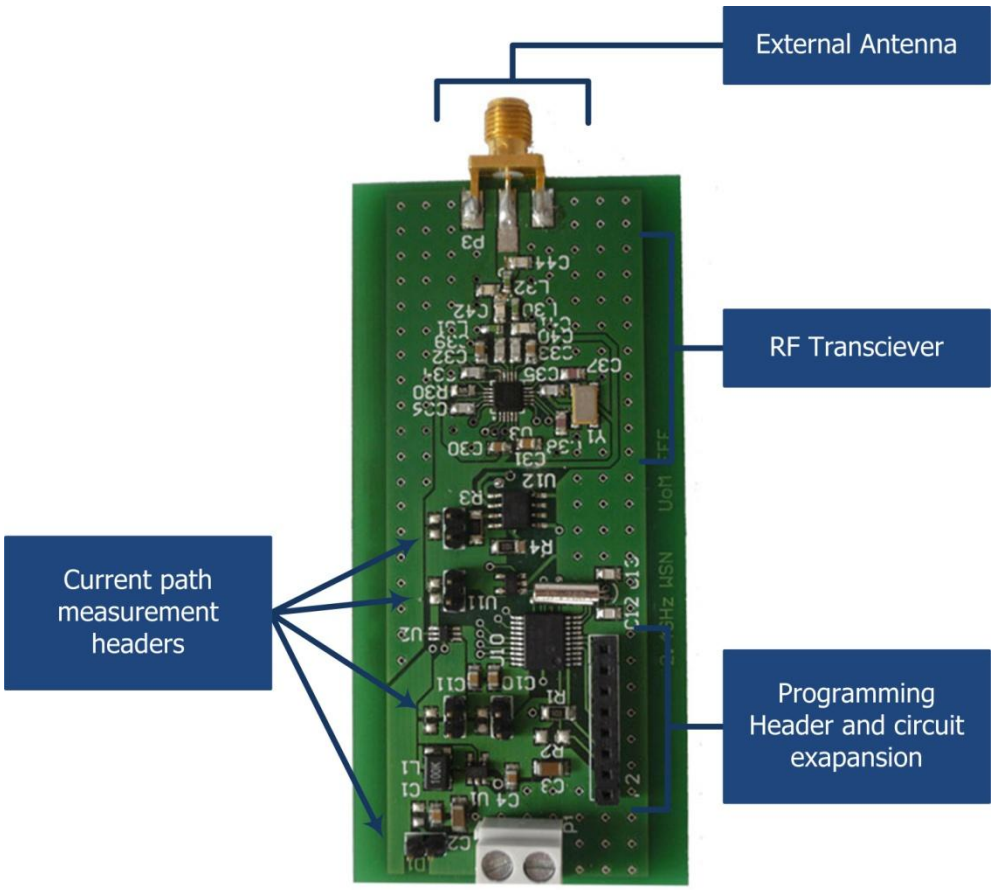

Figure 8.2 - Prototype Wireless Sensor Node

8.3.1 Deep Sleep Measurements

The aim has been to achieve an inactive current draw of less than 1 µA. The node hardware has been designed so that the current draw can be measured in various locations in the system. The current path measurement headers have been labelled in Figure 8.2 of the low power node.

Setting out provisions for being able to measure the current draw for separate parts of the system has the advantage that it is possible to spot possible leakage currents. These leakage currents could be causing the current draw on the batteries to be higher than intended, and in some cases can be larger than the deep sleep current.

The simplest advantage though is that the deep sleep current of the microcontroller can be measured directly.

To measure the deep sleep current, the device was programmed to power on every minute for 10 seconds then power into deep sleep for 50 seconds. This allowed for repeat measurements of the deep sleep current.

Using a 6.5 digit Digital multimeter the deep sleep current was consistently measured between 1.2 µA and 900 nA ± 0.1%. This was only achieved through eliminating the leakage currents present when first powered on, which in one case resulted in sleep currents of 900 µA due to a bad solder joint. Importantly the design has met with the initial design requirements of the low power wireless node.

8.3.2 Problems encountered

The major problem in the development of the low power node was time. There was however some problems encountered during the development.

The layout of the CC2500 transceiver and balun filter was taken from a reference design by Texas Instruments [50]; however the components used for the balun filter were selected based on case size from the same component ranges as used in the reference design.

Attempts to operate the transceiver, and exchange communications failed. The cause was traced to the balun filter after modifying the PCB to connect to a CC2500 module from Quasar. With the attached module wireless communication was successful but by this point time had become a problem.

8.4 Further Work and Conclusions

Unfortunately due to time on the research project running out, the development of the low power node concluded without being fully functional. The design of the low power wireless node had not been in the original plan for the research project but provided a suitable way to apply the conclusions made from the experimental data.

With further development the suggested design could be adapted to include application specific sensors, and a balun filter that enables the wireless operation of the node.

The selection of components however did enable the device to achieve the deep sleep current in the region of 1 µA, which if implemented will help bring the average operational load current down into the region of 100 µA. Based loosely on the experimental data, it could be possible to achieve an operational service life of over two years.

Full details on the design of the wireless sensor node can be found in Appendix G, with additional data such as datasheets and source code available on the attached DVD. A list of contents of the DVD is contained in Appendix H.

Chapter 9.

Conclusions and Further Work

Through experimental measurements and analysis this research project has investigated the performance of Alkaline Manganese batteries and applied the knowledge gained to the area of low power wireless applications.

This research combines the behaviour of alkaline manganese cells from experimental results and not simulation, and their use in wireless sensor nodes. This is an area of research, to the author's knowledge, that does not exist or has not been published.

Neither the data available from the manufacturer's cell datasheet [45], nor the manufacturer's datasheet on the Alkaline Manganese chemistry [20] provided the necessary information for batteries being discharged at currents below 5 mA.

In low power wireless applications it is expected that the batteries would be discharged from a pulsed current waveform, with the discharge current varying between active and inactive states. Data on pulsed discharges is not contained in the manufacturer's data, and very little academic research has been published with experimental data.

The lack of research and data surrounding the use of alkaline cells in low power wireless devices has prompted this research project. The following concludes the various areas of the research project, summarizing what has been achieved.

9.1 EXPERIMENTAL WORK

In order to gain an understanding of battery behaviour a measurement system, described in Chapter 4, has been developed and built for the single purpose of performing controlled battery discharges. The system has a modular design so that the configuration can be changed, in the event that the research focus changed over the 2 year project period.

The measurement system has been a great success, with the three boards built totalling operational time well in excess of 350 days and in total discharging over 100 alkaline cells. The data collected for each discharge test could reach in excess of 360,000 measurements or 11.5 MB of raw data. Through the use of an accompanying Windows application developed for the measurement system, the raw data can be processed into meaningful data points that can be plotted graphically and analysed.

In addition to the measurement system was the temperature controlled aluminium encasement. Using a thermoelectric device to either heat or cool the encasement, a total of ten experiments were carried out in an attempt to perform partial battery discharges at a controlled temperature.

It did take two iterations in design in order to achieve temperatures below zero degrees, but unfortunately even in the second iteration the temperature switch control stopped working due to condensation. These were minor problems, as a result additional experiments were carried out and the battery behaviour was exposed as being unpredictable at sustained low temperatures.

9.2 ANALYSIS

As already mentioned in earlier chapters, the data gathered for this research is not substantial enough to claim statistical significance. The data that has been gathered does offer a clear insight into the behaviour of the cells when under varying scenarios.

The analysis has been completed on two fronts, firstly on the behaviour of the cells and the effects from temperature, and secondly analysis of how the behaviour could be exploited in a low power wireless device to extend the service life.

9.2.1 Discharge method

Data available from the manufacturer concentrates on the constant current discharge of the cells for lifetime estimation. In a low power embedded device it is expected that the device would enter an inactive state, and in order to preserve energy the load during the inactive state would be significantly lower than when operational. This behaviour referred to as pulsed discharge has been a major area of analysis.

Importantly using this method of discharge allows for the cells to recover charge during the inactive periods. The right combination of a long inactive period and a discharge current down in the µA range can maximize the service life of the cells. In a low power wireless device, the length of the inactive period is determined by the network behaviour.

9.2.2 Deployment

From the measurement of temperature during all of the discharge tests, coupled with partial battery discharges at temperature extremes, it has been made clear that temperature has a great bearing on the final service life of the batteries.

Early research found that no existing published research projects have been able to operate a wireless sensor network for more than 6 months when powered from standard alkaline cells.

It has been suggested that the network protocol could be optimized by gathering data on the environment the wireless network is to be deployed into. Experimental work has backed the theory that the cells perform better at higher temperatures, so can network traffic be routed using temperature as a variable in the routing algorithm?

This could remove some burden from wireless nodes that for example do not see any sunlight, improving the service life of the network nodes that may be hampered by their operational temperature.

9.2.3 Low power wireless node

The aim has been to justify that it is possible to operate a wireless sensor network from standard alkaline cells for two years or more. Using the data on battery behaviour, and existing research on deployments, a low power wireless sensor node has been designed.

Using the latest low power embedded technology it has been possible to achieve sleep currents in the region of 1 µA. This has required the design of a power management scheme that removes the inefficiencies of any voltage regulation during the sleep state of the node.

The design and build of a prototype had not been originally planned but it offered an excellent way to practically exploit what had been learnt from analysing the battery behaviour. Unfortunately due to time restrictions the nodes have not been deployed into a wireless network.

9.3 FURTHER WORK

In Section 7.1.3 a lifetime estimation model is suggested based on experimental work. From further experimental work it could be possible to see a correlation between constant current discharges and pulsed discharges with the same average discharge current over a single duty cycle. This correlation could be used in conjunction with the constant current lifetime estimation curve, allowing for example the lifetime estimation of cells being used in a wireless sensor node.

For this model to be a reliable source of lifetime estimation substantially more battery discharges would need to be carried out and this would require a large investment in time to achieve.

In Chapter 8 the design of a low powered wireless node is suggested and implemented, unfortunately the deployment of wireless sensor network using these nodes was left incomplete.

The aim had been to deploy a wireless network with the sole purpose of gathering data specifically focused on battery performance. By having the network collect measurements on temperature and cell voltage, along with network protocol data such as dropped packets, a greater picture could be built up on how the wireless network service life could be increased.

9.4 SUMMARY

The research project has explored through experimental work the behaviour of alkaline cells and put in context of using them for powering a wireless sensor node. Given the lack of existing research in this area this research project gives a good foundation for further work.

References

[1] K. Martinez et al., "Deploying a Sensor Network in an Extreme Environment," in *IEEE International Conference on Sensor Networks, Ubiquitous, and Trustworthy Computing*, Taichung, Taiwan, 2006, vol. 1, pp. 186-193.

[2] E. Lou, D. Zbinden, P. Mosberger, D. L. Hill, and V. J. Raso, "A wireless personal wearable network system to understand the biomechanics of orthotic for the treatment of scoliosis," in *2008 30th Annual International Conference of the IEEE Engineering in Medicine and Biology Society*, Vancouver, pp. 3426-3429.

[3] R. Szewczyk, A. Mainwaring, J. Polastre, J. Anderson, and D. Culler, "An analysis of a large scale habitat monitoring application," in *Proceedings of the 2nd international conference on Embedded networked sensor systems, SenSys 2004*, Baltimore, MD, USA, p. 214.

[4] M. Vetterli, "SensorScope: Experiences with a Wireless Building Monitoring Sensor Network - Infoscience," presented at the Workshop on Real-World Wireless Sensor Networks (REALWSN'05), Stockhom, 2005.

[5] J. Wilson, "Chapter 22. Wireless Sensor Networks," in *Sensor Technology Handbook*, Har/Cdr edition., Oxford/GB: Elsevier Science & Technology, 2005, p. 575.

[6] D. Linden, "Part II. Primary Batteries, Chapter 7. Primary Battery Introduction," in *Handbook of batteries*, New York, NY, USA: McGraw-Hill, 2002, p. 7.4, Figure 7.1.

[7] MIT School of Engineering, "Lewis Frederick Urry - Inventor of the Alkaline Cell," *Lemelson-MIT*, Mar-2005. [Online]. Available: http://web.mit.edu/invent/iow/urry.html. [Accessed: 11-Feb-2011].

[8] "Batteryless energy harvesting for embedded designs," *EE Times*, 08-Jan-2009. [Online]. Available: http://www.eetimes.com/design/embedded/4008326/Batteryless-energy-harvesting-for-embedded-designs?pageNumber=3. [Accessed: 24-Jun-2011].

[9] Mintel, *Batteries - UK - February 2010*. Mintel, 2010.

[10] Microchip, "eXtreme Low Power PIC® Microcontrollers with XLP Technology." [Online]. Available: http://www.microchip.com/en_us/technology/xlp/. [Accessed: 13-Dec-2010].

[11] D. Linden, "Part I. Principles of Operation, Chapter 6," in *Handbook of Batteries*, New York, NY, USA: McGraw-Hill, 2002.

[12] K. Langendoen, A. Baggio, and O. Visser, "Murphy Loves Potatoes Experiences from a Pilot Sensor Network Deployment in Precision Agriculture," in *Proceedings 20th IEEE International Parallel & Distributed Processing Symposium*, Rhodes Island, Greece, 2006, pp. 1-8.

[13] Texas Instruments, "Energy Harvesting." [Online]. Available: http://www.ti.com/ww/en/apps/energy-harvesting/index.shtml. [Accessed: 23-Jun-2011].

[14]"Cymbet EnerChip Energy Storage." [Online]. Available: http://www.cymbet.com/content/products.asp. [Accessed: 24-Jun-2011].

[15] D. Linden, "Part II. Primary Batteries, Chapter 10. Alkaline-Manganese Batteries," in *Handbook of batteries*, New York, NY, USA: McGraw-Hill, 2002, p. 10.29 Figure 10.22(a).

[16] D. Linden, "Part II. Primary Batteries, Section 14. Lithium Batteries," in *Handbook of batteries*, New York, NY, USA: McGraw-Hill, 2002, p. 14.62 Figure 14.49.

[17] Ravishankar Rao, S. Vrudhula, and D. N. Rakhmatov, "Battery modelling for energy-aware system design," *Computer*, vol. 36, no. 12, pp. 77-87, Dec. 2003.

[18] C. Ma, Y. Yang, and Z. Zhang, "Constructing Battery-Aware Virtual Backbones in Wireless Sensor Networks," *EURASIP Journal on Wireless Communications and Networking*, pp. 1-15, 2007.

[19] C. F. Chiasserini and R. R. Rao, "Pulsed battery discharge in communication devices," in *Proceedings of the 5th annual ACM/IEEE international conference on Mobile computing and networking - MobiCom '99*, Seattle, Washington, United States, 1999, pp. 88-95.

[20] Duracell, "Alkaline-Manganese Dioxide," *OEM Datasheet Alkaline-Manganese Dioxide Cells*. [Online]. Available: http://www1.duracell.com/oem/Pdf/others/ATB-full.pdf. [Accessed: 01-Jun-2011].

[21]"IEEE-SA -IEEE Get 802 Program." [Online]. Available: http://standards.ieee.org/about/get/802/802.15.html. [Accessed: 28-Jun-2011].

[22] E. Callaway et al., "Home networking with IEEE 802.15.4: a developing standard for low-rate wireless personal area networks," *IEEE Communications Magazine*, vol. 40, no. 8, pp. 70-77, Aug. 2002.

[23] A. Mainwaring, D. Culler, J. Polastre, R. Szewczyk, and J. Anderson, "Wireless sensor networks for habitat monitoring," in *Proceedings of the 1st ACM international workshop on Wireless sensor networks and applications - WSNA '02*, Atlanta, Georgia, USA, 2002, p. 88.

[24] Wei Ye, J. Heidemann, and D. Estrin, "An Energy-Efficient MAC Protocol for wireless sensor networks," in *Proceedings.Twenty-First Annual Joint Conference of the IEEE Computer and Communications Societies*, New York, NY, USA, pp. 1567-1576.

[25] T. Trathnigg, J. Moser, and R. Weiss, "An Energy-Efficient MAC Protocol for Low Traffic Wireless Sensor Networks," in *2008 International Wireless Communications and Mobile Computing Conference*, Crete Island, Greece, 2008, pp. 377-382.

[26] A. B. da Cunha, B. R. de Almeida, and D. C. da Silva, "Remaining Capacity Measurement and Analysis of Alkaline Batteries for Wireless Sensor Nodes," *Instrumentation and Measurement, IEEE Transactions on*, vol. 58, no. 6, pp. 1816-1822, 2009.

[27] G. Barrenetxea, F. Ingelrest, G. Schaefer, and M. Vetterli, "The hitchhiker's guide to successful wireless sensor network deployments," in *Proceedings of the 6th ACM conference on Embedded network sensor systems - SenSys '08*, Raleigh, NC, USA, 2008, p. 43.

[28] P. M. Wightman and M. A. Labrador, "Topology maintenance: Extending the lifetime of wireless sensor networks," in *2009 IEEE Latin-American Conference on Communications*, Medellin, 2009, pp. 1-6.

[29] J. N. Al-Karaki and A. E. Kamal, "Routing techniques in wireless sensor networks: a survey," *IEEE Wireless Communications*, vol. 11, no. 6, pp. 6-28, Dec. 2004.

[30] V. K. Chaurasiya, S. R. Kumar, S. Verma, and G. C. Nandi, "Traffic based clustering in wireless sensor network," in *2008 Fourth International Conference on Wireless Communication and Sensor Networks*, Indore, India, 2008, pp. 83-88.

[31] K. Langendoen and G. Halkes, "Chapter 34 - Energy-Efficient Medium Access Control," in *Embedded System Handbook*, Second., CRC Press, 2005.

[32] J. L. Hill and D. E. Culler, "Mica: a wireless platform for deeply embedded networks," *IEEE Micro*, vol. 22, no. 6, pp. 12-24, Nov. 2002.

[33] S. Moon, T. Kim, and H. Cha, "Enabling Low Power Listening on IEEE 802.15.4-Based Sensor Nodes," in *2007 IEEE Wireless Communications and Networking Conference*, Kowloon, China, 2007, pp. 2305-2310.

[34] T. van Dam and K. Langendoen, "An adaptive energy-efficient MAC protocol for wireless sensor networks," in *Proceedings of the first international conference on Embedded networked sensor systems - SenSys '03*, Los Angeles, California, USA, 2003, p. 171.

[35] D. N. Rakhmatov and S. B. K. Vrudhula, "An analytical high-level battery model for use in energy management of portable electronic systems," in *IEEE/ACM International Conference on Computer Aided Design. ICCAD 2001. IEEE/ACM Digest of Technical Papers (Cat. No.01CH37281)*, San Jose, CA, USA, pp. 488-493.

[36] J. Newman, "DUALFOIL." [Online]. Available: http://www.cchem.berkeley.edu/jsngrp/fortran.html. [Accessed: 30-Jun-2011].

[37] M. Handy and D. Timmermann, "Simulation of Mobile Wireless Networks with Accurate Modelling of Non-linear Battery Effects," *In proceedings of Applied simulation and modeling*, 2003.

[38] M. A. Spohn, P. S. Sausen, F. Salvadori, and M. Campos, "Simulation of Blind Flooding over Wireless Sensor Networks Based on a Realistic Battery Model," in *Seventh International Conference on Networking (icn 2008)*, Cancun, Mexico, 2008, pp. 545-550.

[39] Sung Park, A. Savvides, and M. B. Srivastava, "Battery capacity measurement and analysis using lithium coin cell battery," in *Low Power Electronics and Design, International Symposium on, 2001.*, 2001, pp. 382-387.

[40] Maxim, "Inaccuracies of Estimating Remaining Cell Capacity with Voltage Measurements Alone - Maxim," *Application Note 121*. [Online]. Available: http://www.maxim-ic.com/app-notes/index.mvp/id/121. [Accessed: 30-Jun-2011].

[41] Energizer, "Alkaline Manganese Dioxide - Handbook and Application Manual." Energizer.

[42] Vishay, "The FET Constant-Current Source/Limiter." [Online]. Available: http://www.vishay.com/docs/70596/70596.pdf. [Accessed: 06-May-2011].

[43] Tellurex, "Introduction to Thermoelectrics." [Online]. Available: http://www.tellurex.com/pdf/introduction-to-thermoelectrics.pdf. [Accessed: 08-Jun-2011].

[44] Laird Technologies, "Thermoelectric Assembly Tips." [Online]. Available: http://www.lairdtech.com/WorkArea/linkit.aspx?LinkIdentifier=id&ItemID=2147483685. [Accessed: 22-Jan-2011].

[45] Duracell, "Duracell: Technical/OEM," *MN1500 Battery Online Data Sheet*. [Online]. Available: http://www1.duracell.com/oem/primary/alkaline/mn1500.asp. [Accessed: 13-Jul-2011].

[46] M. T. Penella and M. Gasulla, "Battery Squeezing under Low-Power Pulsed Loads," in *2008 IEEE Instrumentation and Measurement Technology Conference*, Victoria, BC, Canada, 2008, pp. 1184-1188.

[47]"UCB Mica2 Mote Power Benchmark Summary Numbers." [Online]. Available: http://www.eecs.harvard.edu/~shnayder/ptossim/mica2bench/summary.html. [Accessed: 04-Jun-2011].

[48]"DC/DC Converter (Integrated Switch) - Step-Up Regulator - TPS61097-33 - TI.com." [Online]. Available: http://focus.ti.com/docs/prod/folders/print/tps61097-33.html. [Accessed: 22-Jul-2011].

[49] Y. Liu et al., "Long-term large-scale sensing in the forest: recent advances and future directions of GreenOrbs," *Frontiers of Computer Science in China*, vol. 4, no. 3, pp. 334-338, Aug. 2010.

[50] Texas Instruments, "CC2500EM Reference Design." [Online]. Available: http://focus.ti.com/docs/toolsw/folders/print/cc2500em_refdes.html. [Accessed: 19-Jul-2011].

Appendix A

MN1500 Alkaline Manganese Battery Datasheet

DURACELL®
COPPERTOP

MN1500
Size: AA (LR6)
Alkaline-Manganese Dioxide Battery

Zn/MnO_2

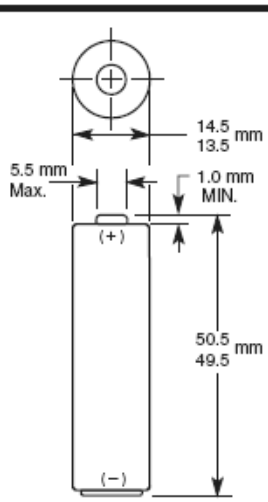

Dimensions shown are ANSI standards

Nominal Voltage:	1.5 V
Operating Voltage	1.6 - 0.75V
Impedance:	120 m-ohm @ 1kHz
Typical Weight:	24 gm (0.8 oz.)
Typical Volume:	8.4 cm^3 (0.5 $in.^3$)
Terminals:	Flat
Storage Temperature Range:	-20°C to 35°C
Operating Temperature Range:	-20°C to 54°C (-4°F to 130°F)
ANSI: / **IEC:**	15A / LR6

TYPICAL DISCHARGE CHARACTERISTICS AT 21°C (70°F)

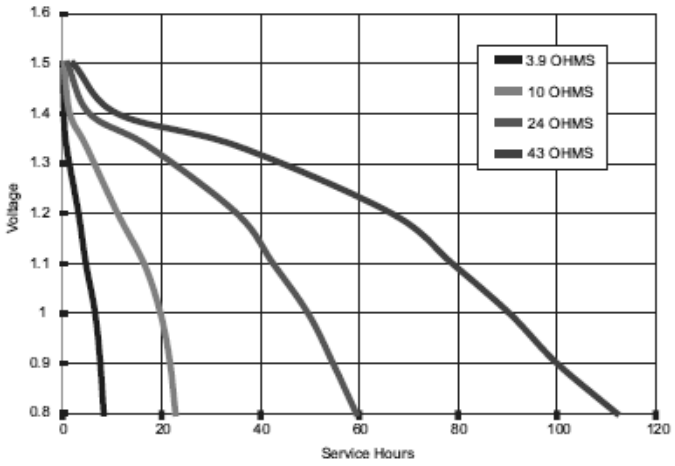

DURACELL BATTERIES
Berkshire Corporate Park
Bethel, CT 06801 U.S.A.
Telephone: Toll-free 1-800-544-6454
Internet: www.duracell.com

* Delivered capacity is dependent on the applied load, operating temperature and cut-off voltage. Please refer to the charts and discharge data shown for examples of the energy / service life that the battery will provide for various load conditions.

This data is subject to change. Performance information is typical. Contact Duracell for the latest information

8/06

DURACELL®
COPPERTOP

MN1500
Size: AA (LR6)
Alkaline-Manganese Dioxide Battery

Zn/MnO_2

TYPICAL CONSTANT CURRENT DISCHARGE CHARACTERISTICS AT 21°C (70°F)

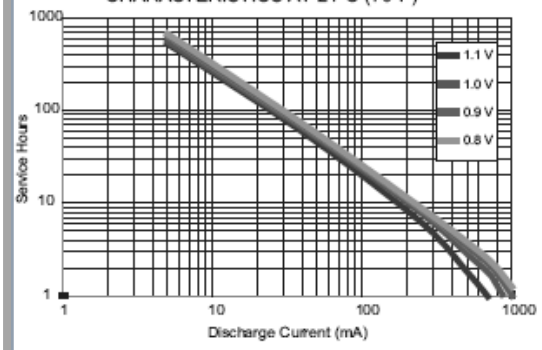

TYPICAL DISCHARGE CHARACTERISTICS AT 21°C (70°F)

This is the graph that is repeatedly referred to during the various chapters.

TYPICAL DISCHARGE CHARACTERISTICS AT 21°C (70°F)

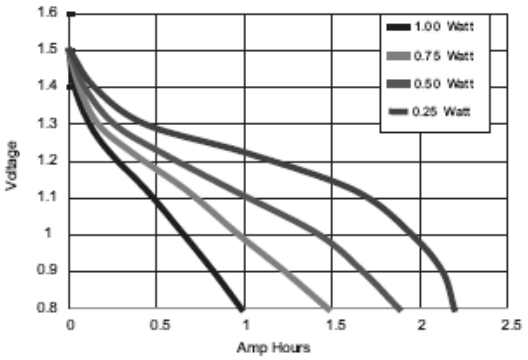

TYPICAL DISCHARGE PERFORMANCE AT 21°C (70°F)

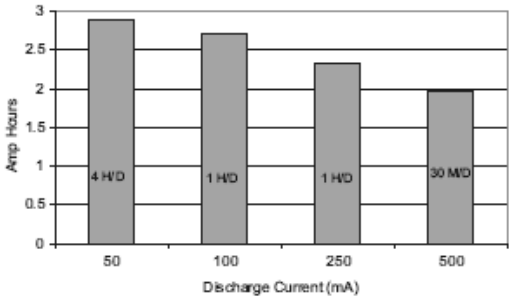

TYPICAL DC RESISTANCE CHARACTERISTICS AT 21°C (70°F)

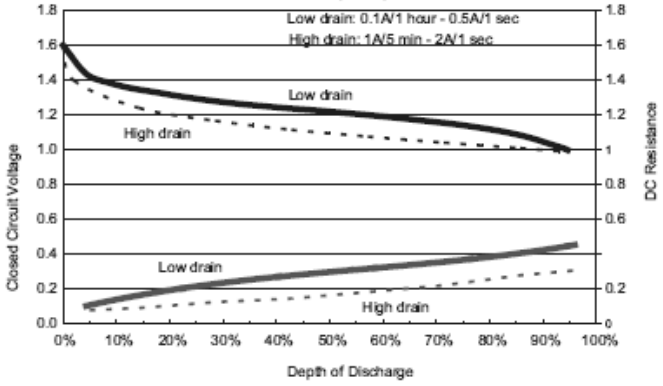

DURACELL BATTERIES
Berkshire Corporate Park
Bethel, CT 06801 U.S.A.
Telephone: Toll-free 1-800-544-5454
Internet: www.duracell.com

* Delivered capacity is dependent on the applied load, operating temperature and cut-off voltage. Please refer to the charts and discharge data shown for examples of the energy / service life that the battery will provide for various load conditions.

Appendix B
System Hardware

This appendix covers the measurement system hardware, including the schematics for the measurement system and the modules that were used for the experimental work. In addition to this there are photographs of the Measurement system and details on the precision and accuracy of the system.

B.1 Measurement System Schematics

This section contains the following:

- Measurement Core Schematics
    - Parent Schematic
    - Battery Module
    - Microcontroller and supporting components
    - Serial Peripheral Interface
        - IO Expander
        - SD Card Interface
        - External DAC
        - Additional ADC
- JFET Constant Current Module
- Voltage Controlled Constant Current Module
- Voltage Measurement Module

B.1.1 System Core Schematics

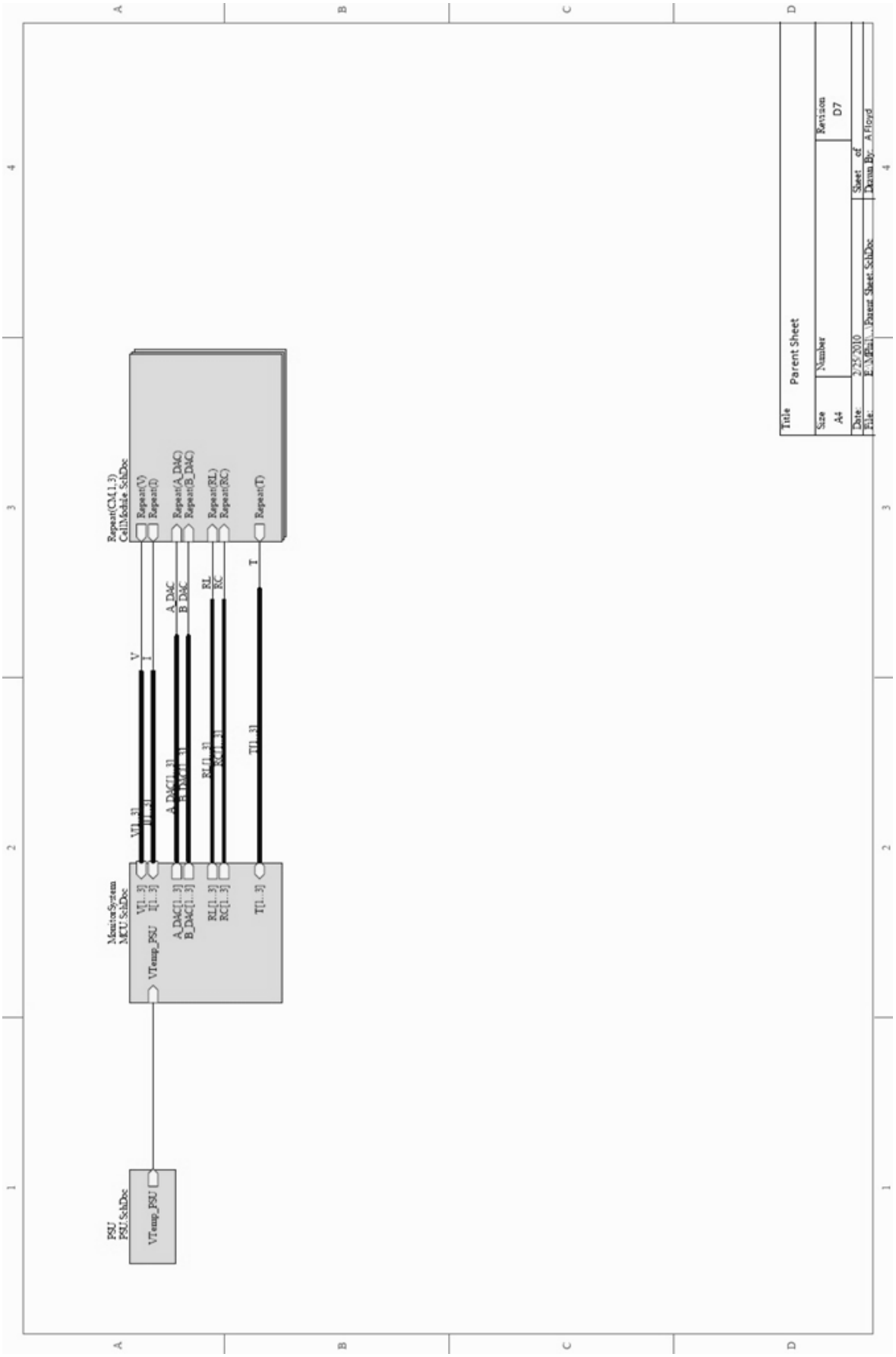

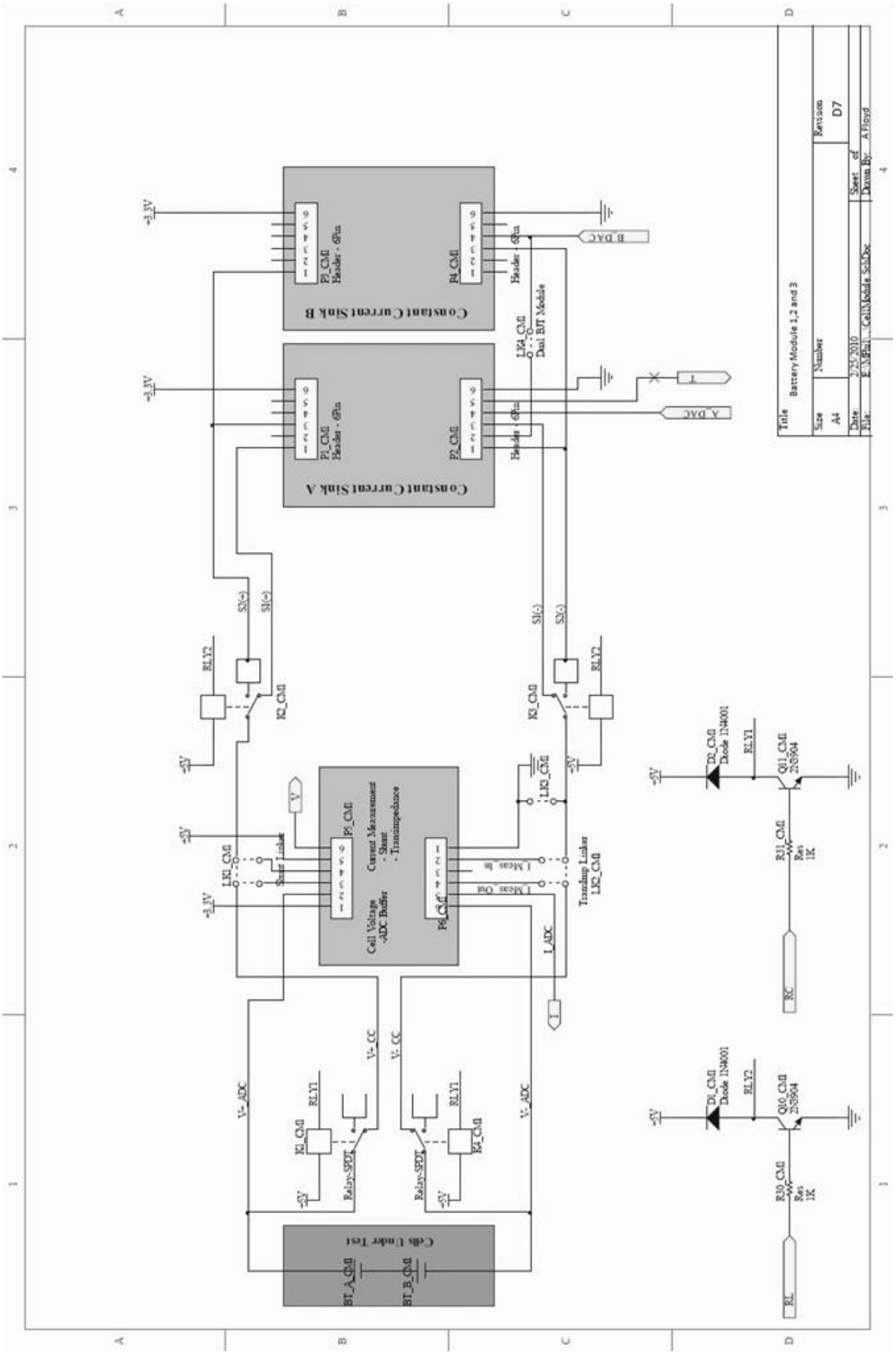
Constant Current Sink B
Constant Current Sink A
Cell Voltage
-ADC Buffer
Current Measurement
- Shunt
- Transimpedance
Cable Under Test
Battery Module 1,2 and 3
Dual BIT Module
Shunt Linker
Transimp Linker
Relays-SPDT
Diode 1N4001
2N3904
Rev
A Floyd
D7

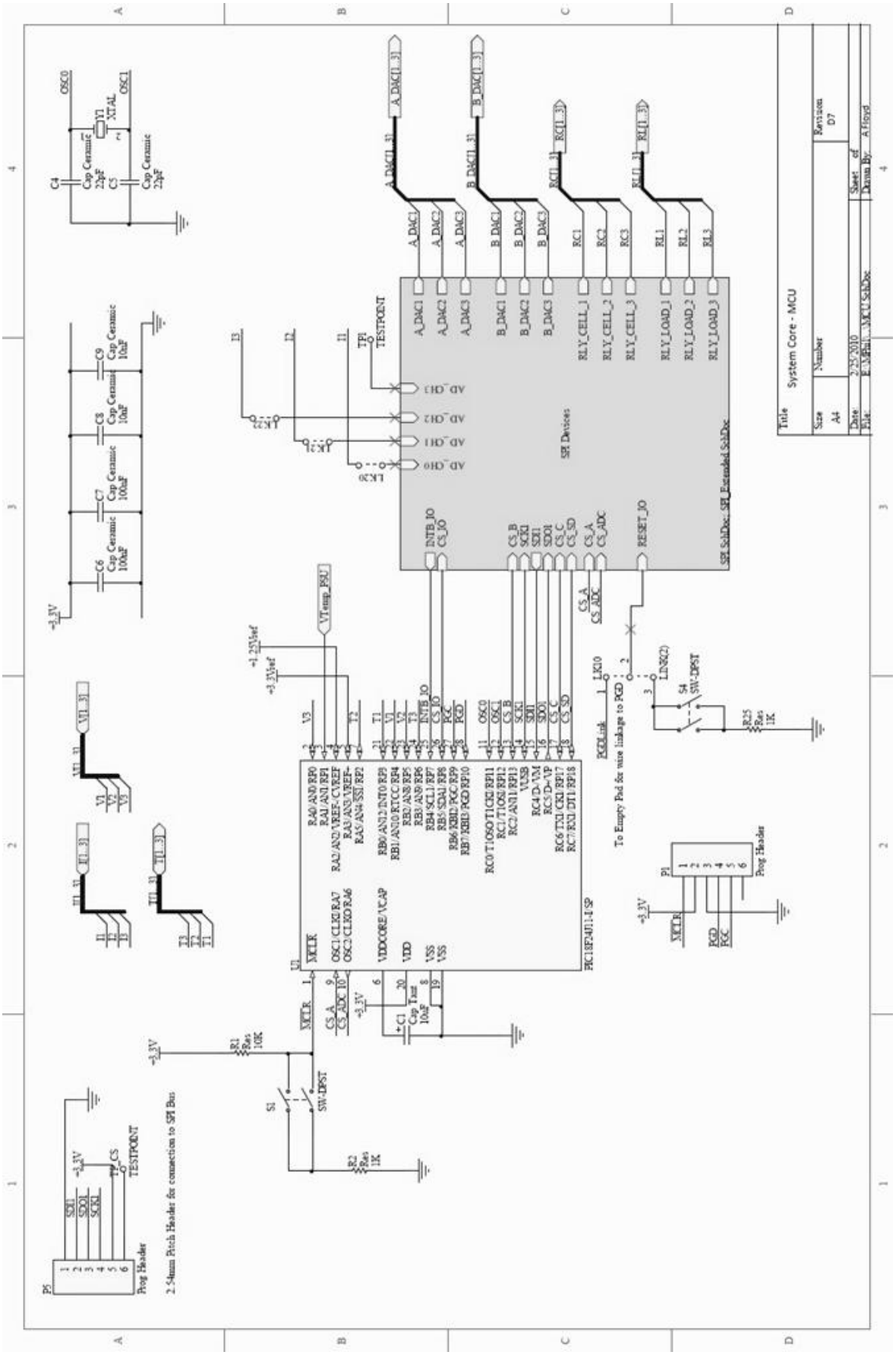
Title
System Core - MCU
Size
A4
Number
Revision
D7
Date:
2/25/2010
Sheet of
File:
E:\Mplab\...\MCU.SchDoc
Drawn By:
A.Floyd
SPI Devices
SPI SchDoc
SPI_Extended.SchDoc
PIC18F4431-I/SP
Cap Ceramic 22pF
Cap Ceramic 100nF
Cap Ceramic 10nF
Cap Tant 10uF
XTAL
SW-DPST
Res 10K
Res 1K
Prog Header
2.54mm Pitch Header for connection to SPI Bus
To Empty Pad for wire linkage to PGD
TESTPOINT
PCOLink

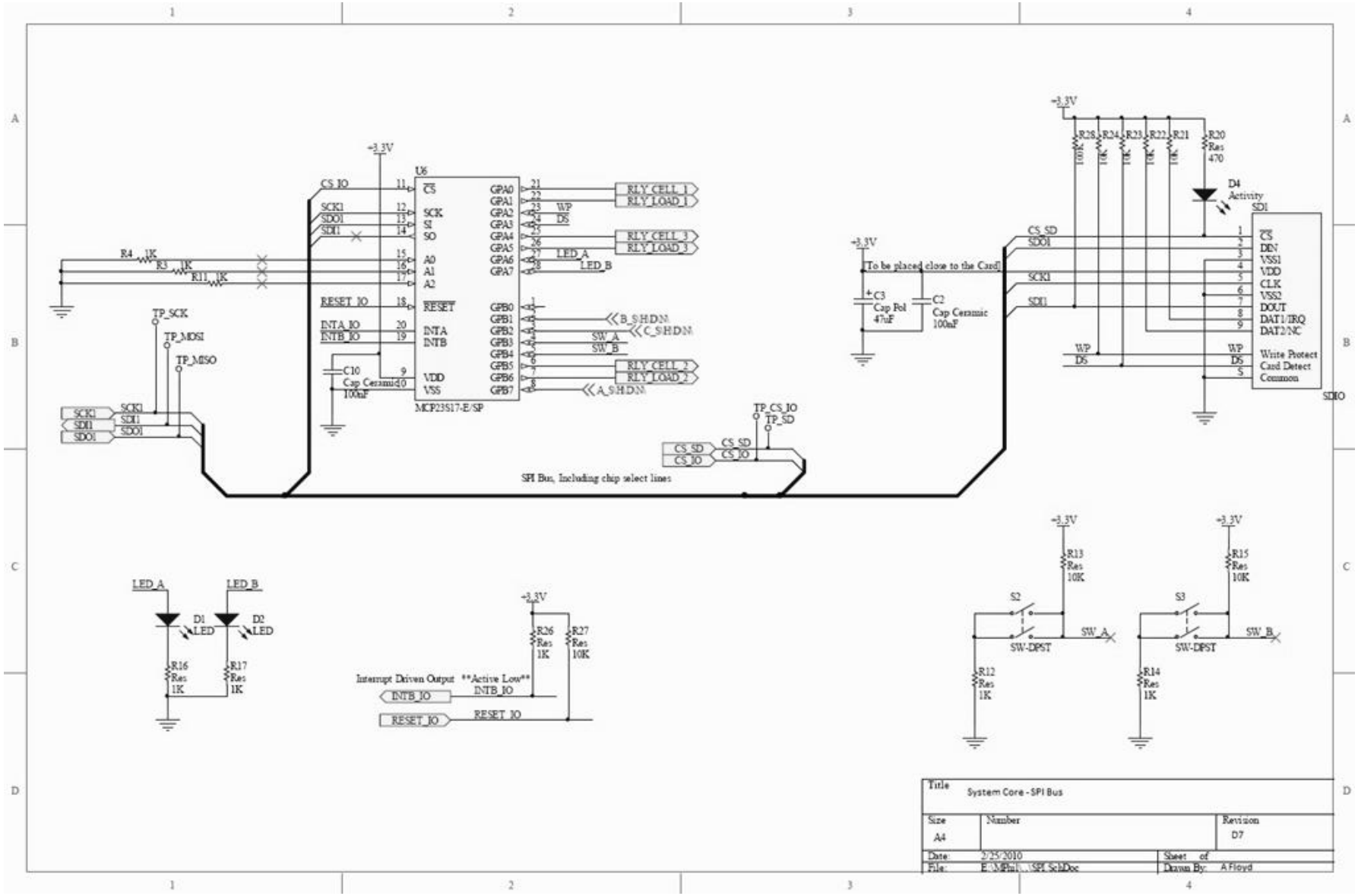
+3.3V
U6
MCP23S17-E/SP
CS_IO
SCK1
SDO1
SDI1
RESET_IO
INTA_IO
INTB_IO
R4 1K
R3 1K
R11 1K
C10
Cap Ceramic
100nF
TP_SCK
TP_MOSI
TP_MISO
TP_CS_IO
TP_SD
CS_SD
SPI Bus, Including chip select lines
RLY_CELL_1
RLY_LOAD_1
RLY_CELL_3
RLY_LOAD_3
RLY_CELL_2
RLY_LOAD_2
LED_A
LED_B
B_SHDN
C_SHDN
A_SHDN
SW_A
SW_B
WP
DS
To be placed close to the Card
C3
Cap Pol
47uF
C2
Cap Ceramic
100nF
R28
R24
R23
R22
R21
R20
Res
470
D4
Activity
SDI
CS
DIN
VSS1
VDD
CLK
VSS2
DOUT
DAT1/IRQ
DAT2/NC
Write Protect
Card Detect
Common
SDIO
D1
LED
D2
LED
R16
Res
1K
R17
Res
1K
Interrupt Driven Output **Active Low**
R26
Res
1K
R27
Res
10K
R13
Res
10K
R15
Res
10K
S2
S3
SW-DPST
R12
Res
1K
R14
Res
1K
Title
System Core - SPI Bus
Size
A4
Number
Revision
D7
Date:
2/25/2010
Sheet of
File:
E:\Mpfl...\SPI.SchDoc
Drawn By:
A Floyd

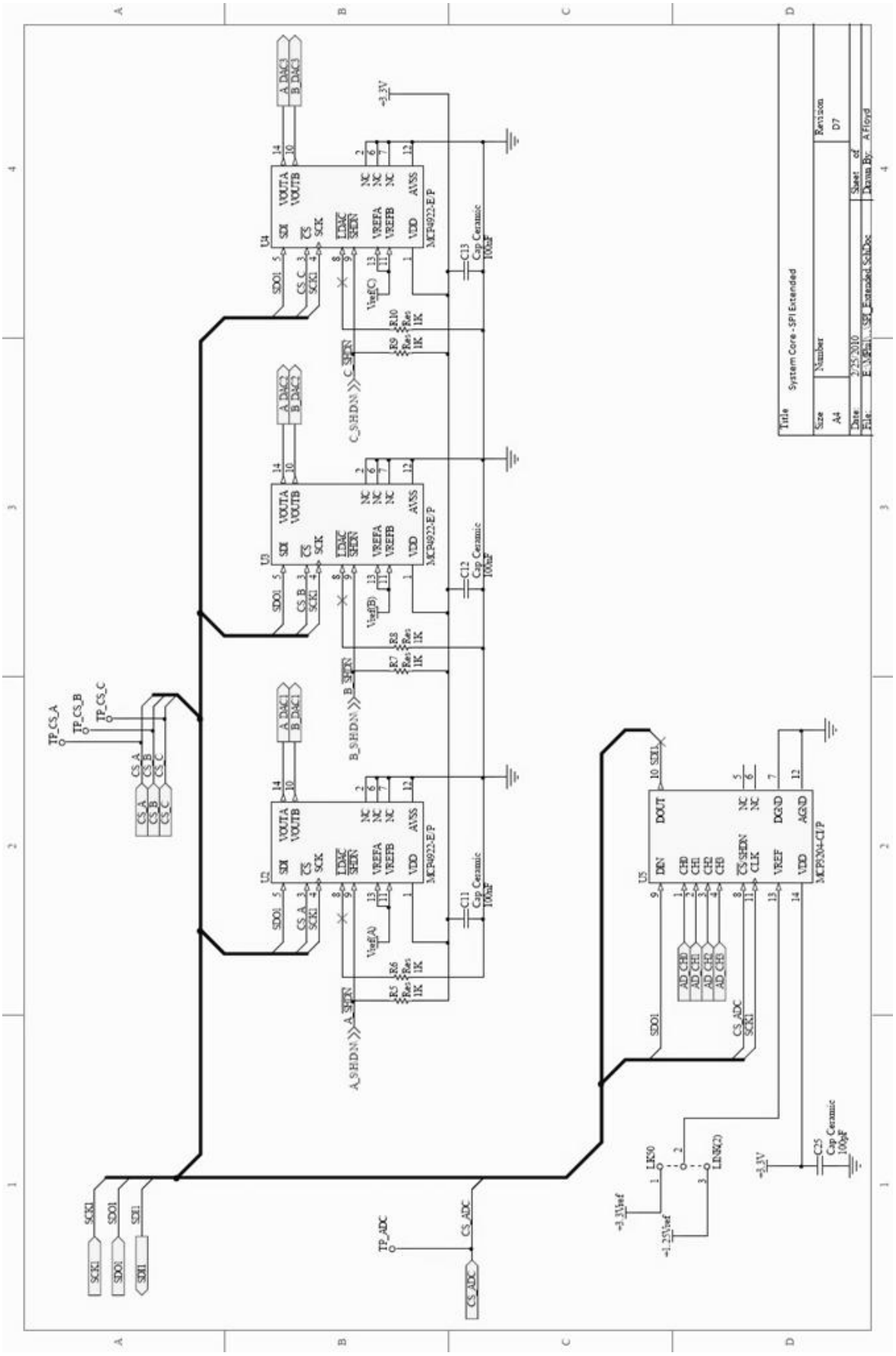
System Core - SPI Extended
Size A4
Number
Revision D7
Date: 2/25/2010
File: E:\Misc\...\SPI_Extended.SchDoc
Sheet of
Drawn By: AFloyd
MCP4922-E/P
MCP3304-CI/P
A_SHDN
B_SHDN
C_SHDN
TP_CS_A
TP_CS_B
TP_CS_C
TP_ADC
CS_ADC
SCK1
SDO1
SDI1
+3.3V
+3.3Vref
+1.25Vref
Cap Ceramic 100nF
Res 1K

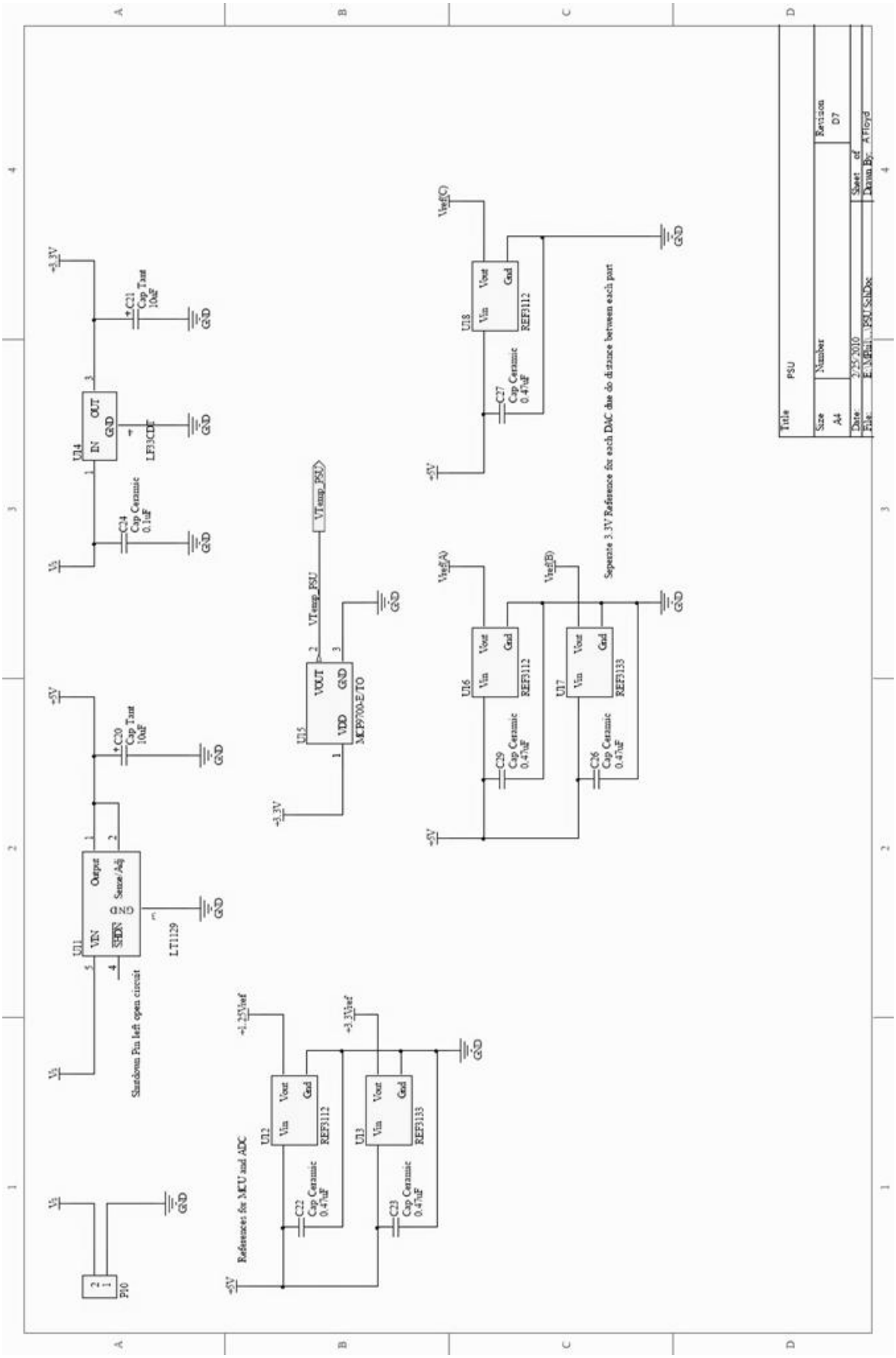
Title PSU
Size A4
Number
Revision D7
Date 2/25/2010
File E:\Mikro...\PSU.SchDoc
Sheet of
Drawn By: A Floyd
Separate 3.3V Reference for each DAC due do distance between each part
Shutdown Pin left open circuit
References for MCU and ADC
U11 LT1129
U12 REF3112
U13 REF3133
U14 LF33CDT
U15 MCP9700-E/TO
U16 REF3112
U17 REF3133
U18 REF3112
C21 Cap Tant 10uF
C22 Cap Ceramic 0.47uF
C23 Cap Ceramic 0.47uF
C24 Cap Ceramic 0.1uF
C26 Cap Ceramic 0.47uF
C27 Cap Ceramic 0.47uF
C29 Cap Ceramic 0.47uF
C30 Cap Tant 10uF
P10
VTemp_PSU
VrefA
VrefB
VrefC
+5V
+3.3V
GND

B.1.2 JFET Constant Current Module

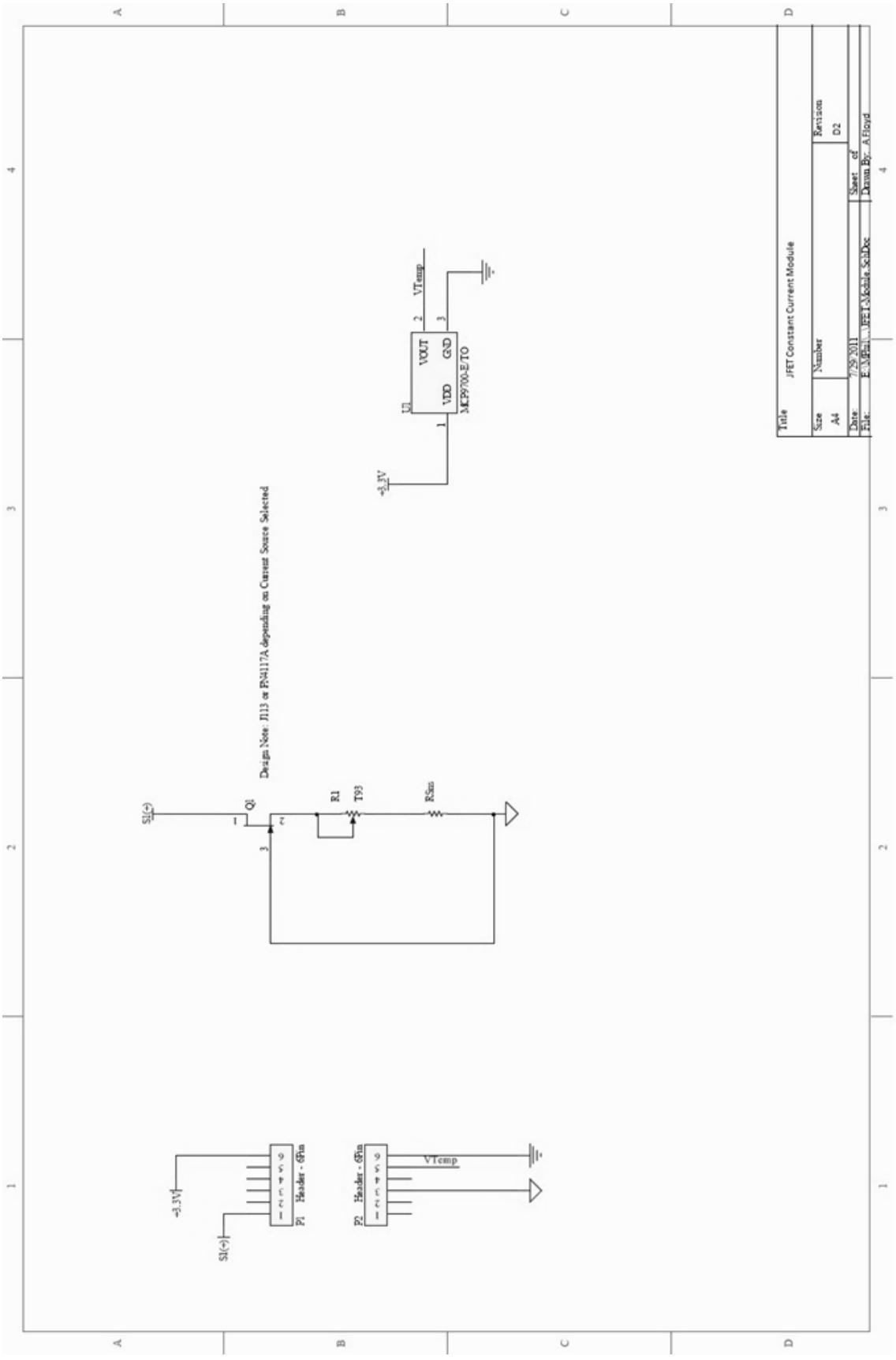

B.1.3 Voltage Controlled Constant Current Module

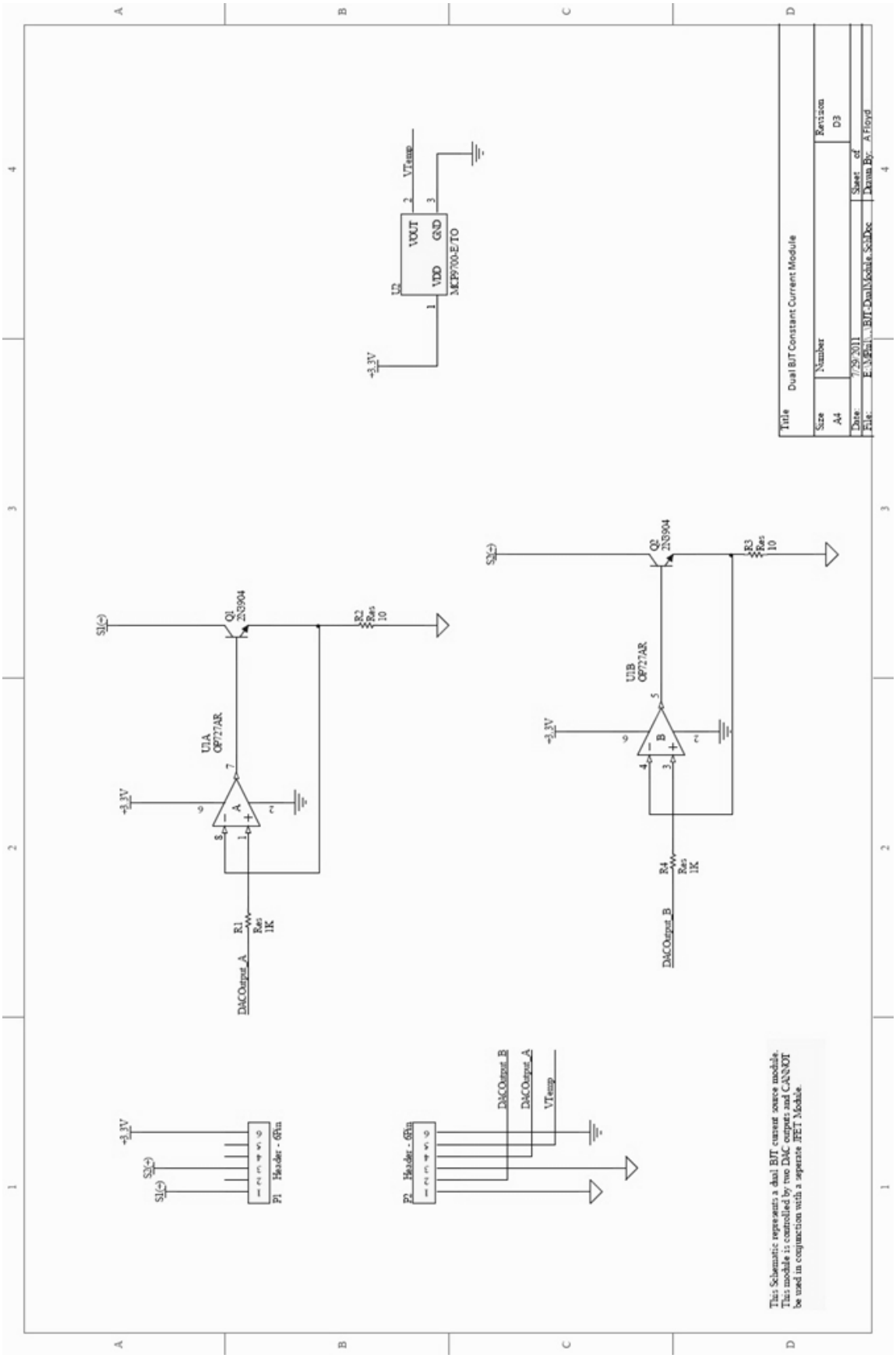

B.1.4 Voltage Measurement Module

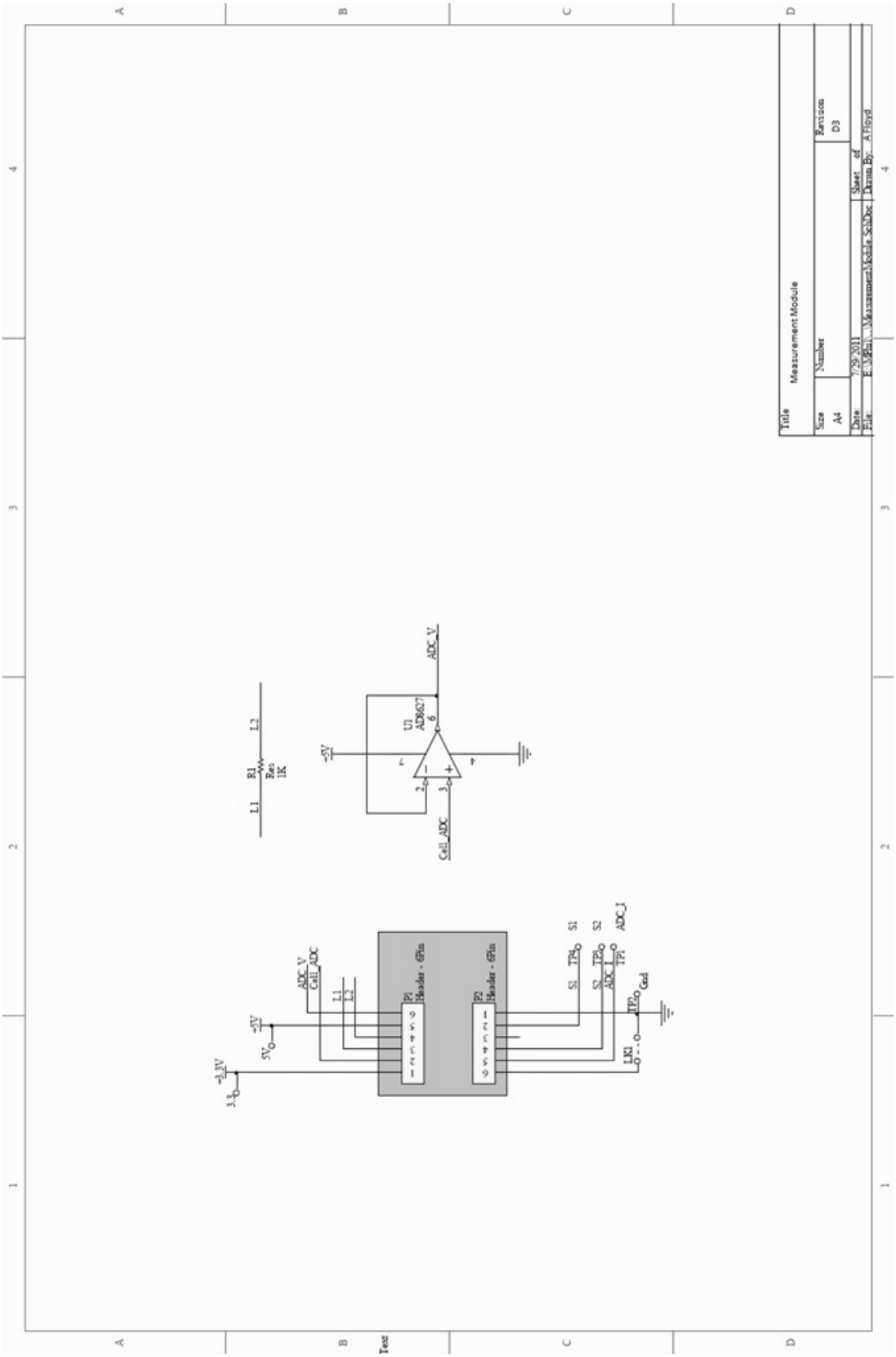

B.2 Measurement System Photographs

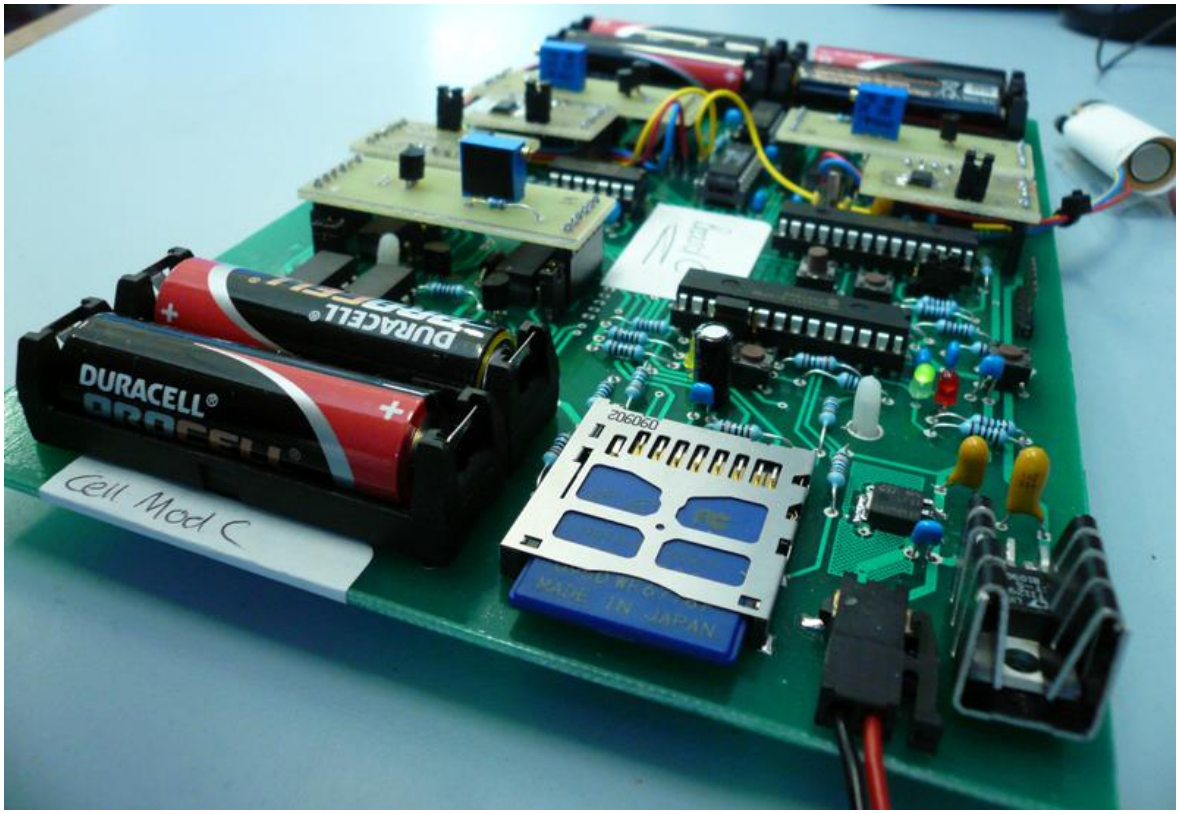

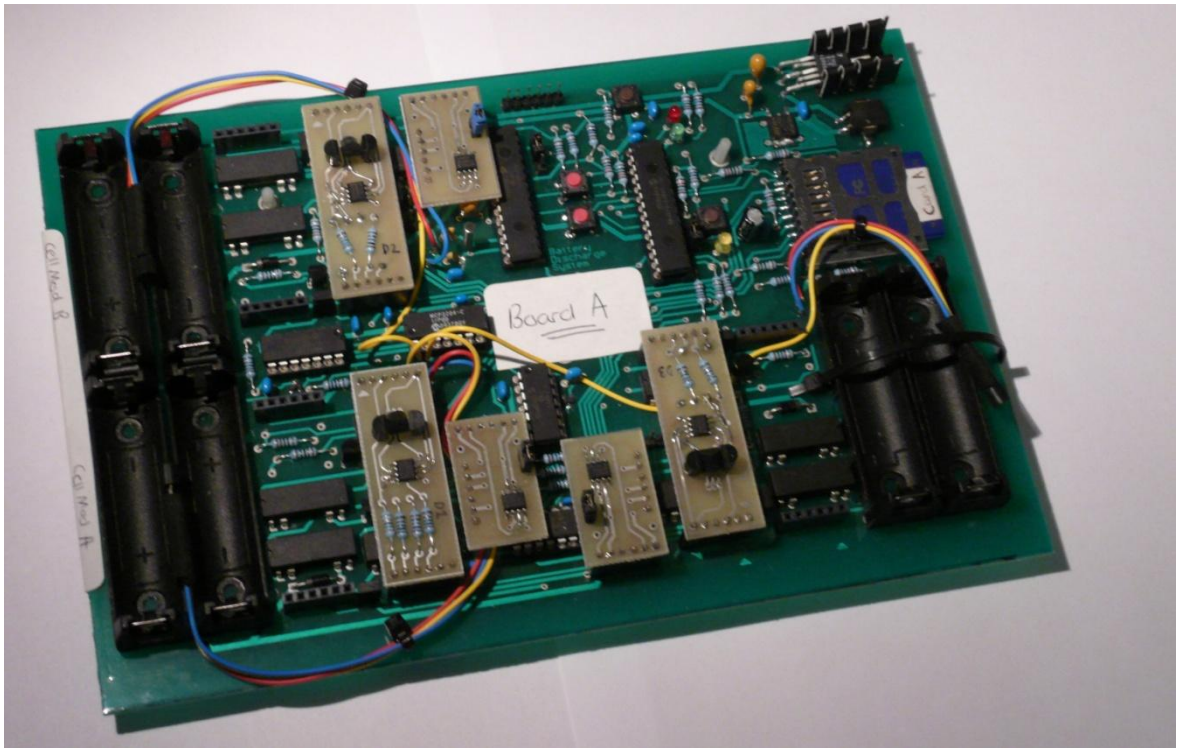

B.3 Measurement System Precision and Accuracy

All of the constant current sources were configured using a 6.5 digit digital multimeter and the temperature coefficient of the load resistors considered. Given that all experiments will take place close to 23 °C ambient it has been assumed that temperature will not have a significant effect on the calibration of the constant current sources. All of the constant current sources were therefore configured to within ±2 % accuracy.

The seven 10 bit ADC channels use precision voltage references of 1.25 V and 3.3 V to sample the input. The voltage references have a maximum error of 0.2% in accuracy. Based on the input range of the ADC therefore gives a resolution of 2 mV.

The four auxiliary ADC channels use a 12 bit ADC. These channels however are sampled between the ground of the IC and either a reference voltage of 1.25 V or 3.3 V. When using a maximum reference of 1.25 V, the ADC has a resolution of 305 µV, and when using 3.3 V a resolution of 800 µV.

The auxiliary channels for the majority of experiments were connected to a linear active thermistor IC. This thermistor has a resolution of 10.0 mV/ °C; this means the greatest degree of error is with this thermistor and not the ADC.

The accuracy of the thermistor IC used is ± 2 °C in the range of 0 °C and 70 °C.

Appendix C

System Software

The following appendix details the software of both the measurement system and the accompanying windows software for data processing.

This is followed by the format of the data stored on the SD card and the data frame that is logged into the binary file at every sampling period.

C.1 SYSTEM SETUP

The following is an example setup:

- **DAC setup for if 'BJT LOAD' selected**

```
// DAC Calibration Values
//DAC A is connected to 100 Ohm Sense resistor i.e. providing 1mA & 10mA
#define CAL_DAC_A1      0x014D//@1mA    OR  0x0D00//@10mA
#define CAL_DAC_B1      0x014D//@1mA    OR  0x0D00//@10mA
#define CAL_DAC_C1      0x014D//@1mA    OR  0x0D00//@10mA

//DAC B is connected to 10 Ohm Sense Resistor i.e. providing 10mA & 100mA
#define CAL_DAC_A2      0x0D6C//@100mA  OR  0x014D//@10mA
#define CAL_DAC_B2      0x0D58//@100mA  OR  0x014D//@10mA
#define CAL_DAC_C2      0x0D70//@100mA  OR  0x014D//@10mA
```

- **Load Type**

```
#define MODA_LOAD                   DUAL_LOAD
#define MODA_LOAD1_TYPE             BJT_LOAD            //Inactive Load
#define MODA_LOAD2_TYPE             BJT_LOAD            //Active Load
```

- **Timing ratios**

```
#define MODA_RATIO_LOAD1            10
#define MODA_RATIO_LOAD2            60

#define MODA_LOAD1_PERIOD           AMASK_1_MIN         //RATIO1*LOAD1_PERIOD
#define MODA_LOAD2_PERIOD           AMASK_1_SEC         //RATIO2*LOAD2_PERIOD

#define MODA_LOAD1_PVALUE           PVALUE_1_MIN        //Period counts
#define MODA_LOAD2_PVALUE           PVALUE_1_SEC        //Period counts
```

- **Post sampling period setup**

```
//PostActive i.e. how many load2 periods within 1 load1 period for PostActive state
#define MODA_LOAD_POSTCOUNT         30
//PostInactive  i.e. how many load2 periods within 1 load1 period for PostInactive state
#define MODA LOAD PRECOUNT          30
```

- **End of test cell voltage measured by the ADC**

```
//ADC Cut Off values
#define MODA_CUTOFF                 25      //(1.3V VCell) Cell put into Open Circuit
#define MODA_TESTCUT                175     //(1.6V VCell) Point of End of Test
```

The example setup above is for a discharge test summarized as the following:

- Using voltage controlled constant current module set at 1 mA (Inactive) and 100 mA (Active) depending on the timing period.
- The timing ratios are set at 10 minutes for the inactive period and 1 minute for the active period.
- At the beginning and end of the inactive period there will be a 30 second period of increased sampling (PRECOUNT and POSTCOUNT)

  The test will end at cell voltage of 1.6 V but will not put he cells into open circuit until 1.3 V is reached.

C.2 WINDOWS APPLICATION

The following will give a brief explanation of the accompanying windows software for processing the data gathered on the SD card.

C.2.1 IMPORT

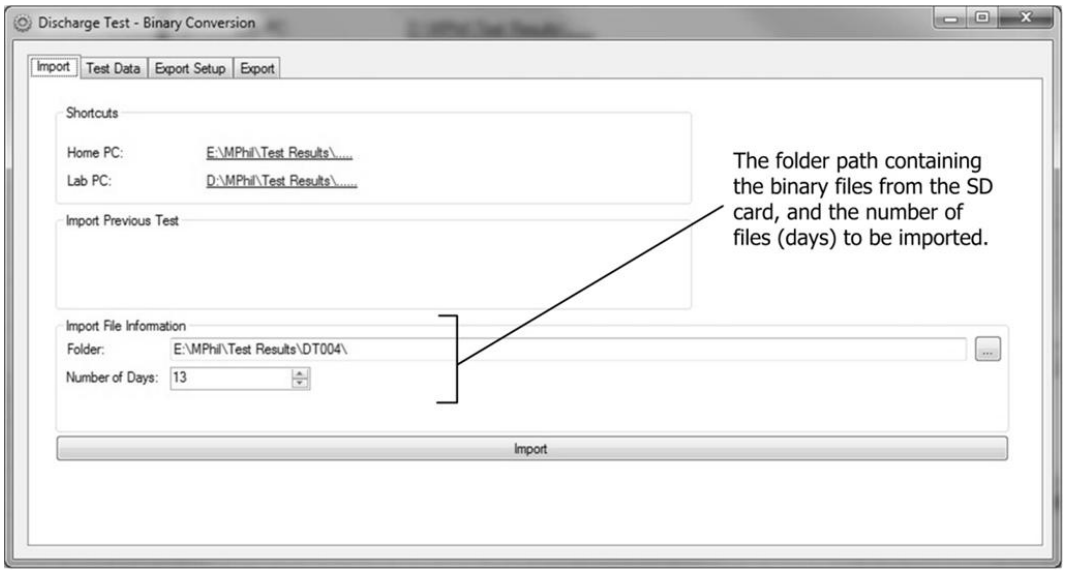

C.2.2 TEST SETUP SUMMARY

This is a summary of the test that is imported from the binary files.

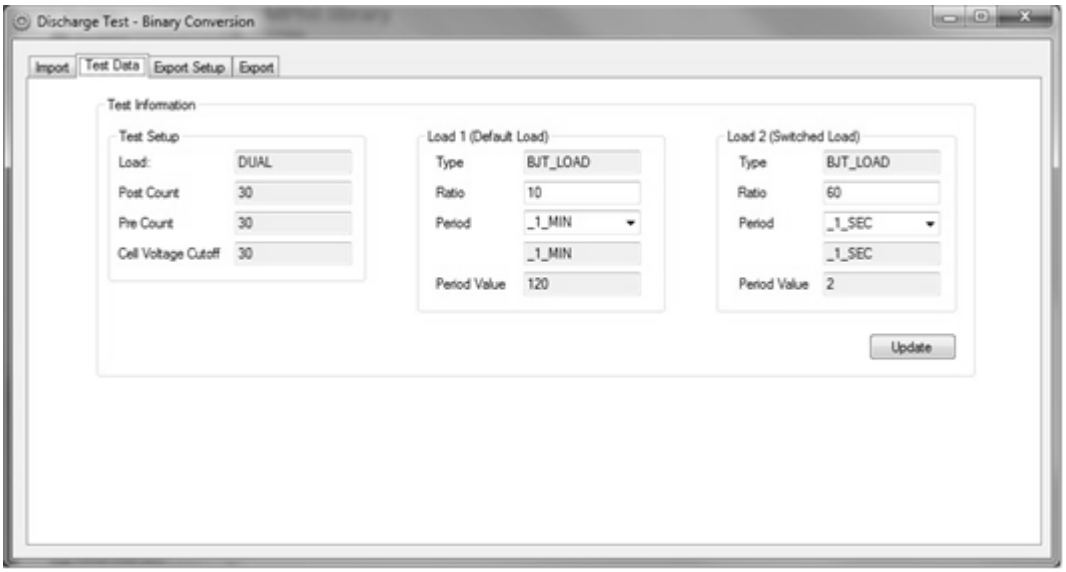

C.2.3 Export Settings

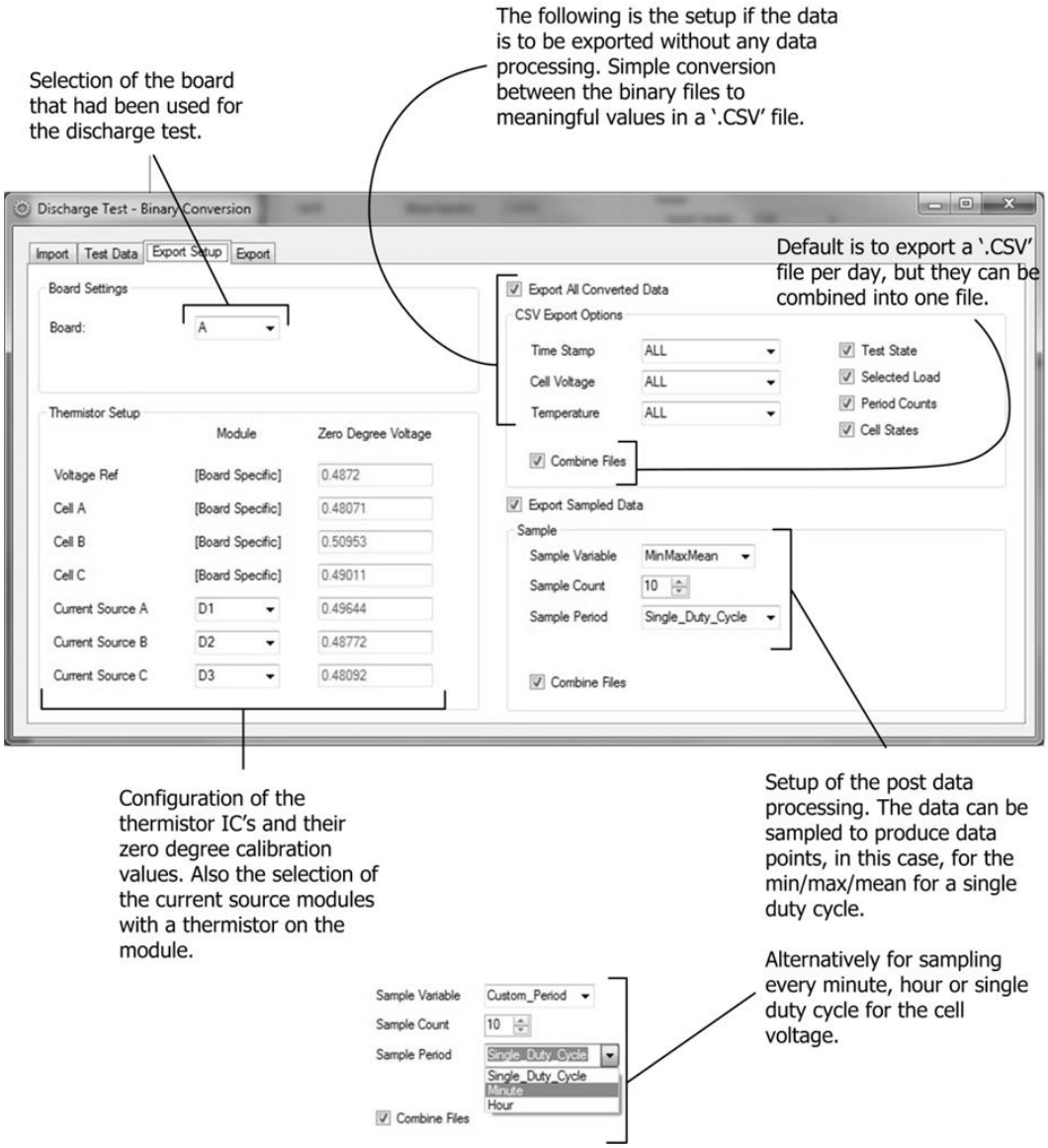

C.2.4 Export files

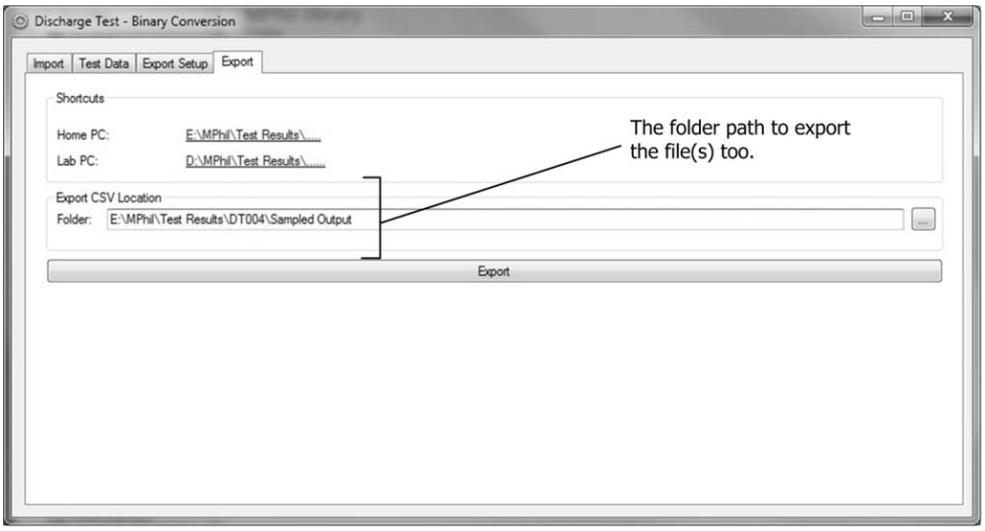

C.3 DATA STORAGE

The following table summarises the 32 Byte frame recorded for every sample.

Data	Value Range	Index	Length (Bytes)
Frame ID	0x10	0	1
Seconds	0x00 to 0x59	1	1
Minutes	0x00 to 0x59	2	1
Hours	0x00 to 0x23	3	1
Day	0x01 to 0x31	4	1
Month	0x01 to 0x12	5	1
State and Load	0x00 to 0xFF	6	1
Cell Voltage CH1	0x0000 to 0x03FF	7	2
Cell Voltage CH2	0x0000 to 0x03FF	9	2
Cell Voltage CH3	0x0000 to 0x03FF	11	2
Temperature CH1	0x0000 to 0x03FF	15	2
Temperature CH2	0x0000 to 0x03FF	17	2
Temperature CH3	0x0000 to 0x03FF	19	2
VRef Temperature	0x0000 to 0x03FF	13	2
Count Period	0x00 to 0xFF	21	1
Count Post	0x00 to 0xFF	22	1
Count Pre	0x00 to 0xFF	23	1
Cell States	0x00 to 0xFF	24	1
External ADC CH1	0x0000 to 0x0FFF	25	2
External ADC CH1	0x0000 to 0x0FFF	27	2
External ADC CH1	0x0000 to 0x0FFF	29	2
Checksum	0x00 to 0xFF	31	1

Appendix D

Temperature Controlled Encasement

The temperature controlled encasement has been designed for the sole purpose of being able to discharge a pair of cells whilst being kept at a desired temperature above or below ambient, to see the effects of temperature on cells.

The following appendix provides more information on the design of the encasement, including the mechanical drawings and details on the design iteration, and then a summary of where the framework could be improved.

D.1 MECHANICAL DESIGN

There have been two designs, D1 and D2, used for the encasement of the cells. The change from the initial design was due to not being able to achieve the desired temperature below freezing.

An exploded view of the initial design D1 seen in Figure D.2, and a picture of the final assembly with and without the insulation can be seen Figure D.2. The exploded view of the second design, D2, can be found in Section 4.6.2 Figure 4.6. In section D.1.1 the mechanical drawing of the encasement can be found.

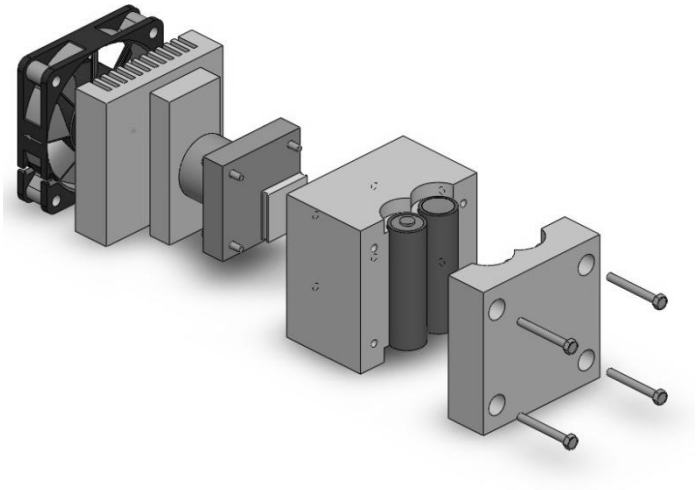

Figure D.1 - Exploded view of initial encasement design

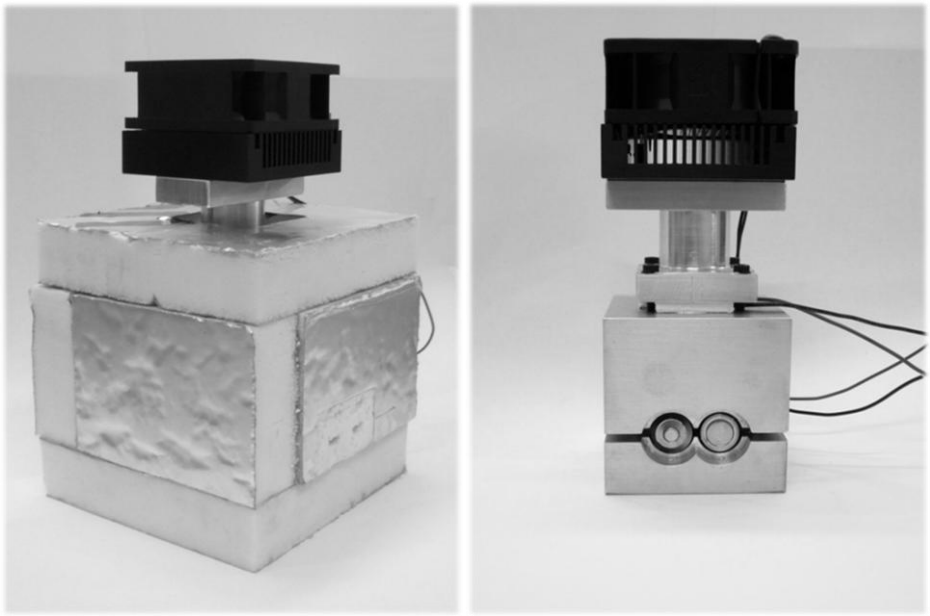

Figure D.2 - Pictures of initial encasement design with and without insulation

A major problem of the first design was that to change the batteries out of the encasement meant disassembling the entire encasement. Changes in the second design iteration meant that the batteries could be accessed from the bottom of the insulation, ensuring that once the peltier device had been bound to the aluminium encasement using thermal paste it would not need to be removed. This feature can be seen in Figure D.3 alongside an image of the final design with insulation.

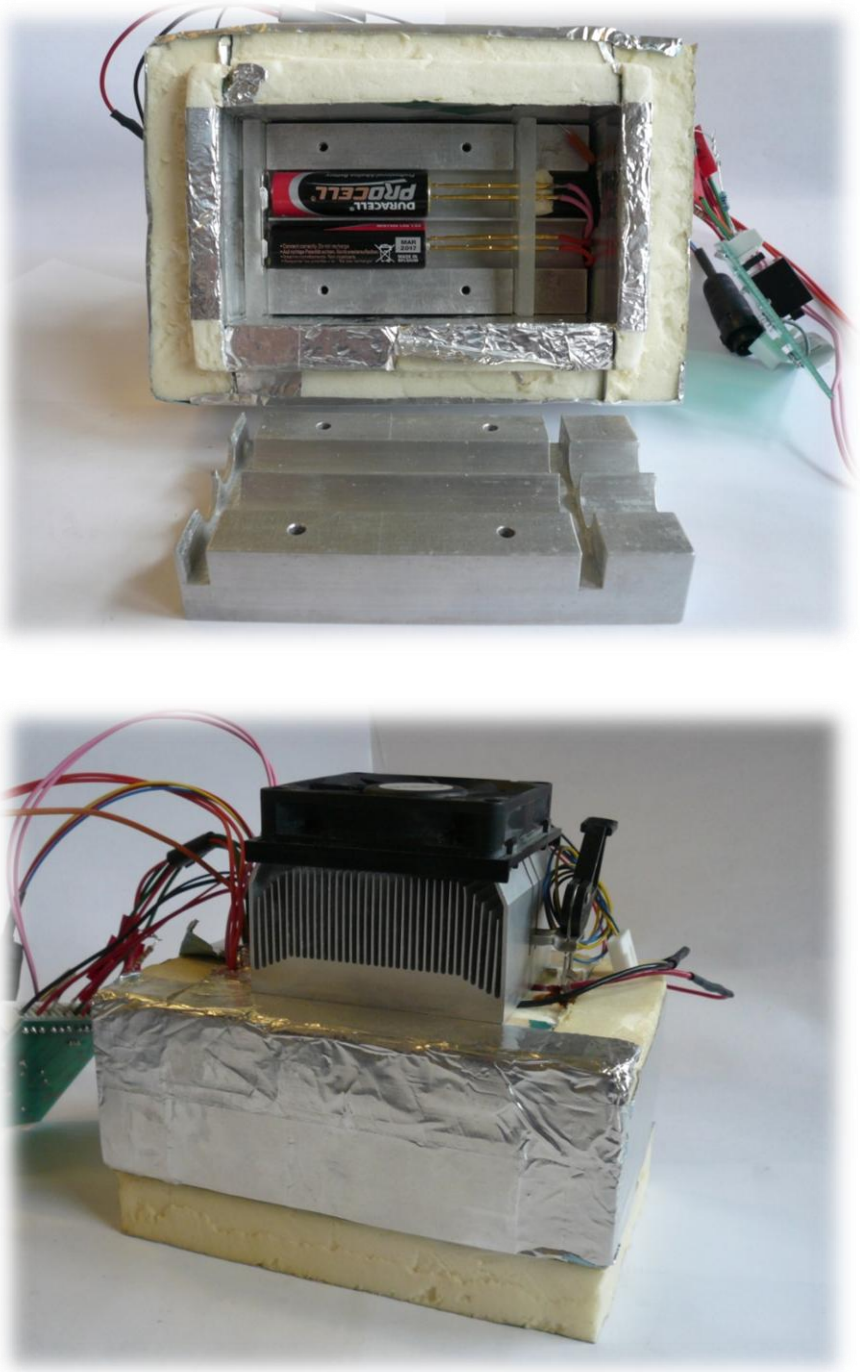

Figure D.3 - Images of final design iteration assembled

D.1.1 Mechanical Drawings of Design D2

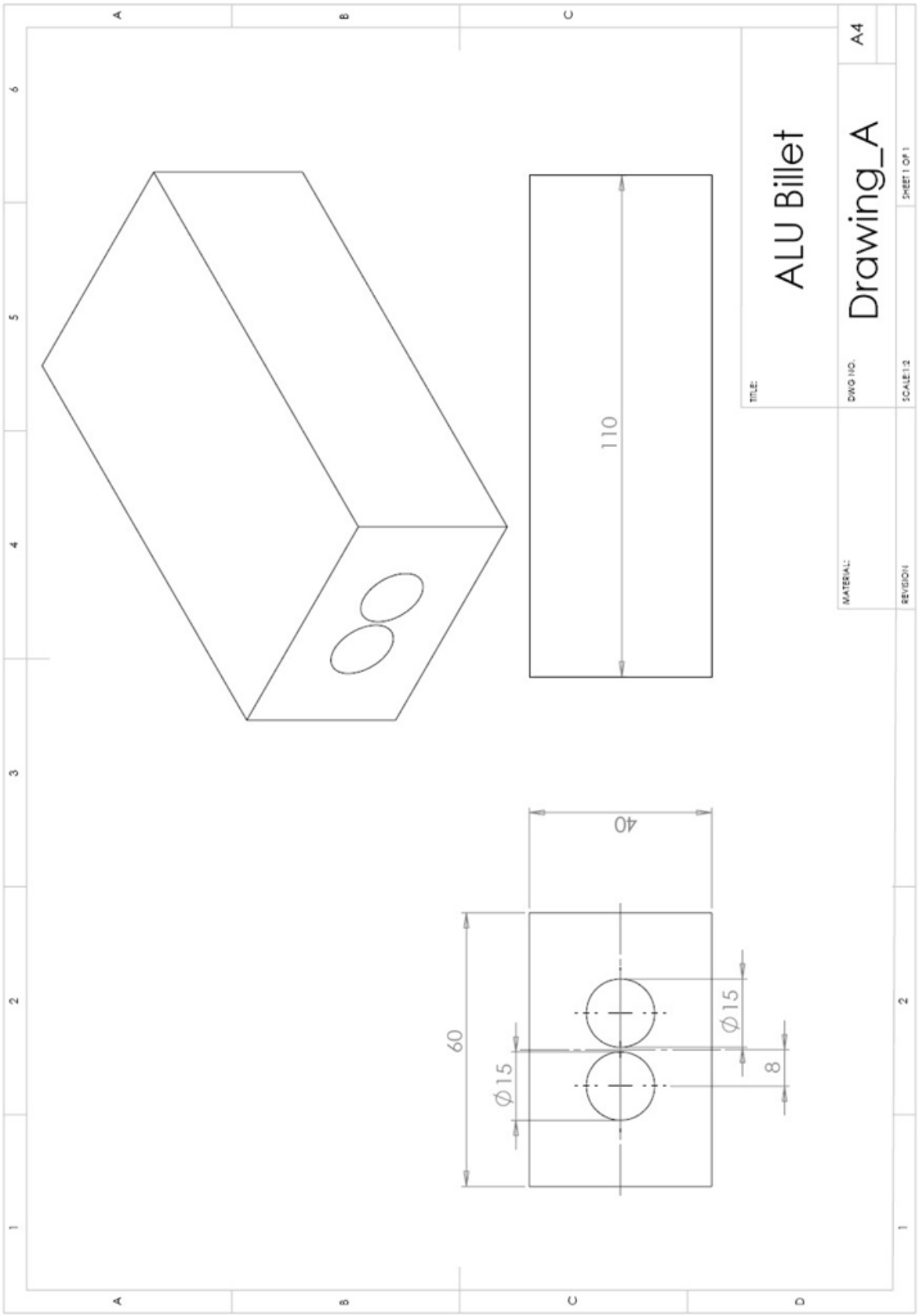

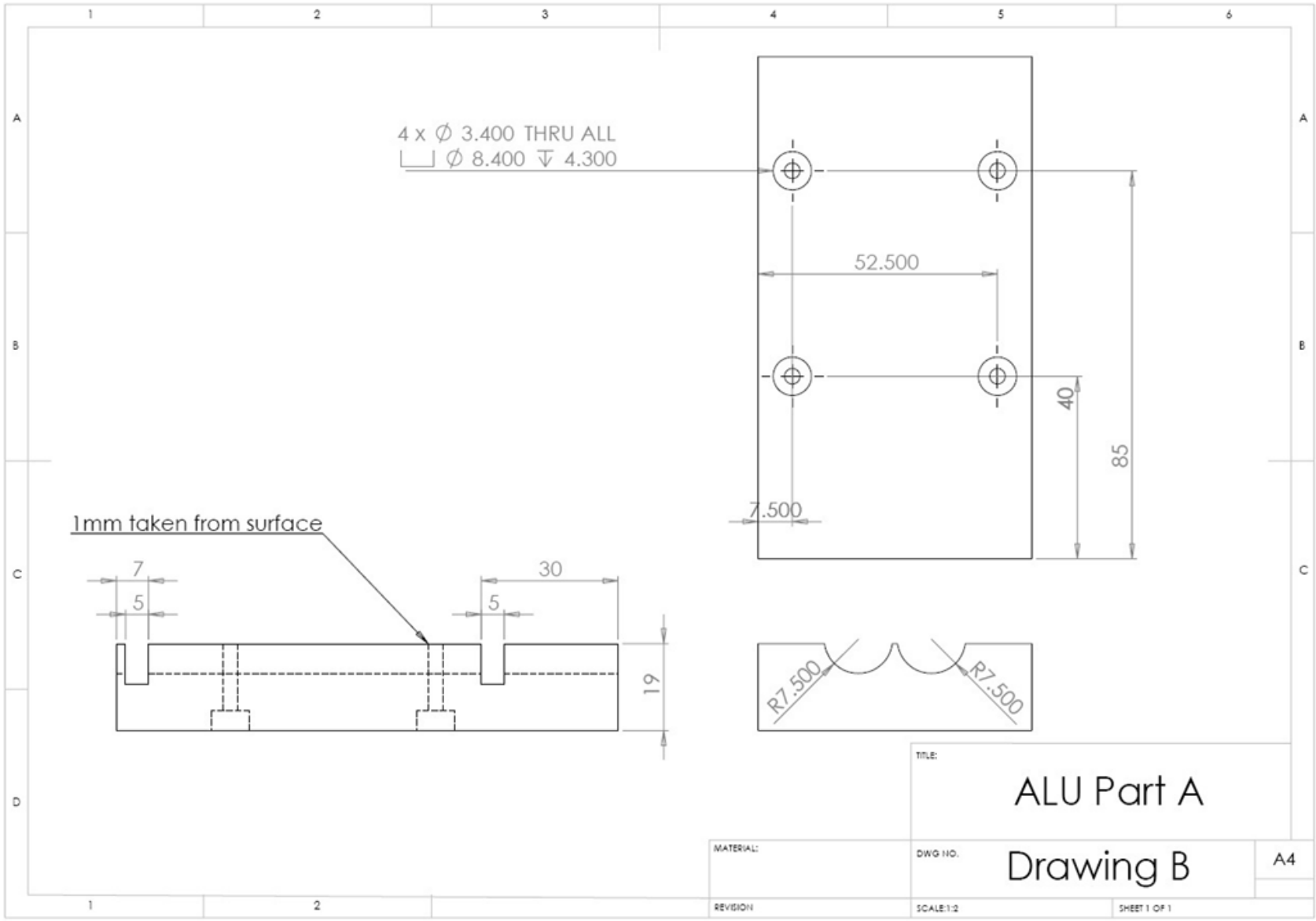
4 x ∅ 3.400 THRU ALL
⌴ ∅ 8.400 ↧ 4.300
52.500
40
85
7.500
1mm taken from surface
7
5
30
5
19
R7.500
R7.500
TITLE:
ALU Part A
MATERIAL:
DWG NO.
Drawing B
A4
REVISION
SCALE:1:2
SHEET 1 OF 1

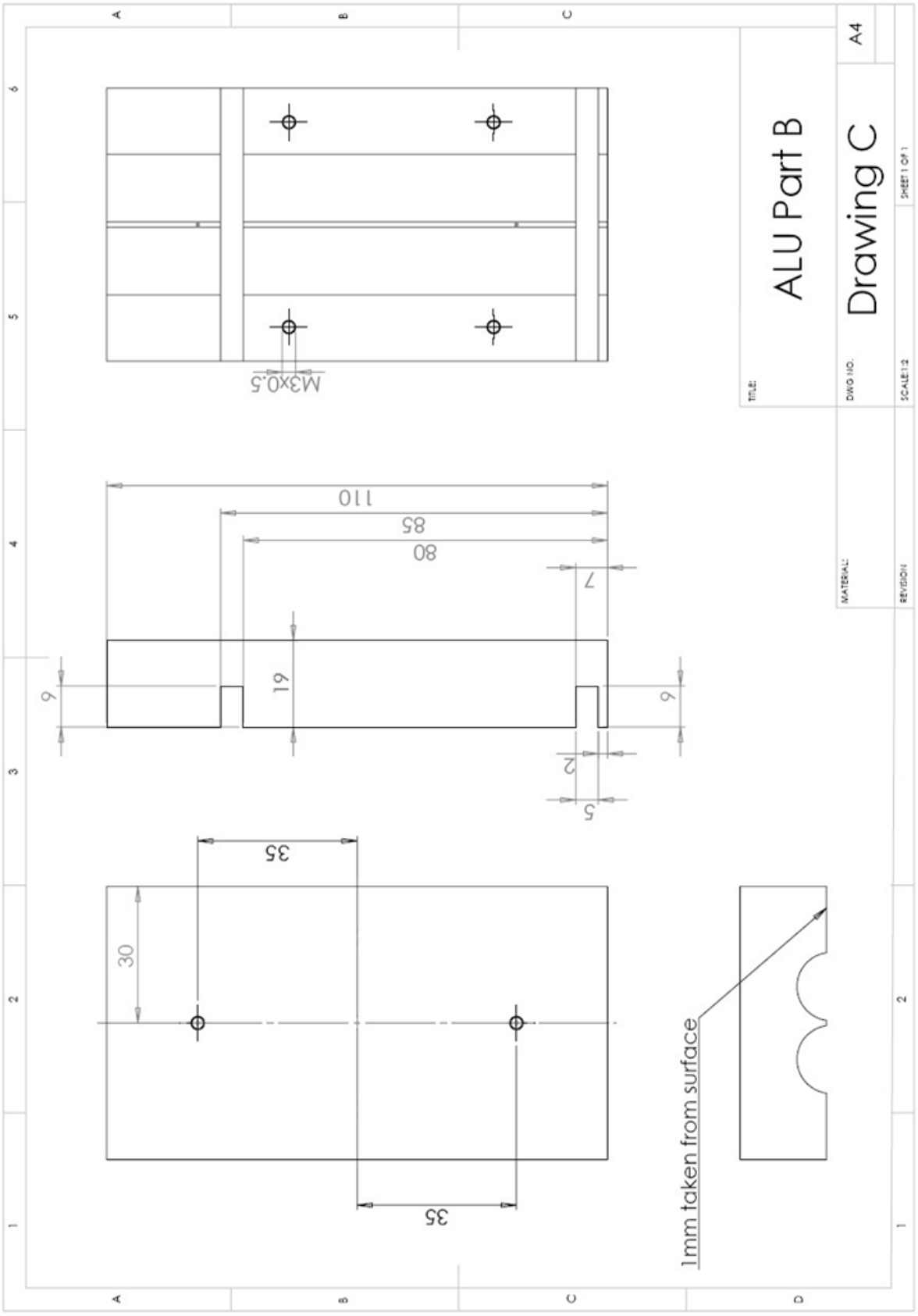
A4
ALU Part B
Drawing C
TITLE:
DWG NO.
SCALE:1:2
SHEET 1 OF 1
MATERIAL:
REVISION
M3x0.5
110
85
80
7
19
6
6
2
5
35
30
35
1mm taken from surface

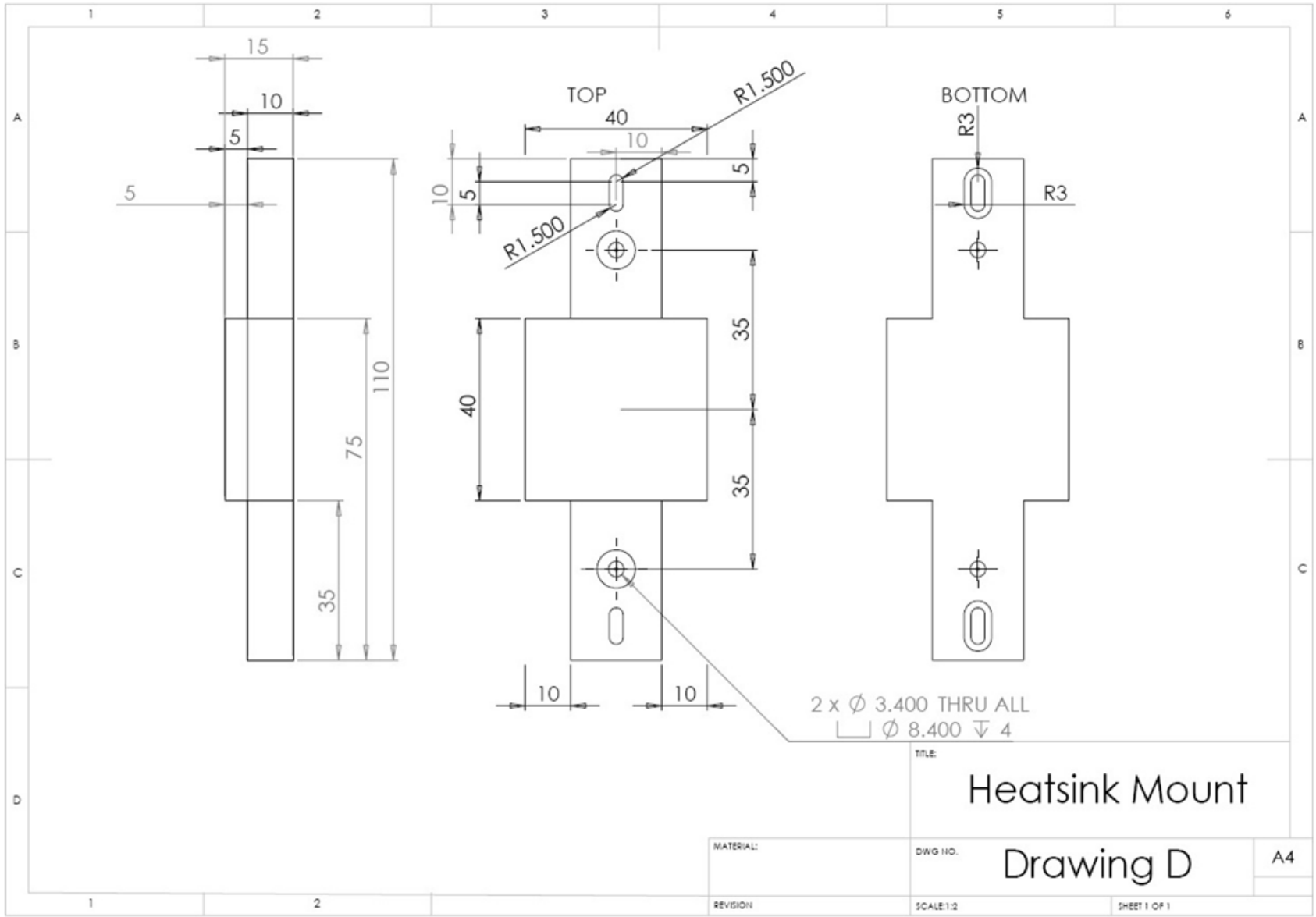
15
10
5
5
110
75
35
TOP
R1.500
40
10
5
10
5
R1.500
35
40
35
10
10
BOTTOM
R3
R3
2 x ∅ 3.400 THRU ALL
⌴ ∅ 8.400 ↧ 4
TITLE:
Heatsink Mount
MATERIAL:
DWG NO.
Drawing D
A4
REVISION
SCALE:1:2
SHEET 1 OF 1

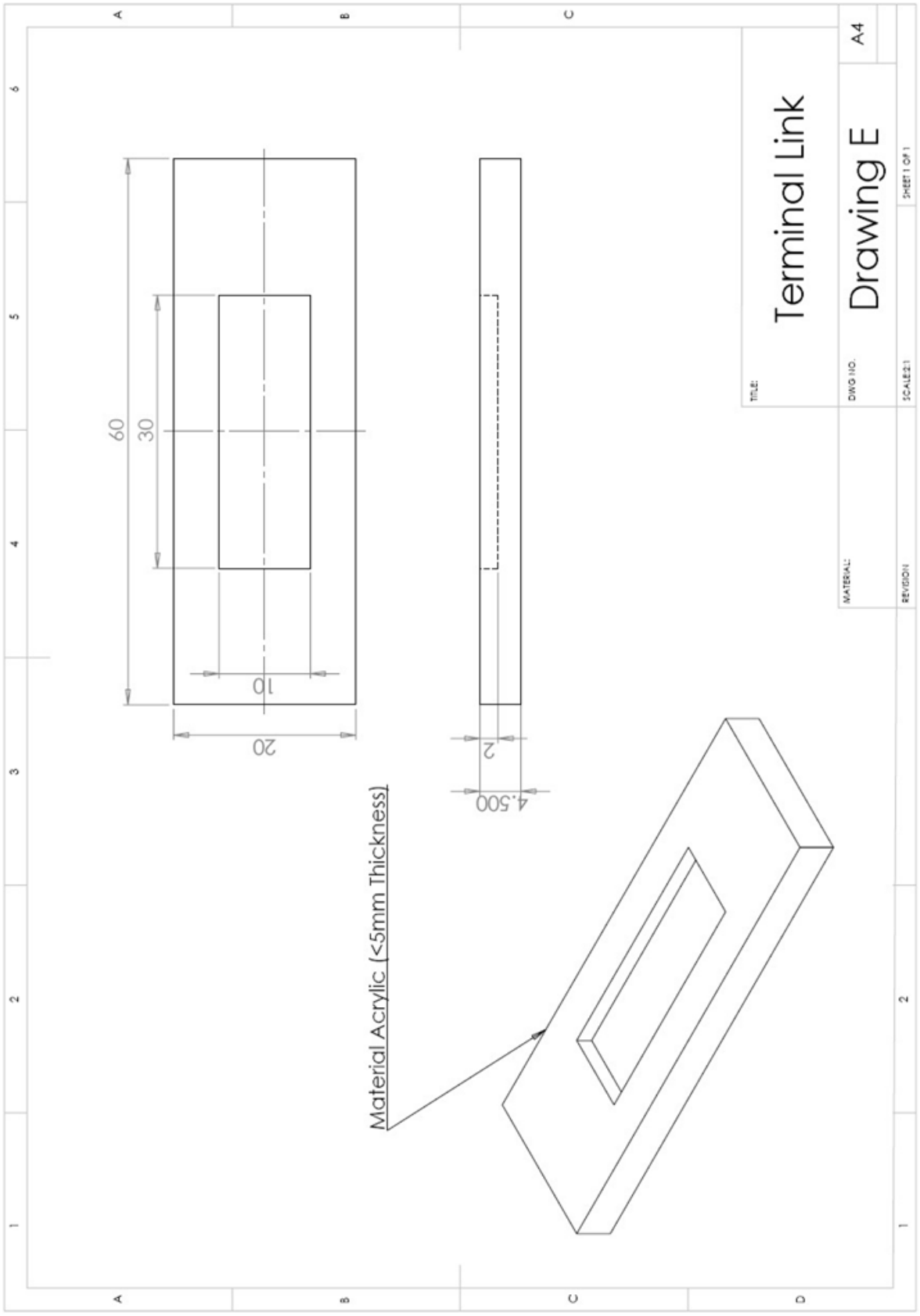
Terminal Link
Drawing E
A4
60
30
10
20
2
4.500
Material Acrylic (<5mm Thickness)

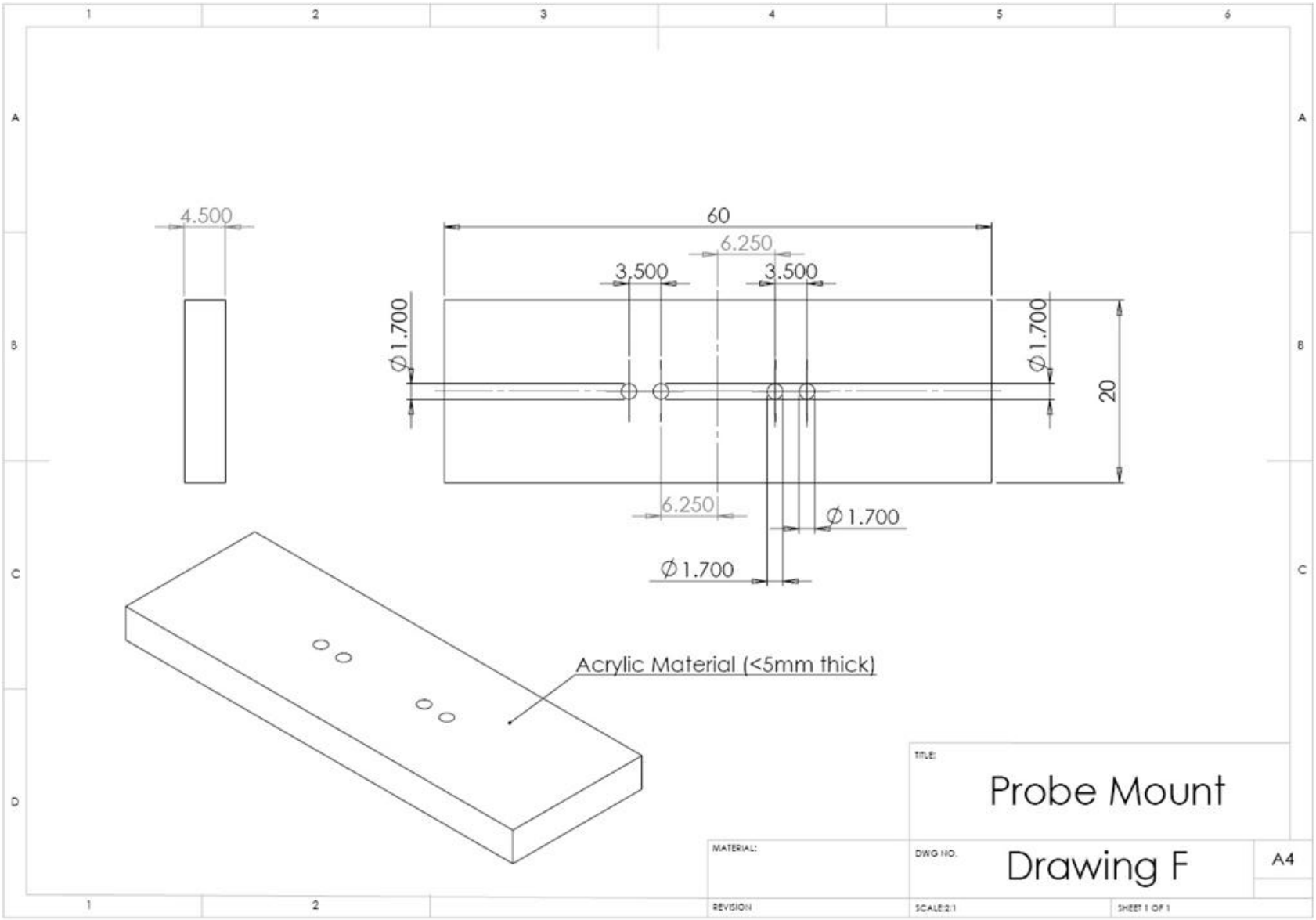
4.500
60
6.250
3.500
3.500
Ø1.700
Ø1.700
20
6.250
Ø1.700
Ø1.700
Acrylic Material (<5mm thick)
TITLE:
Probe Mount
Drawing F
A4
MATERIAL:
DWG NO.
REVISION
SCALE:2:1
SHEET 1 OF 1

D.2 CONTROL DESIGN AND OPERATION

The temperature control was performed using a temperature switch TC622VAT IC from Microchip, to switch the Peltier module on or off via a relay.

The switching temperature is determined by a single variable resistor connected to the temperature switch IC. Built into this device is 2 °C of hysteresis.

The temperature switch provides both an active high and active low output when the set temperature is reached. Depending on the direction of the temperature, one of these outputs is used to switch the relay, connecting the Peltier module, on or off.

To increase the rate of heat being pumped across the Peltier module, the voltage across the terminals was varied in order to increase or decrease the current flowing through the module. Likewise the direction of the current was change through swapping the Peltier module terminal connections over.

The rating of the Peltier module used was initially 18.5 W, this was later replaced by a 110 W device in order to pump enough heat away from the aluminum encasement to reach below freezing. Initial tests showed that to achieve temperatures below freezing, the D1 encasement and 18.5 W Peltier module was not enough.

The insulation used was Kingspan Therma insulation with a thickness of 25 mm. This insulation was used in both design iterations. The insulation was broken into sections and glued together to enclose the encasement. Additional aluminum tape was also used to provide further insulation.

Appendix E

Additional Data for Controlled Battery Discharges

The following appendix contains additional data/plots for the different sections detailed in Chapter 5 Controlled Battery Discharge.

E.1 COMPARISON OF PULSED AND CONSTANT CURRENT DISCHARGE

The continuation of Section 5.3 to provide comparison between pulsed and constant current discharge for the batteries B and C that were discharged in the same discharge tests.

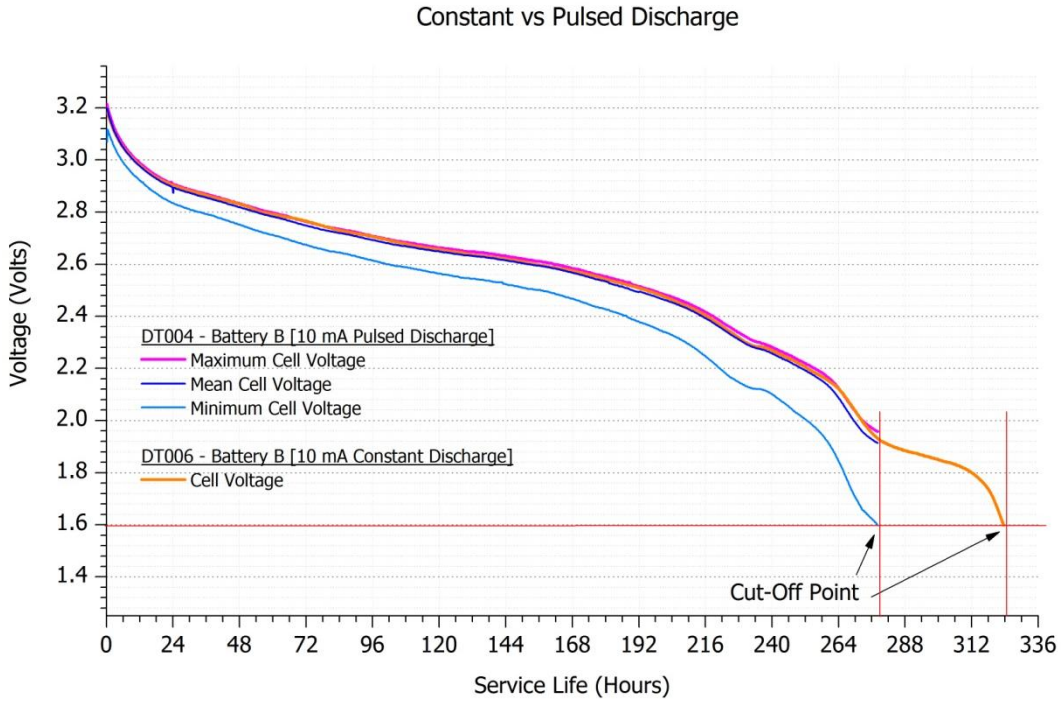

Figure E.1 - Battery B from DT004 and DT006

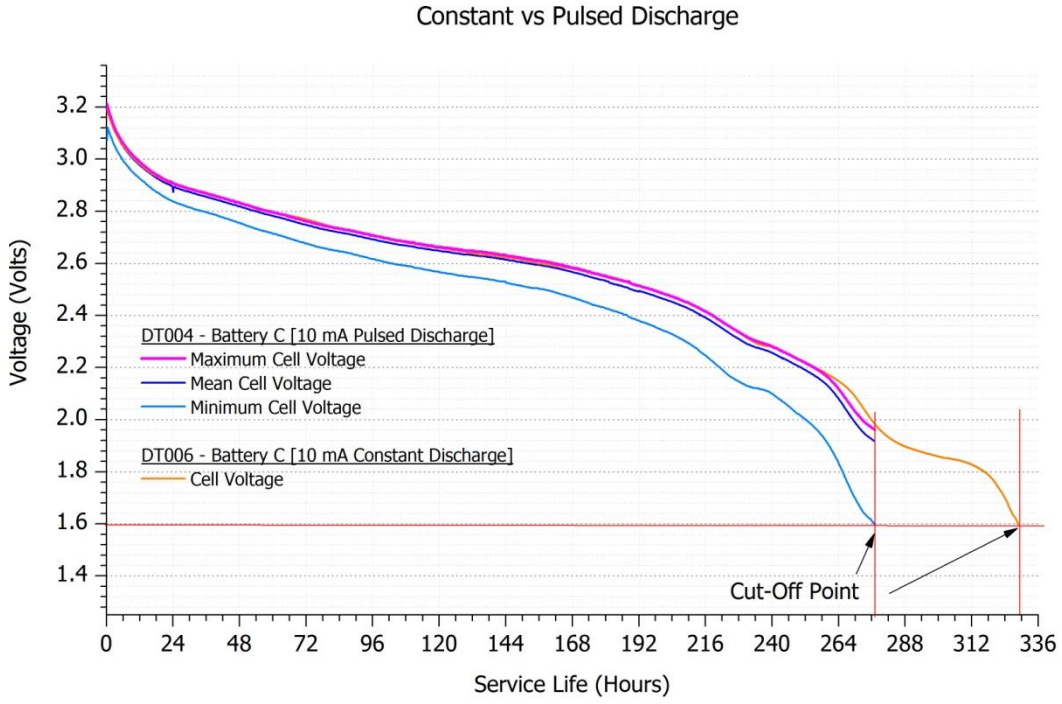

Figure E.2 - Battery C from DT004 and DT006

E.2 CELL TO CELL VARIATION

In Section 5.4 the cell voltage of all 3 pairs of cells from discharge test DT005 are compared. The following are the same plots for tests DT001, DT002 and DT007 as mentioned in the same section.

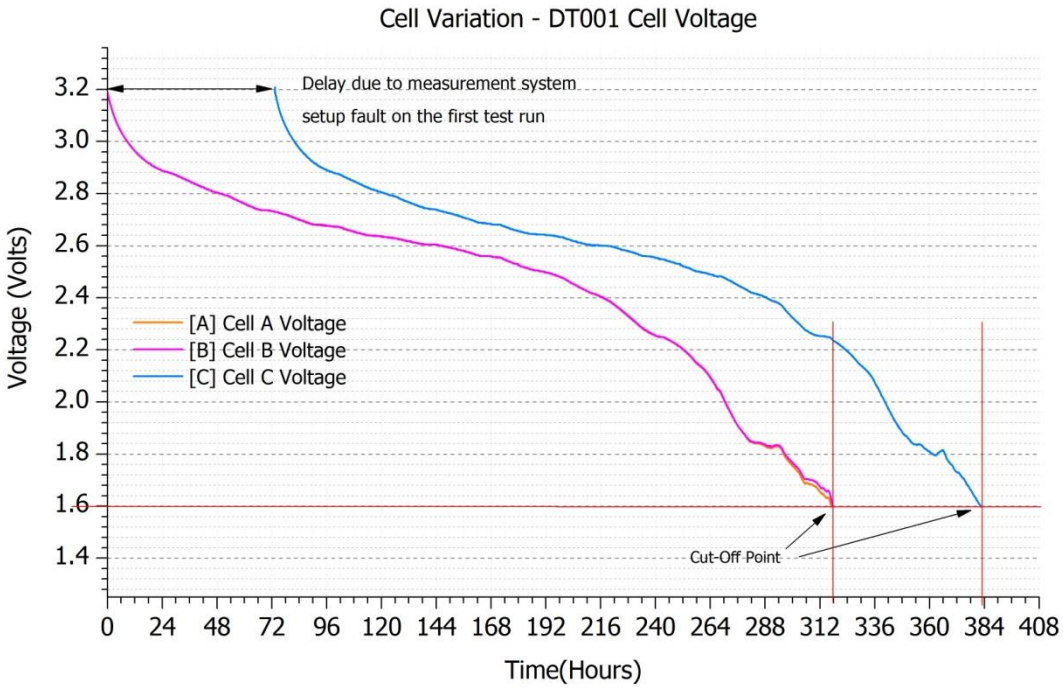

Figure E.3 - Cell variation for constant current discharge test DT001

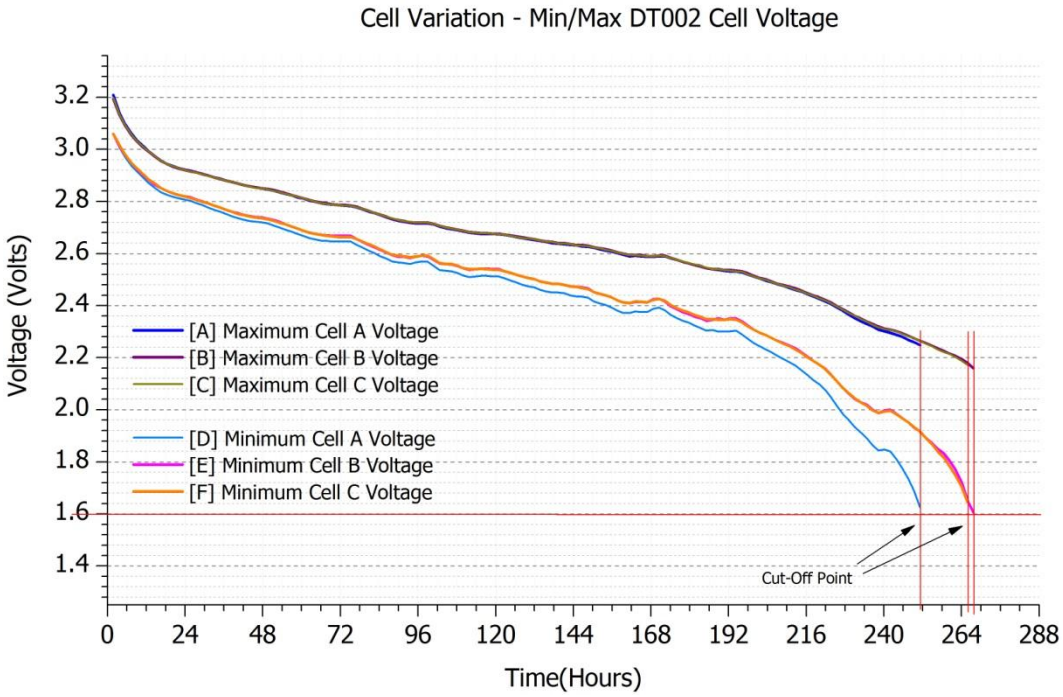

Figure E.4 - Cell variation for pulsed current discharge test DT002

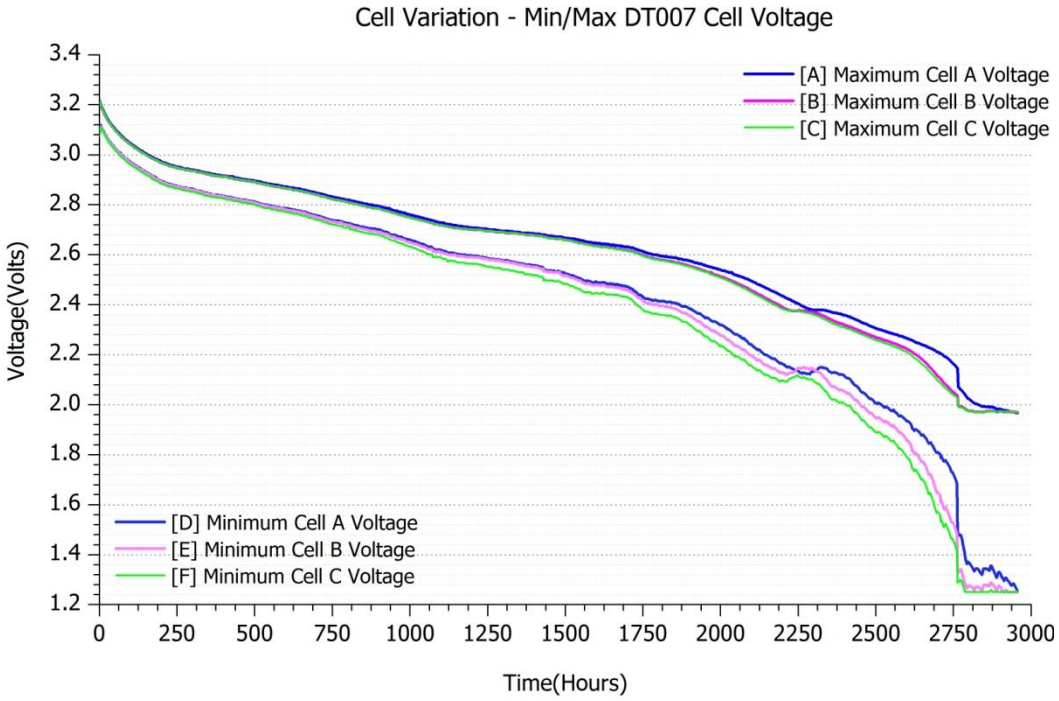

Figure E.5 - Cell variation for pulsed current discharge test DT007

All of the above plots highlight the cell to cell variation in discharge test DT001, DT002, and DT007. The same plots could be produced for all of the tests but the above three were highlighted in Section 5.4 as best representing the possible variation between cells.

Appendix F

Additional Data for Environmental Effects

The following appendix contains additional data/plots for the different sections detailed in Chapter 6 Environmental Effects.

F.1 TEMPERATURE CHANGE

Temperature change in Section 1.1 uses discharge test DT007 for comparison between change in temperature and change in cell voltage. The following plots are further examples of temperature variation with cell voltage.

F.1.1 EXAMPLES OF CHANGE WITH TEMPERATURE

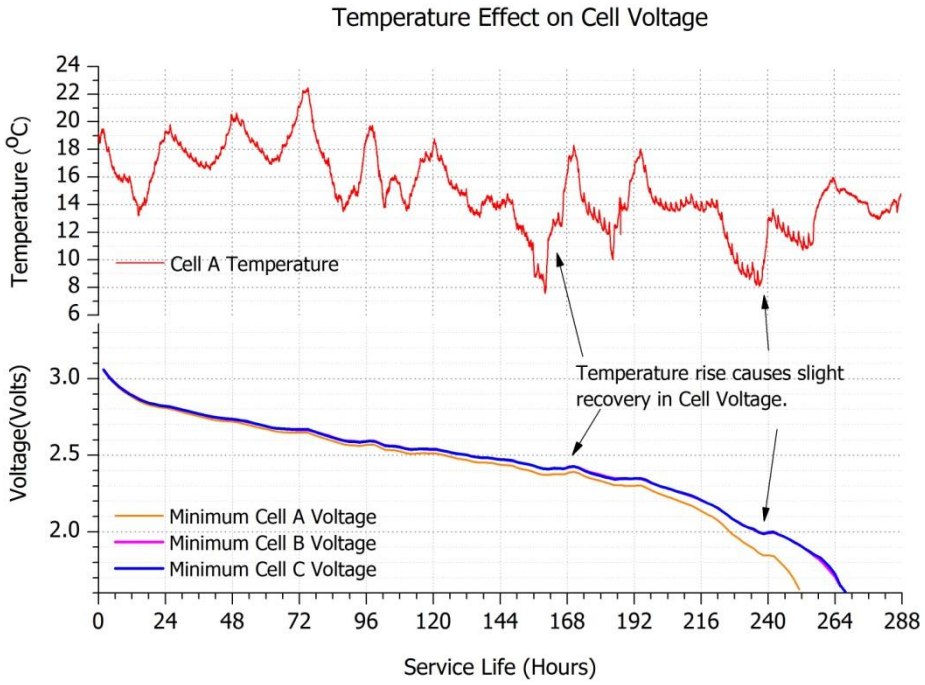

Figure F.1 - Temperature and Cell voltage comparison from discharge test DT002

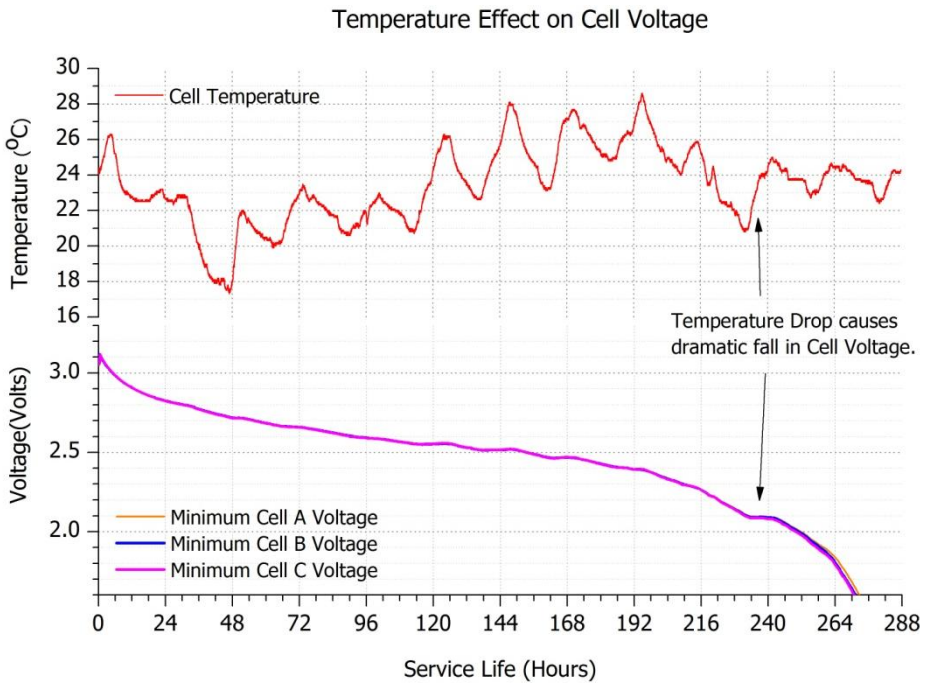

Figure F.2 - Temperature and Cell voltage comparison from discharge test DT003

F.1.2 EXAMPLES OF NO CHANGE WITH TEMPERATURE

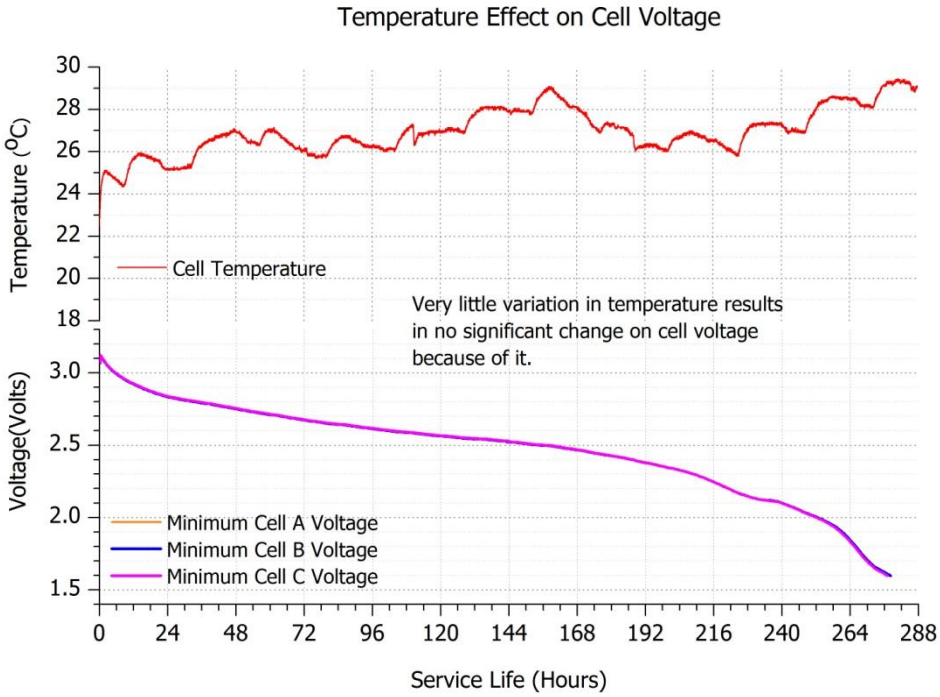

Figure F 3 - Temperature and Cell voltage comparison from discharge test DT004

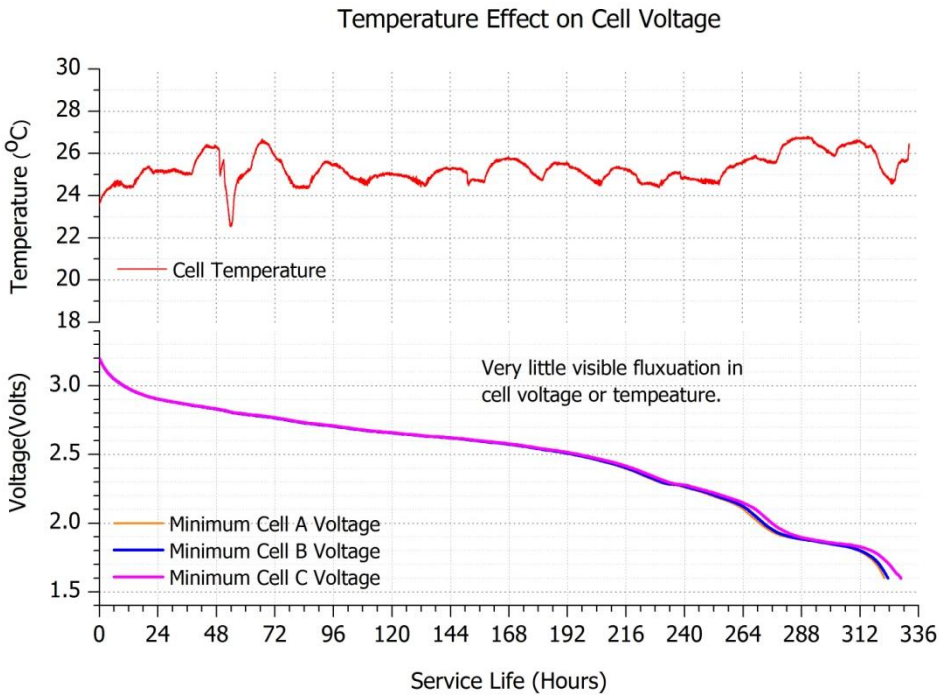

Figure F 4 - Temperature and Cell voltage comparison from discharge test DT006

F.2 TEMPERATURE EXTREMES

The following are additional plots and data related to discharge tests at extreme temperatures.

F.2.1 HIGH TEMPERATURE DISCHARGE

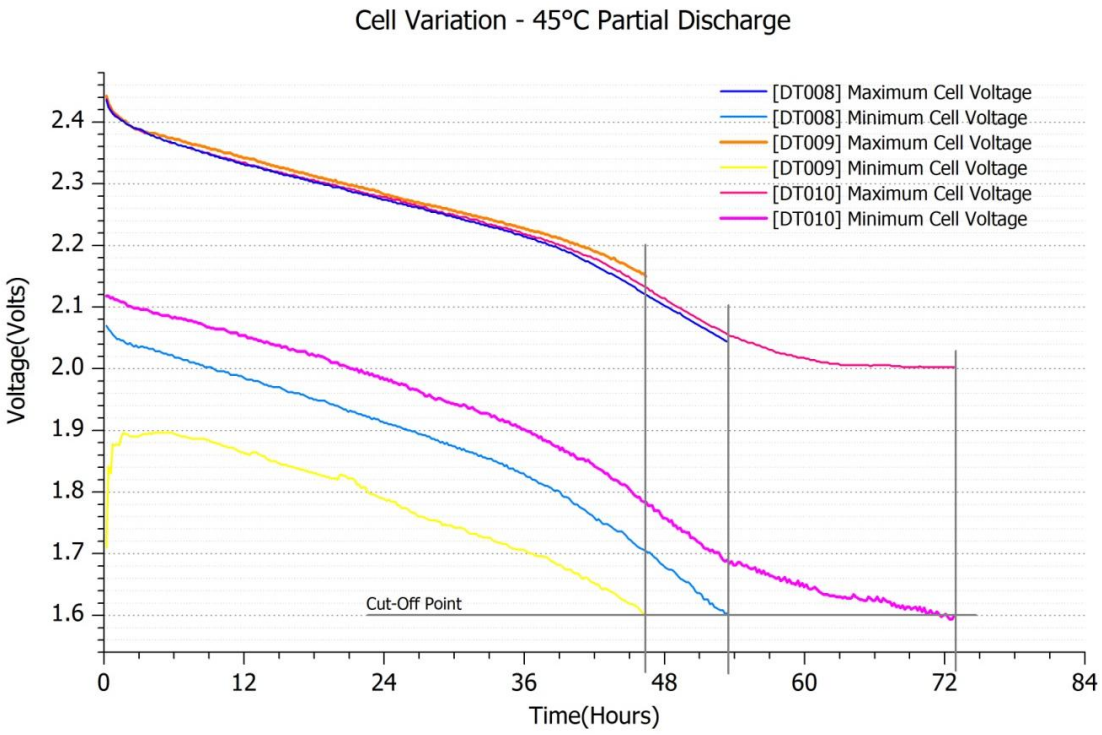

Figure F.5 - Variation between cells at high temperature

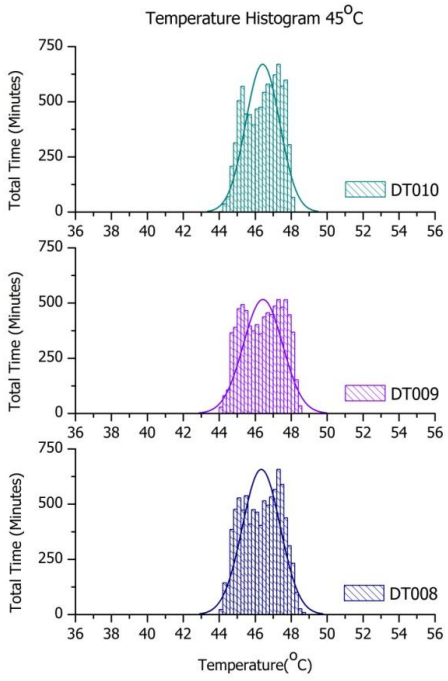

Figure F.6 - Temperature histogram for each of the discharges at 45 °C

F.2.2 Low Temperature Discharge

The following are the cell voltage and temperature profiles for all discharge tests whilst attempting to operate at -5 °C. First looking at the cells discharged close to -5 °C, the temperature profiles for DT014 and DT018 can be seen in Figure F.7.

The temperature profiles show that the peaks of the curves sit at slightly below the -5 °C target. The profile for DT018 is heavily skewed above -5 °C but is still within 1 or 2 °C of the target temperature. Test DT014 however is skewed below the mean, and appears that the temperature 5 °C was held for a considerable length of time during the discharge test.

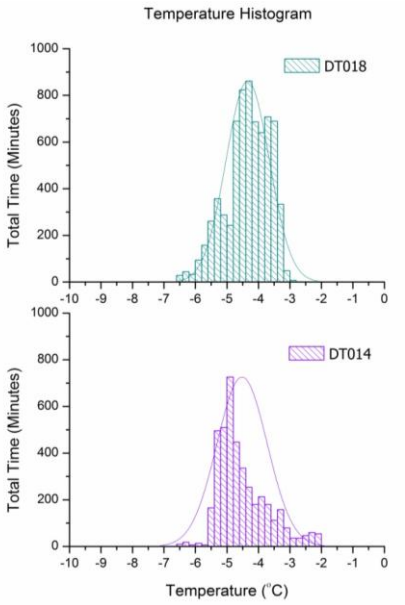

Figure F.7 - Temperature histogram of discharge

The resulting cell voltage curves produced very mixed results as shown in Figure F.8 and Figure F.9. It is worth mentioning that the minimum voltage that can be measured by the measurement system is 1.25 V, due to the range of the ADC as detailed in Section 4.4.1.

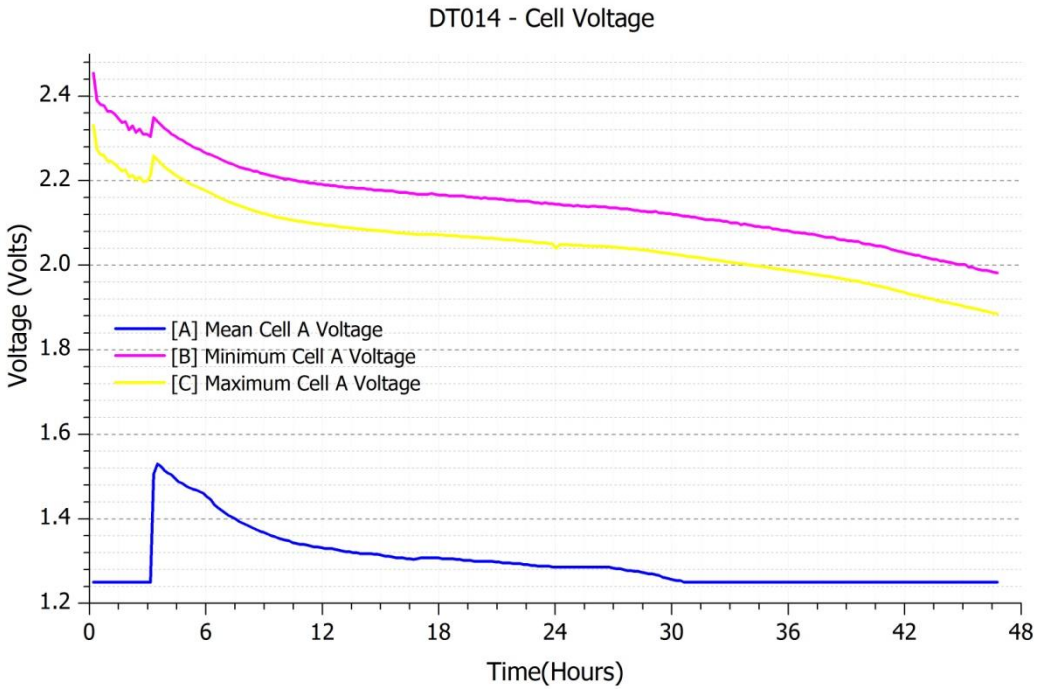

Figure F.8 - Cell voltage of partial discharge at a temperature below -2°C

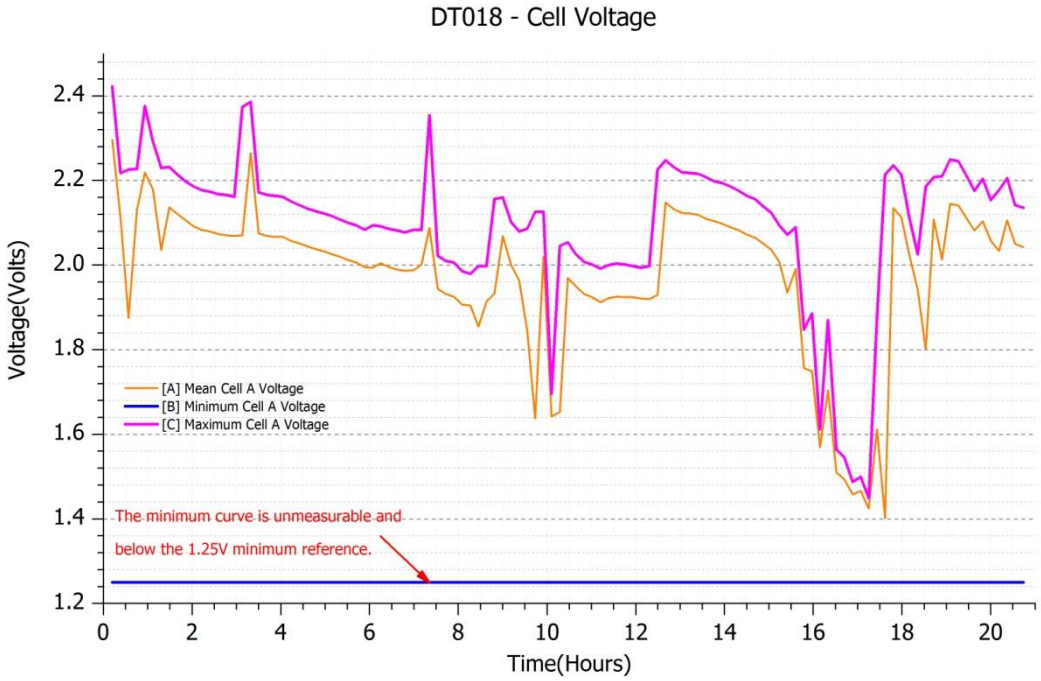

Figure F.9 - Cell voltage of partial discharge that exhibited unpredictable behaviour

There is a clear anomaly in DT014 within the first 3 hours of the discharge test, during this time the cell voltage when under the active load dropped to 1.25V and below, only for the cell to recover to a minimum of 1.52V. This same behaviour was observed in test DT009 and shown in Figure F.5 where the initial minimum cell voltage, under the active load, recovered.

The result of DT018 shows the unpredictable nature of the cells at low temperature. From the very beginning of the test, the cell voltage under active load was being measured by a DMM at less than 500 mV, but due to the recovery seen previously, the test was left to run its course. It is difficult to know if the cell chemistry was affected during the partial discharge or if the length of time the cell was stored in a partially discharged state had a part to play.

As mentioned previously, two tests inadvertently discharged the cells at temperatures close to -10°C. The resulting temperature profiles are shown in Figure F.10, and the corresponding cell voltage curves in Figure F.11 and Figure F.12.

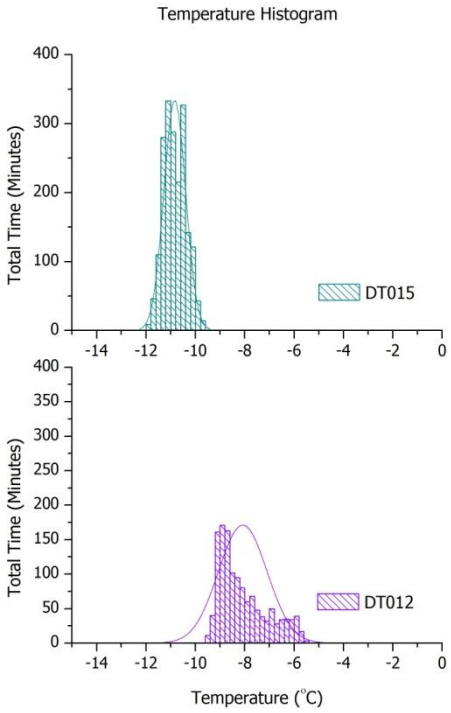

Figure F.10 - Temperature histograms

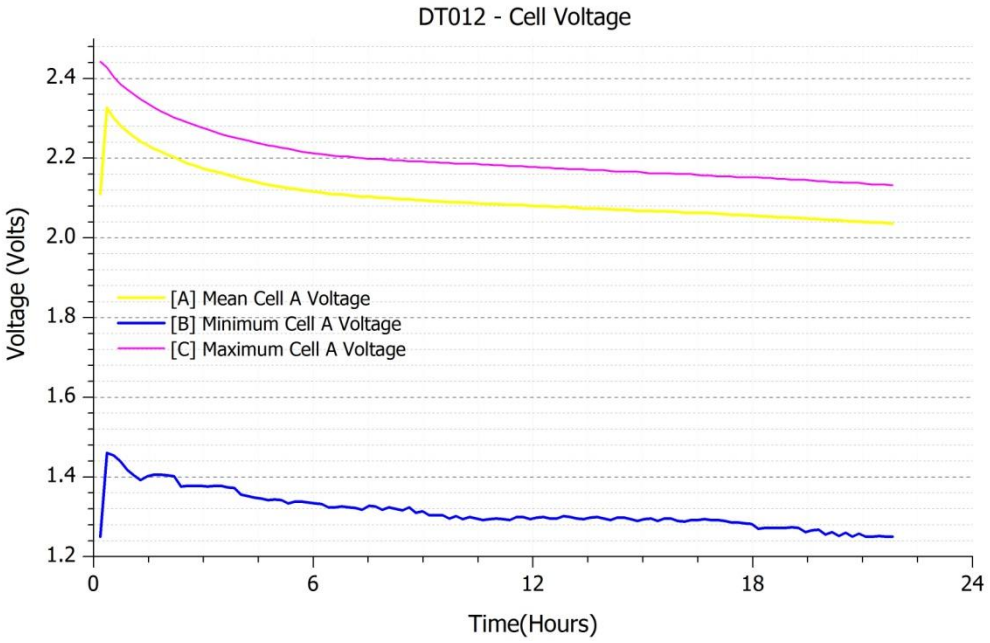

Figure F.11 - Cell voltage of partial discharge at temperatures close to -10°C

The result from DT012 again shows evidence of the minimum cell voltage when under the active load, recovering after an initial period of time. In this case the minimum cell voltage was measured at 1.25 V or below for only the first duty cycle of length 11 minutes.

The most noticeable result is the minimum curve from DT015, because despite the mean temperature being -11 °C, the cell voltage remains above the 1.6 V cut-off voltage for just under 6 hours.

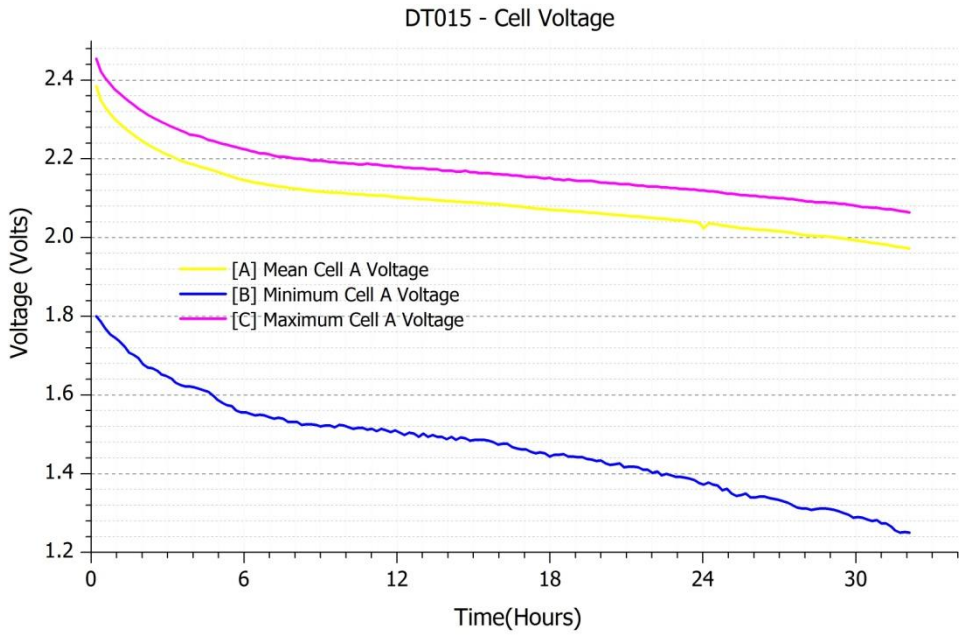

Figure F.12 - Cell voltage of partial discharge at temperatures close to -10°C

Appendix G

Low Power Wireless Sensor Node

The following appendix provides further design details of the low power wireless sensor node that has been designed. This includes a bill of materials, schematics, and PCB layout.

The design itself is not complete and needs modifications to be completely functional. The problems will be highlighted and information given on the reference designs used.

G.1 Low Power Node Schematics

This section contains the following:

- Low power node
  - Power Supply
  - Application (Microcontroller + peripherals)
  - RF Transceiver and Balun Filter
- RS232 and Programming Adapter

G.1.1 Low Power Node

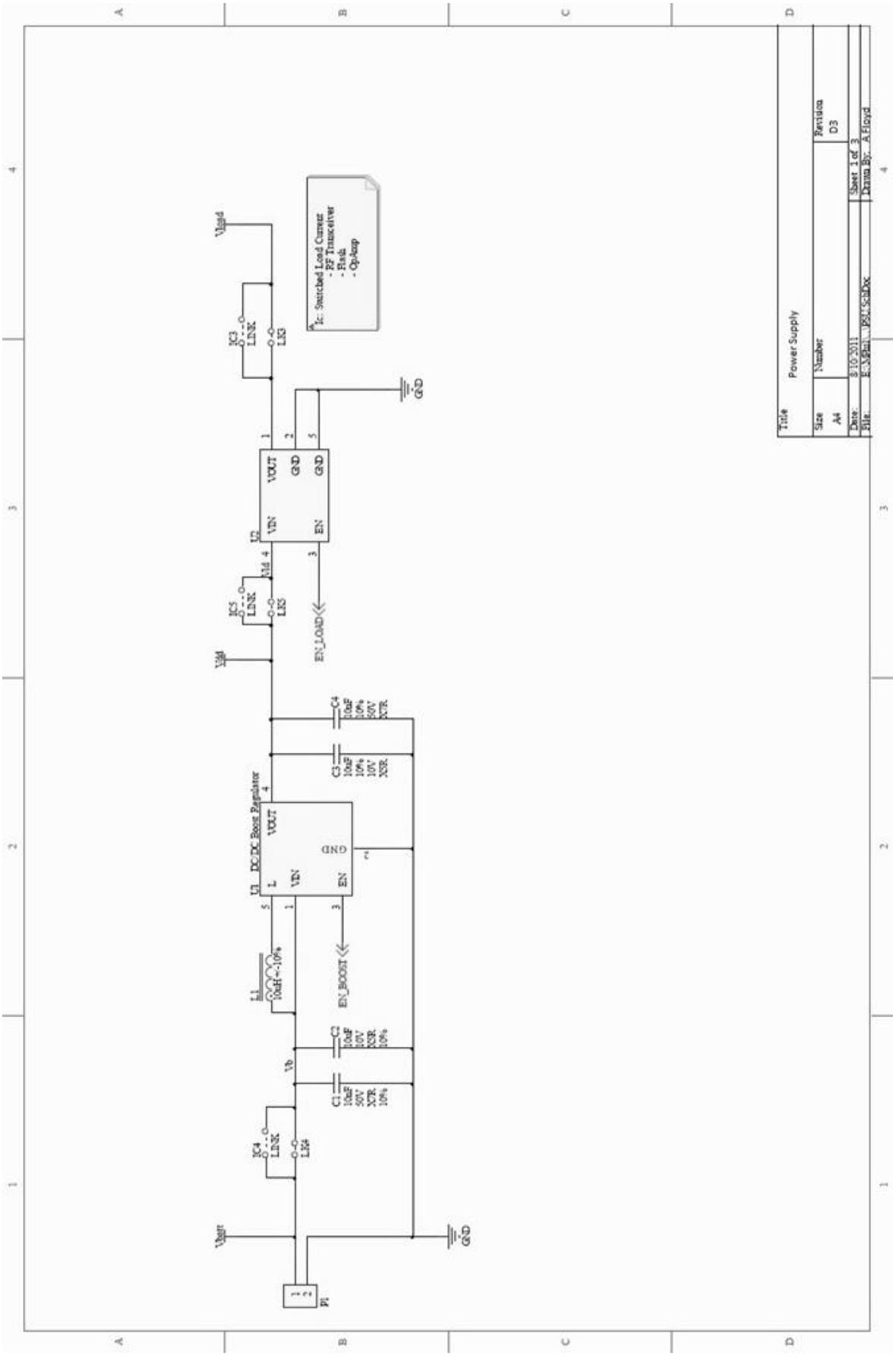

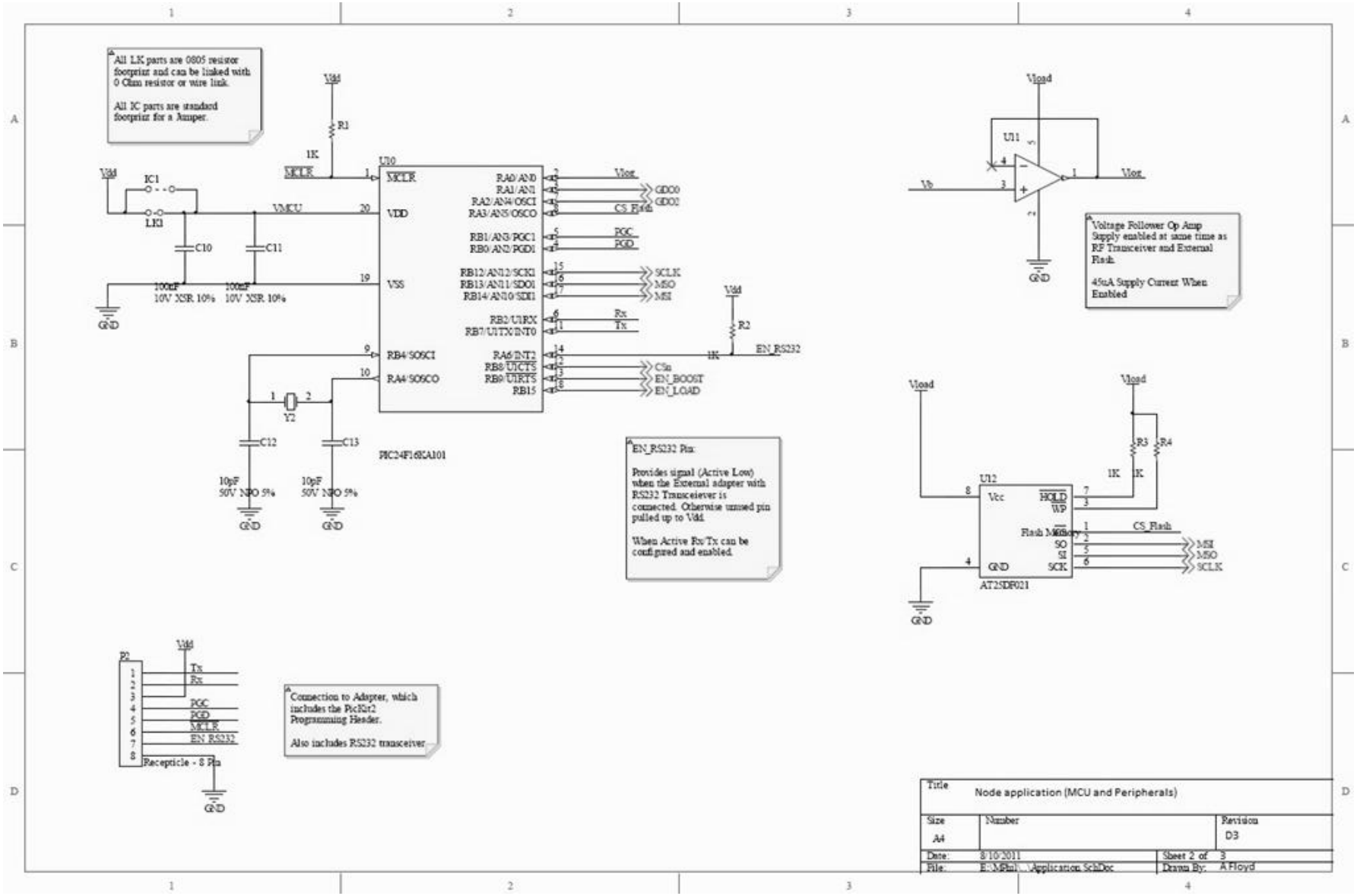
All LK parts are 0805 resistor footprint and can be linked with 0 Ohm resistor or wire link.
All IC parts are standard footprint for a Jumper.
Vdd
R1
1K
MCLR
U10
IC1
LK1
VMCU
C10
C11
100nF
10V X5R 10%
100nF
10V X5R 10%
GND
VDD
VSS
RA0/AN0
RA1/AN1
RA2/AN4/OSCI
RA3/AN5/OSCO
RB1/AN3/PGC1
RB0/AN2/PGD1
RB12/AN12/SCK1
RB13/AN11/SDO1
RB14/AN10/SDI1
RB2/U1RX
RB7/U1TX/INT0
RB4/SOSCI
RA4/SOSCO
RA6/INT2
RB8/U1CTS
RB9/U1RTS
RB15
Vlost
GDO0
GDO2
CS_Flash
PGC
PGD
SCLK
MSO
MSI
Rx
Tx
R2
EN_RS232
CSn
EN_BOOST
EN_LOAD
Y2
C12
C13
10pF
50V NPO 5%
10pF
50V NPO 5%
PIC24F16KA101
EN_RS232 Pin:
Provides signal (Active Low) when the External adapter with RS232 Transceiver is connected. Otherwise unused pin pulled up to Vdd.
When Active Rx/Tx can be configured and enabled.
Vload
U11
Vb
Vlost
Voltage Follower Op Amp
Supply enabled at same time as RF Transceiver and External Flash.
45uA Supply Current When Enabled
R3
R4
1K
1K
U12
Vcc
HOLD
WP
Flash Memory
SO
SI
SCK
GND
CS_Flash
MSI
MSO
SCLK
AT25DF021
P2
Tx
Rx
PGC
PGD
MCLR
EN_RS232
Recepticle - 8 Pin
Connection to Adapter, which includes the PicKit2 Programming Header.
Also includes RS232 transceiver
Title
Node application (MCU and Peripherals)
Size
A4
Number
Revision
D3
Date:
8/10/2011
Sheet 2 of 3
File:
E:\Mihir\...\Application.SchDoc
Drawn By:
A Floyd

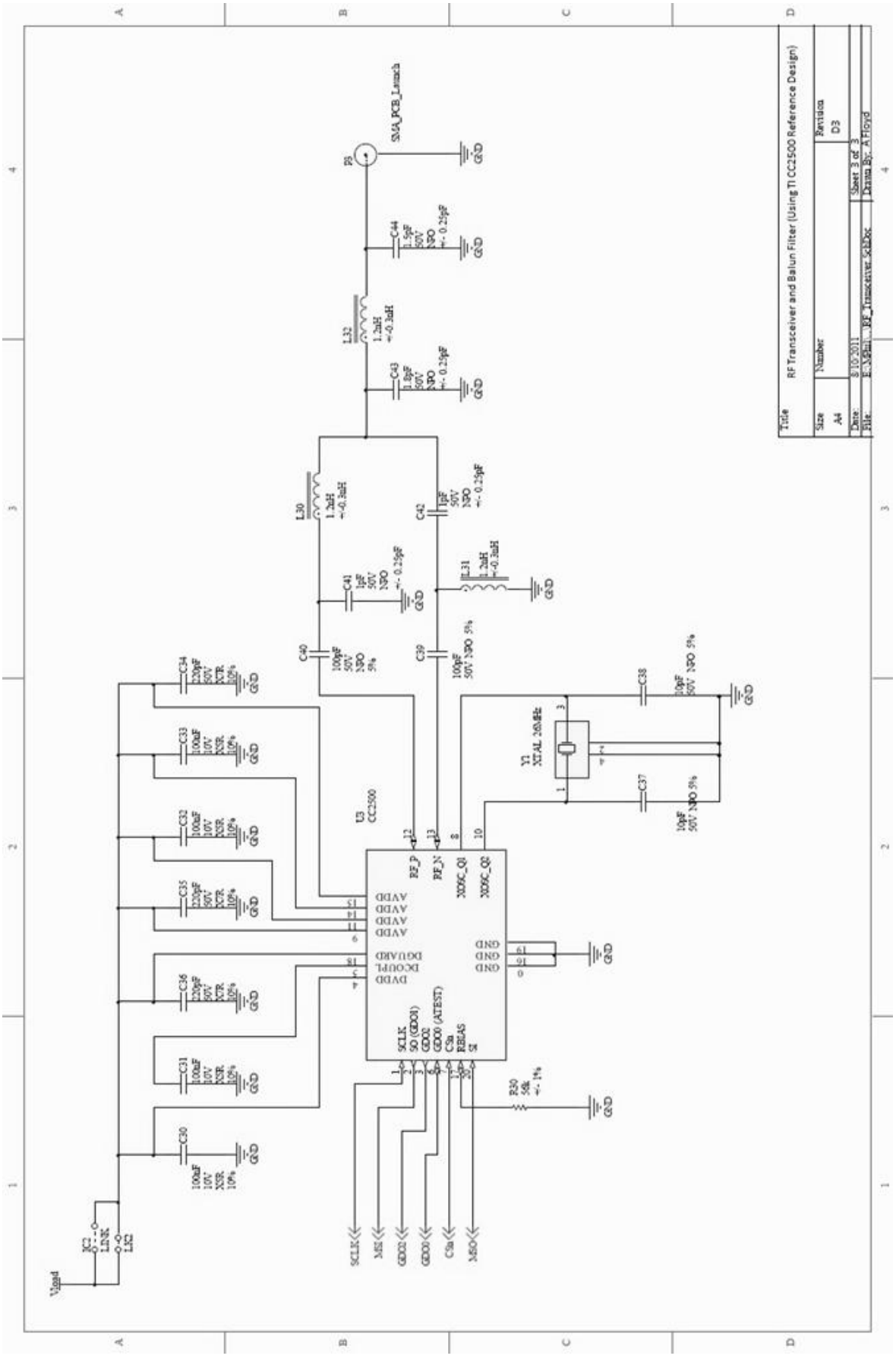
RF Transceiver and Balun Filter (Using TI CC2500 Reference Design)
Revision
D3
Number
Size
A4
Date: 8/10/2011
Sheet 3 of 3
File: E:\Misc\RF_Transceiver.SchDoc
Drawn By: A Floyd
SMA_PCB_Launch
U3
CC2500
Y1
XTAL 26.0MHz
L30
L31
L32
C30
C31
C32
C33
C34
C35
C36
C37
C38
C39
C40
C41
C42
C43
C44
R30
56k
+/- 1%
SCLK
MISO
GDO2
GDO0
CSn
MOSI
Vbnd
GND

G.1.2 Low Power Node Adapter

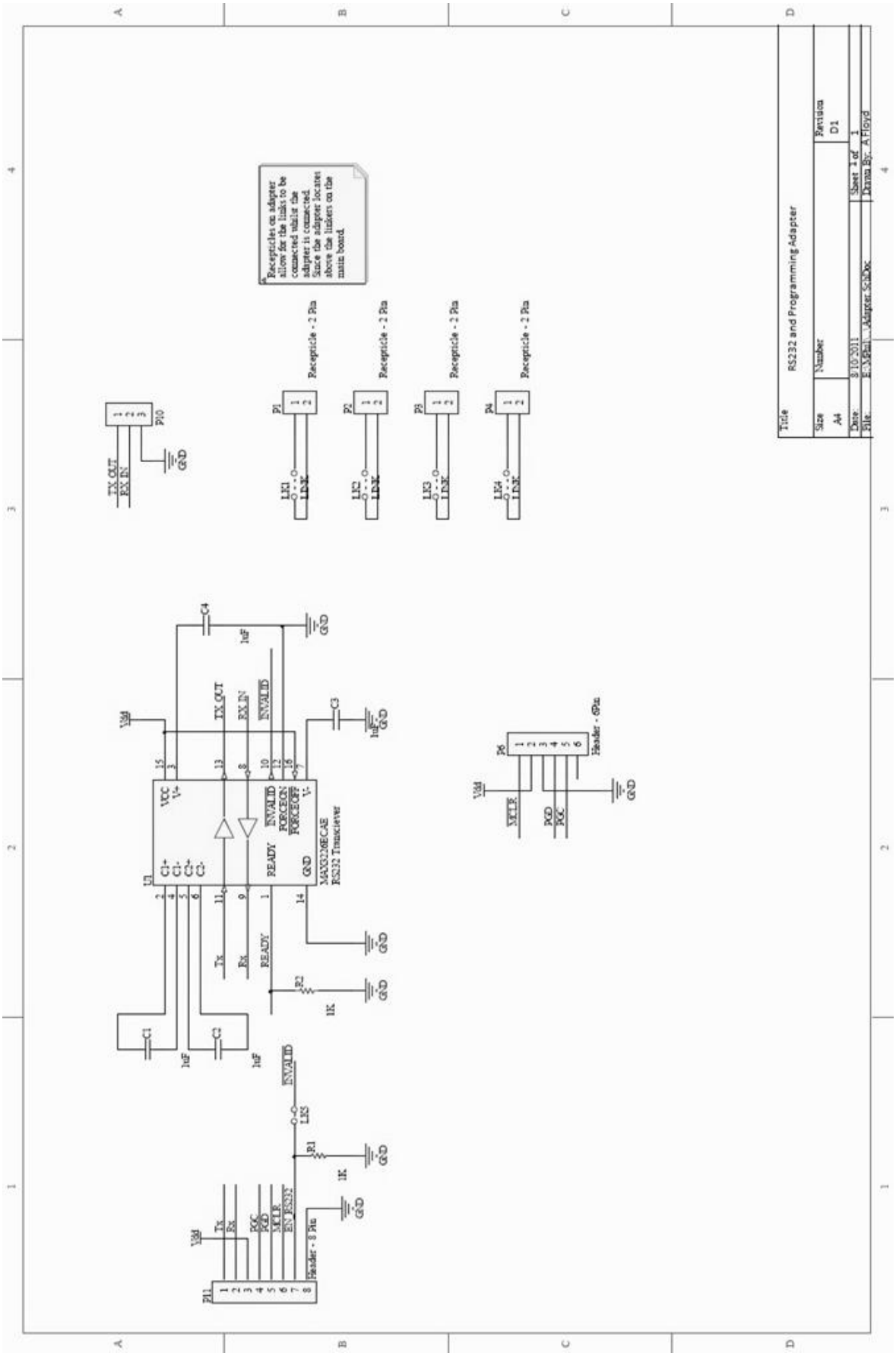

Description	Designator	Farnell	Mouser	Quantity	Manufacturer	Model
32.768kHz Crystal Oscillator	Y2	9509682		1	AEL	
100nF Capacitor	C10, C11, C30, C31, C32, C33	8820120		6	Murata	GRM21BR71H104KA01L
10nF Capacitor	C1, C4	1828948		2	Murata	GRM216R71H103KA01D
100pF Capacitor	C39, C40	1828933		2	Murata	GRM2165C1H101JA01D
10pF Capacitor	C12, C13, C37, C38	1828929		4	Murata	GRM2165C1H100JZ01D
10uF Capacitor	C2, C3	1828811		2	Murata	GRM31 Series
Boost Converter, 0.9VIN, 3.3VOUT	U1	1755714		1	Texas Instruments	TPS61097
2-Megabit SPI Serial Flash	U12	1715438		1	ATMEL	AT25DF021
56k 0805 SMT Resistor	R30	1712808		1		
PIC24F16KA101	U10	1707628		1	Microchip	PIC24F16KA101
SAMTEC Recepticle, 8 Pin	P2	1667514		1	SAMTEC	CES-108-01-T-S
High Side Power Switch	U2	1663123		1	Micra	MIC94070YC6
SMA PCB Launch	P3	1608592		1	Johnson/Emerson	142-0701-801
1.2nH Inductor	L30, L31, L32	1515377		3	Murata	LQG18HN1N2S00D
CC2500 2.4GHz Transciever	U3	1248487		1	Texas Instruments	CC2500
OP Amp, 1MHz, 45uA, CMOS, Rail-to-Rail	U11	1207047		1	Texas Instruments	OPA348AIDBVTG4
Screw Terminal, 2-Way	P1	1177875		1	Lumberg	KRM 02
10uH Inductor	L1	1174073		1	Sigma Inductors	3613C100K
1.8pF Capacitor	C43		81-GRM2165C1H1R8CD	1	Murata	GRM2165C1H1R8CD01D
1pF Capacitor	C41, C42		81-GRM40C010C50D	2	Murata	GRM2165C1H1R0CD01D
1.5pF Capacitor	C44		81-GRM40C1R5C50D	1	Murata	GRM2165C1H1R5CD01D
220pF Capacitor	C34, C35, C36		81-GRM40X221K50D	3	Murata	GRM216R71H221KA01D
Link	IC1, IC2, IC3, IC4, IC5			5		
Exposed Pads for solder link	LK1, LK2, LK3, LK4, LK5			5		
1K SMT Resistor	R1, R2, R3, R4			4		
26MHz Crystal Oscillator	Y1		815-ABM3B-26-T	1	ABRACON	ABM3B

G.3 PCB LAYOUT

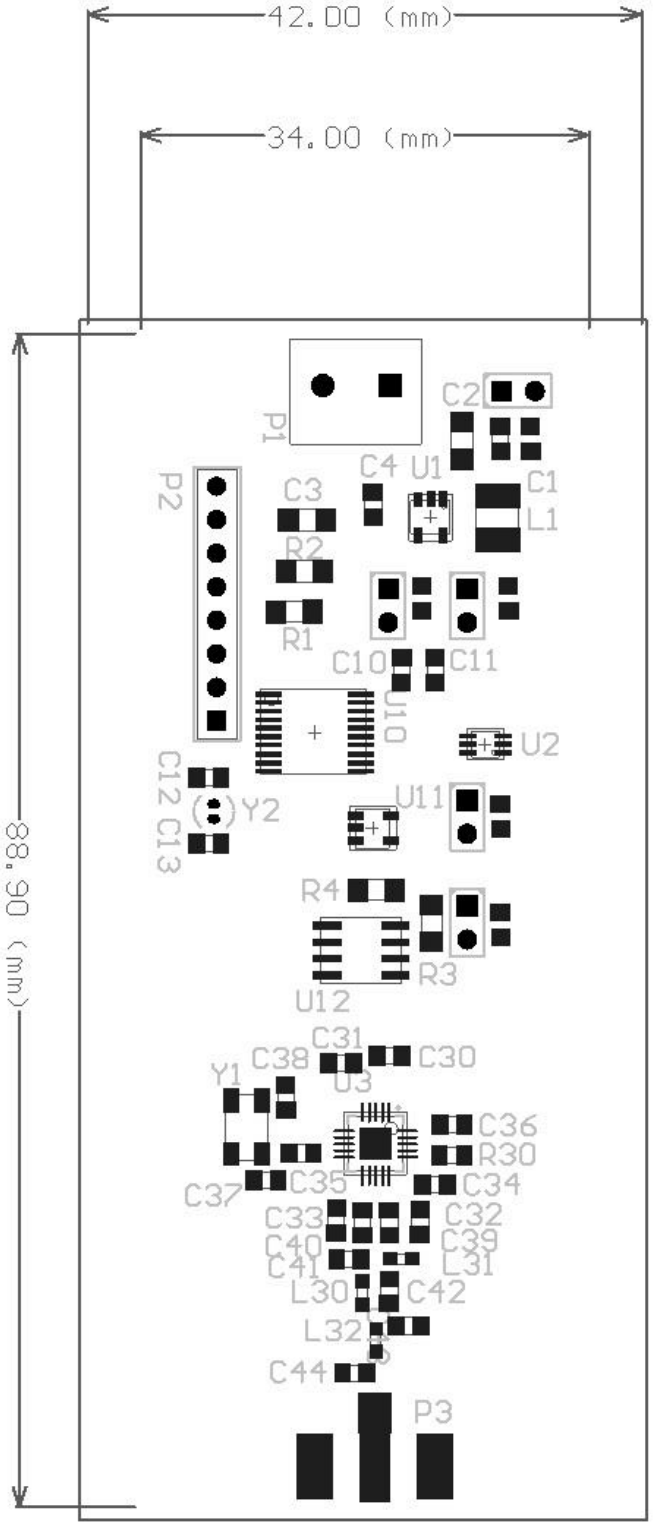

All PCB files can be found on the CD, along with Gerber files and final artwork

G.4 STATE OF DEVELOPMENT

At the time of completion of this research project the low power node was in the following state:

- In order to operate the RF transceiver, and send or receive any wireless communications, a module from Quasar was used to bypass the CC2500 transceiver and balun filter on the PCB.
- With the module from Quasar attached the embedded software was tested.
- The software uses the software library designed for use with Texas Instruments microcontrollers. This software library has been ported to work on Microchip devices as found in the design.
- The ported software has not been fully tested and cannot be deemed to be operational.
- Problems related to timings were found during the end of development where packet transmission was only achievable with a breakpoint set after the transmission routine.

The problem with the node design lies with the selection of parts for the balun filter. The reference design from Texas Instruments was used for passive values and manufacturers. The decision was made to use the same parts but of a larger case size / footprint from the same range of parts from the same manufacturers. This change in case sizes resulted in the nodes being non-operational.

If the reference design from Texas Instruments is followed exactly then it is possible for the node to become operational. This would require the assembly of the PCBs by a third party as the University's reflow soldering facilities currently cannot cope with parts as small as 0402.

Appendix H

Attached DVD Contents

The attached DVD contains files grouped into the following categories:

- Poster
- Measurement System
    - This includes all the design files and software projects
- Temperature Controlled Encasement
    - Includes the datasheets and Solidworks 3D CAD
- Experimental Results
    - Contains the files of each discharge test from DT001 to DT020
- Experimental Analysis
    - Contains the OriginPro 8 project files for graphical analysis
- Low Power Wireless Node
    - Includes the datasheets, PCB design files, and software
- Zotero Bibliographic Management RDF Export
    - An export from the open source bibliography software used for this research

H.1 FOLDER LIST

H.1 ..\Poster

H.2 ..\Measurement System

- H.2.1 ..\Part Datasheets
- H.2.2 ..\PCB Design
- H.2.3 ..\Embedded Software
- H.2.4 ..\Windows Software

H.3 ..\Temperature Controlled Encasement

- H.3.1 ..\Part Datasheets
- H.3.2 ..\Solidworks Assembly

H.4 ..\Experimental Results

- H.4.1 ..\DT001 to DT020
  - ..\ ..\Binary Files
  - ..\ ..\Sampled Output
  - ..\ ..\Standard Output

H.5 ..\Experimental Analysis

- H.5.1 ..\DT001 to DT020

H.6 ..\Low Power Wireless Node

- H.6.1 ..\Part Datasheets
- H.6.2 ..\PCB Design
- H.6.3 ..\Embedded Software
- H.6.4 ..\Texas Instruments Software Examples

H.7 ..\Zotero Bibliographic Management RDF Export